

**NASA TECHNICAL  
MEMORANDUM**

**NASA TM X-73900**

**NASA TM X-73900**

(NASA-TM-X-73900) LABORATORY CALIBRATION OF  
AAFE RADIOMETER/SCATTEROMETER (RADSCAT)  
(NASA) 155 p HC A08/MF A01 CSCL 14B

N77-12363

Unclas  
G3/35 55744

LABORATORY CALIBRATION OF AAFE RADIOMETER/SCATTEROMETER (RADSCAT)

by Lyle C. Schroeder, W. L. Jones, Jr., and John L. Mitchell

November 1976



This informal documentation medium is used to provide accelerated or special release of technical information to selected users. The contents may not meet NASA formal editing and publication standards, may be revised, or may be incorporated in another publication.

**NASA**

National Aeronautics and  
Space Administration

Langley Research Center  
Hampton, Virginia 23665

1. Report No. NASA TMX-73900		2. Government Accession No.		3. Recipient's Catalog No.	
4. Title and Subtitle Laboratory Calibration of AAFE Radiometer/Scatterometer (RADSCAT)				5. Report Date November 1976	
				6. Performing Organization Code	
7. Author(s) Lyle C. Schroeder, W. L. Jones, Jr., John L. Mitchell* *(Vought Corporation)				8. Performing Organization Report No.	
9. Performing Organization Name and Address NASA Langley Research Center Hampton, Virginia 23665				10. Work Unit No.	
				11. Contract or Grant No.	
12. Sponsoring Agency Name and Address National Aeronautics and Space Administration Washington, D. C.				13. Type of Report and Period Covered Technical Memorandum	
				14. Sponsoring Agency Code	
15. Supplementary Notes					
16. Abstract The AAFE RADiometer/SCATterometer (RADSCAT) instrument, which is described in this report, was developed to measure ocean surface brightness temperature and radar backscatter coefficient from an aircraft. A brief description of the electrical and mechanical instrument configuration, followed by an extensive discussion of laboratory tests and results are contained herein. This information is required to provide parameters for data reduction, and a basis for analysis of the measurement errors of data taken with this instrument.					
17. Key Words (Suggested by Author(s)) Microwave Scatterometer Microwave Radiometer Radar Scattering Coefficient Brightness Temperature			18. Distribution Statement Unclassified - Unlimited		
19. Security Classif. (of this report) Unclassified	20. Security Classif. (of this page) Unclassified	21. No. of Pages 151	22. Price* \$6.25		

ORIGINAL PAGE IS  
OF POOR QUALITY

CONTENTS

	Page
SUMMARY . . . . .	1
INTRODUCTION . . . . .	1
INSTRUMENT DESCRIPTION . . . . .	2
Antenna Subsystem . . . . .	3
Electromechanical Subsystem . . . . .	3
RF Subsystem . . . . .	5
RF Processor Subsystem . . . . .	6
Digital Controller Subsystem . . . . .	9
Alternating Scan Angle Mode . . . . .	10
Fixed Scan Angle Mode . . . . .	11
Calibration Sequence . . . . .	11
Scat Operational State . . . . .	12
RAD Operation . . . . .	13
Output Data Formats . . . . .	13
Digital Controller Changes . . . . .	14
Power Subsystem . . . . .	15
Temperature Control Subsystem . . . . .	15
RADSCAT Analog Outputs . . . . .	15
CALIBRATION TESTS . . . . .	15
Scatterometer Testing . . . . .	16
Channel Linearity . . . . .	16
Channel Overlap . . . . .	17
IF Passband Response . . . . .	17
System Dynamic Range . . . . .	21
Saturated-to-Unsaturated Tests . . . . .	27
Calibration Stability . . . . .	28
Calibration Loop Attenuation . . . . .	29
Sphere Test "Factor" . . . . .	29
Radiometer Testing . . . . .	30
Radiometer Response to Fixed Temperature Loads . . . . .	30
Additional Radiometer Testing . . . . .	32

	Page
Other Calibration Tests . . . . .	35
Thermistor Calibrations . . . . .	35
AGC Calibrations . . . . .	36
Antenna Gimbal Angle . . . . .	36
CONCLUDING REMARKS . . . . .	37
REFERENCES . . . . .	38
TABLES I THROUGH XVIII . . . . .	39 to 57
FIGURES . . . . .	Figures 1 to 41
APPENDIX I - SCATTEROMETER TRANSFER FUNCTION . . . . .	A1-1
APPENDIX II - RADIOMETER TRANSFER FUNCTION . . . . .	A2-1
APPENDIX III - CHARACTERISTICS OF THE AAFE RADSCAT ANTENNA . . . . .	A3-1
APPENDIX IV - OUTPUT DATA FORMAT . . . . .	A4-1

## SUMMARY

The AAFE Radiometer/Scatterometer (RADSCAT) instrument, which is described in this report, was developed to measure ocean surface brightness temperature and radar backscatter coefficient from an aircraft. A brief description of the electrical and mechanical instrument configuration, followed by an extensive discussion of laboratory tests and results, are contained herein. This information is required to provide parameters for data reduction, and a basis for analysis of the measurement errors of data taken with this instrument.

## INTRODUCTION

A combined microwave radiometer-scatterometer (RADSCAT) was developed in the early 1970's under the NASA Langley Research Center's Advanced Applications Flight Experiments (AAFE) Program. This instrument has been used for obtaining microwave remote sensing measurements of ocean surface brightness temperature and radar backscatter coefficient from aircraft altitudes. RADSCAT was designed to be operated at either 9.3 GHz or 13.9 GHz from the open ramp (lower cargo bay door) of a C-130 aircraft over an altitude range from 2,000 feet to 20,000 feet. Figure 1 shows RADSCAT in an operational configuration on the NASA 929 Johnson Space Center aircraft.

During the evolution of this instrument, many evaluation tests have been conducted in the laboratory and in the aircraft (both on the ground and in flight). These tests have led to numerous hardware changes and redefinitions of performance, and an improved microwave instrument.

This report gives a detailed description of RADSCAT, the tests conducted to verify performance, and the instrument parameters at various phases during the development. These descriptions and data will be an aid to interpretation of ocean measurements obtained with this instrument.

## INSTRUMENT DESCRIPTION

The RADSCAT is a combined microwave radiometer/scatterometer which performs absolute brightness temperature and radar scattering coefficient measurements of the earth's surface. A simplified block diagram is given in figure 2. During normal operation the passive (radiometer) and active (scatterometer) measurements are made sequentially using a single pencil beam antenna. The instrument can be operated at either 9.3 or 13.9 GHz. For the scatterometer measurement, pulses from a 1 watt traveling wave tube amplifier are transmitted to the surface. These pulses are long enough to produce "beam filled" conditions, with the antenna foot print totally illuminated by the transmitted pulse. After the transmit period, a sample of the backscattered pulse is selected by a fixed range gate and then simultaneously processed in four overlapping receiver channels (with approximately 60 dB dynamic range). The scattering coefficient, which is proportional to the ratio of power received to power transmitted, is obtained from this processor output, using a transfer function derived in Appendix 1. For the radiometer measurement, the transmitter is turned off and the receiver is alternately switched between the antenna and two internal temperature references in a modified Dicke mode. The antenna microwave brightness temperature is then obtained from the radiometer transfer function which is derived in Appendix 2. A special purpose digital computer is used to control the timing of all operations and to assemble the experimental and telemetry data into suitable formats for analog recording. RADSCAT data reduction methods are described in Ref. 1, and will not be discussed herein.

The major RADSCAT subsystems are discussed in the following sections.

#### Antenna Subsystem

RADSCAT achieves high electrical performance through the use of a single dual-linear polarized, high beam efficiency, mechanically-scanned antenna without a radome. The antenna subsystem consists of a parabolic reflector with separate modified Cutler feeds and orthomode transducers for each operating frequency (9.3 GHz and 13.9 GHz). The characteristics of the antenna used on RADSCAT until January 1975 are presented in Appendix 3. Characteristics of the replacement antennas are discussed in reference 2. A summary of the properties of these antennas is given in Table I.

#### Electromechanical Subsystem

The Electromechanical Subsystem consists of the gimballed platform, carriage assembly, and gimbal controller. This subsystem provides a mounting fixture for RADSCAT in a C-130 aircraft and also provides a control system for scanning the antenna.

The gimbal platform (see figure 3) has a rotating structure and a stationary structure. The rotating structure supports the antenna at its underside and the transmitter/receiver front end components on its top surface. The entire tray is held by gimbal trunnions and rotates in bearings contained in the stationary structure. An antibacklash gear, mounted on the left trunnion, drives an angular-position-indicating potentiometer. The antenna and the microwave transmitter/receiver components are rigidly connected, and can be rotated about  $55^{\circ}$  in incidence angle in discrete steps from the nadir position and along a selected aircraft axis. Originally, the antenna could

only be rotated aft along the aircraft roll axis. However, modifications in February 1975 were made which allow the antenna to be rotated to either side in addition to the aft scanning mode (See figure 1(b) and 1(c)). A frictional damper is connected to the antenna drive system to damp out aerodynamic buffeting of the antenna during flight. The damper consists of a 1-inch diameter brass tube which is pinned to the rim of the antenna reflector and runs through a pivoted damper block in the main support carriage. As the antenna rotates about the gimbal axis, the tube slides through the block. The frictional forces on the tube sliding through the block provide the necessary damping.

The carriage assembly (figure 4) consists of a box beam with rails upon which the carriage moves. An acme screw, coupled to a crank handle by a chain drive, deploys and retracts the carriage. Safety locking pins secure the carriage space to the box in the deployed and retracted positions.

The position of the antenna (gimballed platform) is controlled by a servo system. Up to 8 gimbal positions and corresponding gimbal angles from approximately  $0^{\circ}$  to  $55^{\circ}$  off the nadir in the plane of the aircraft roll or pitch axis may be arbitrarily selected. In flight, the "Gimbal Angle Bias" potentiometer may be adjusted to remove the aircraft pitch bias from all of the gimbal angle positions. In the side scanning mode this adjustment is not used; rather the aircraft ramp is elevated to compensate for aircraft pitch. Antenna angle changes can be initiated automatically by the digital controller or manually by the "Advance" push button. This action advances a stepping switch which changes the input level to the gimbal position servo, and causes the position to change. Once the stepping switch has reached its preset maximum position, it is automatically recycled to the initial position upon the next advance command. While the gimbal is in motion, the digital



controller inhibits normal RADSCAT operation. The inhibiting action is generated digitally from the differentiated gimbal position feedback voltage.

#### RF Subsystem

The RF subsystem consists of a frequency selective receiver front end, an IF amplifier, a scatterometer transmitter, and associated scatterometer and radio-meter calibration components. All of these components are mounted on the rear of the antenna (gimballed tray), and are temperature controlled and/or monitored. The system accuracy is thereby increased by knowing and correcting for the component temperatures and eliminating rotary and flexible waveguide joints in the critical areas of the RF subsystem. The subsystem block diagram is shown in figure 5.

The frequency selective receiver front end which receives both RAD and SCAT signals, consists of the polarization-select switch, the transmit-receive circulator, a triplexer<sup>1</sup> to direct the signal to one of the two frequency Dicke switch assemblies<sup>2</sup>, front ends, and down-converters. The proper IF is selected by a latching coaxial channel-select switch. Since the IF bandwidth of the SCAT processor is very narrow (approximately 8 KHz at half power), the frequency of the transmitter must be tracked by the local oscillator. For this reason, the microwave signals are coherently generated by phase-lock-loop frequency multipliers, using a common 10 MHz crystal oscillator. This multifrequency solid-state source is named the "Coherent Frequency Synthesizer" (CFS). The SCAT transmitter consists of the CFS, a microwave

---

<sup>1</sup>Originally RADSCAT was designed for a third operating frequency, 11.7 GHz, but this frequency was not used.

<sup>2</sup>In January 1975 the Dicke switch assembly was eliminated from the 9.3 GHz channel.

gate, and a traveling wave tube amplifier (TWTA). During a SCAT measurement, the CFS operates continuous wave, while the TWTA RF input drive and the TWTA DC power are pulsed on only during the transmit period. The one watt TWTA output is passed through a comb filter to remove spurious signals. The scatterometer transmitted power is calibrated by means of a calibration loop (SCAT Cal Loop), which consists of two four-port waveguide transfer switches, two directional couplers and an attenuator. During calibration, the TWTA output is switched from the antenna to the SCAT Cal Loop; i.e., switch  $S_1$  directs the signal to the directional coupler DC-3, and switch  $S_2$  isolates the signal from the antenna path. The signal is then coupled by DC-3 through the calibration attenuator to coupler DC-1. The net result is that the output of the TWTA is attenuated and fed into the RF front end. Leakage into the RF front end via  $S_2$  and  $C_7$  is 120 dB below the TWTA output and greater than 55 dB below the calibration signal level.

#### RF Processor Subsystem

The output of the RF Subsystem leaves the gimballed tray via coaxial cable and enters the rack-mounted SCAT processor. Here the signal divides for separate scatterometer and radiometer processing.

A block diagram of the SCAT processor is given in figure 6a. The received signal at 300 MHz IF passes through a pin-diode switch, which acts as a first range gate and selects a 3 microsecond sample of the received pulse. A second range gate is achieved by diode switches on the input and output of the SCAT calibration attenuators, which synchronously close for 2 microseconds. (During operation mode, only the 0 dB leg is used, but during calibration mode, the four calibration attenuators are switched sequentially). Since the second

range gate is centered on the first, the effective width of the received pulse is 2 microseconds.

The signal from the first IF amplifier is filtered to reject images and converted to 100 MHz, where the 8 KHz bandwidth is more easily implemented. Originally the 200 MHz local oscillator for the 300 MHz to 100 MHz conversion was derived from the 10 MHz reference source and a times-20 phase-lock multiplier. This was a poor design because the second harmonic of the local oscillator (400 MHz) also produced a 100 MHz IF which vectorally added to the first order IF. Since the phase of return signal from the ocean's surface was random, the interference effect of the second order IF could be removed by time averaging. However during the internal scatterometer calibration, the signal into the receiver was coherent with all the local oscillators, such that the vector addition of these two signals created a bias which could not be removed by time averaging. This bias produced an error in the calibration level which amounted to as much as  $\pm 2$  dB, depending upon the phase of the 300 MHz signal. In July, 1974 this situation was corrected by installing a separate 10 MHz crystal oscillator to generate the 200 MHz local oscillator. This effectively made both the measurement and the calibration incoherent and thereby eliminated the bias error.

Since the dynamic range of received power can be as much as 60 dB as test conditions of altitude, angle, and scattering coefficient are varied, four square law detectors are used in parallel with sufficient overlap to insure valid data over the entire range from at least one of the detectors. The output of each detector is integrated, A/D converted, and recorded on magnetic tape. Identification of the on-scale channel is accomplished by data processing. During SCAT calibration, attenuators in the second IF are used

to reduce the SCAT calibration signal to a level which produces approximately a midscale level in each SCAT channel. Appendix 1 gives a derivation of the scatterometer transfer function.

In the RAD processor (figure 6b), the 300 MHz signal is square law detected, amplified, inverted and synchronously detected. The radiometer utilizes two warm-temperature references (waveguide loads at  $T_1$  and  $T_2$ ) to provide a two-point calibration of the system and to provide a stable  $\Delta T$  reference for the processor AGC circuit. By proper logic timing a temperature reference equal to  $1/2 (T_1 + T_2)$  is generated to which the antenna temperature is compared. At the same time, the AGC synchronous detector produces the reference temperature difference,  $\Delta T = T_1 - T_2$ , which is smoothed by an integrator and fed back to the AGC amplifier to control the RAD processor gain. Since the AGC voltage is derived from measuring the reference temperature difference, any change in  $\Delta T$  is interpreted as a change in the radiometer system gain, which is subsequently removed by AGC feedback action (the temperature references are more stable than the system gain). The effective time constant for the AGC loop is approximately 2 seconds. The output of the data synchronous detector is summed with a baseline offset voltage at the input of an integrator. The integrated output is A/D converted and recorded on tape. Since it was anticipated that lower antenna temperatures would more often be measured than higher ones, the output of the integrator is maximum (positive) for low temperatures and is minimum for high temperatures to reduce A/D round-off errors. Appendix 2 gives a derivation of the Radiometer system transfer function.

### Digital Controller Subsystem

The digital controller is a special purpose digital computer used to establish the timing of all events and sequences of the RADSCAT instrument and to assemble the experiment and telemetry data into suitable formats for recording on tape. A block diagram of the digital controller is presented in figure 7. The upper half of the figure pertains to the operational controls of the RADSCAT instrument, while the lower half applies to the data processing duties of the digital controller.

The desired mode of operation and other parameters are selectable via front panel controls. For the SCAT measurement, the operational sequence generator establishes the pulse repetition rate, pulse length, receiver range gate timing, and integration time. Also, the controller processes the data for entry onto tape at the conclusion of the SCAT measurement by generating commands for A/D conversion, readout and integrator dump. Hence the SCAT data (4 channels) are multiplexed, digitized, and transferred to temporary storage (SCAT buffer register) until required for readout into the experiment data channel format.

Similarly for the RAD measurement, the digital controller establishes the correct Antenna/Reference switching, the correct Reference 1/Reference 2 switching, sets up the RAD Processor controls, and in addition creates the data processing controls.

Data formatting of measured parameters is also provided by the digital controller. A frame counter creates word (time) slots and shift pulses so that data can be transferred to PCM data channels at appropriate times. As their time or word slots appear in a frame, the SCAT, RAD, and Telemetry data are inserted into the RADSCAT output data register for entry onto tape.

Sync words (specific bit patterns at the beginning of each frame) are provided for both the Experiment and the Telemetry PCM channel. A Sub-Frame counter is also provided for the Telemetry channel due to its length and structure.

The RADSCAT controller provides the capability of two primary modes of operation, Alternating Scan Angle Mode and Fixed Scan Angle Mode. There are several options to the Fixed Scan Angle Mode. All modes and options are selected from the control panel.

#### Alternating Scan Angle Mode

The Alternating Scan Angle Mode (AA) was designed to automatically sequence the antenna aft scan angle in conjunction with the aircraft motion, such that the same surface cell is viewed at several incidence angles (figure 8). In this mode the digital controller steps the antenna through its angular range, pausing to obtain 12 RAD and 12 SCAT measurements at each of 6 pre-selected angles. The controller then returns the antenna to its nadir starting point, calibrates, and repeats the sequence. The antenna polarization can be horizontal (H), vertical (V) or alternating (Alt. - switches polarization after 3 SCAT and 3 RAD measurements). The integration time for the RAD measurement is fixed at 128 msec, but the SCAT integration time in this mode is determined by antenna angle position, as shown in table II. The sequence of SCAT and RAD measurements in the AA mode is shown in figure 9. For data collection requiring cross polarization, the sequence of events is identical to that described above, with the exception that during the SCAT measurement the antenna polarization is switched at the end of the transmitted pulse. In the nomenclature VV, HV, VH, HH, the first letter shows antenna's transmitting polarization and the second letter the receiving polarization.

Hence, VV means transmit vertical, receive vertical; HV means transmit horizontal, receive vertical, etc. Note that the waveguide polarization switch must be replaced by the  $K_u$ -band switching circulator for cross polarization measurements; therefore, cross polarization can be obtained only with the 13.9 GHz frequency.

#### Fixed Scan Angle Mode

In the Fixed Angle (FA) option, the digital controller provides the same timing sequence as above but without issuing any antenna angle advance command. One of the six prescribed angles can be selected manually, and the antenna will stay at that position until another angle is chosen. A RAD and SCAT calibration is automatically performed approximately every two minutes.

a. Short Scat Option - The Short Scat option (SS) is identical to the FA option with two exceptions, namely:

- 1.) The SCAT integration time is always 300 ms.
- 2.) The alternating polarization is not allowed.

The sequence of SCAT and RAD measurements in the SS option are shown in figure 10.

b. RAD Only Option - In RAD only option (RO), the radiometric portion of the instrument is used separately. The sequence of events in this mode (figure 11) consists of repetitive RAD measurements of 128 msec duration followed by a 4 msec data conversion period. Again a standard RAD and SCAT calibration is automatically performed at approximately two minute intervals.

#### Calibration Sequence

The regular RADSCAT calibration cycle used for all modes and options is shown in figure 12(a). (The calibration sequence was changed in January, 1975 from that given in figure 12(a). This modification will be discussed in a later

section.) The SCAT Cal consists of four 100 msec periods (one for each SCAT channel) during which a portion of the transmitter power is fed into the receiver. A separate precision attenuator for each channel (SCAT Cal Attenuator) provides approximately a midscale power reference in each of the four overlapping SCAT channels. Typical output voltage vs. time for the four SCAT channels is also shown in figure 12(b). Note the different levels in each channel; for example, during the second calibration period, SCAT channel 1 is near zero, SCAT channel 2 is midscale, and SCAT channels 3 and 4 are saturated (full scale). After the fourth SCAT channel is calibrated, the RAD CAL is initiated for 10<sup>4</sup> msec. This entire SCAT and RAD Calibration sequence is done three times. The RADSCAT Cal timing is given in table III. A continuous calibrate option (Cont Cal) is available, which repeats the Regular Cal until the sequence is manually terminated.

#### SCAT Operational State

The digital controller establishes the timing sequences during the SCAT operational measurement period. The PRF (12.5 KHz) is fixed by the timing generator, but the transmit pulse width and the delay width are programmed internally for selectable instrument design altitudes of 2,000, 5,000, 10,000, and 20,000 feet (610, 1524, 3048, and 6100 m, respectively). The range gate (receiver) effective pulse width is 2 microseconds and is independent of altitude. The altitude range over which RADSCAT will operate in each range gate is given in figure 13. The corresponding transmit/receive timing diagram for each altitude is given in figure 14. In this figure, the hatched region of the transmitted pulse corresponds to the portion of the received pulse selected by the range gate when the antenna is at nadir and the altitude is equal to the range gate designation. Upon completion of the SCAT operational measurement period, 8 milliseconds are required to multiplex, A/D convert, and transfer the data from the 4 SCAT channels to a temporary buffer prior to insertion of the data into the Experiment data stream.



## RAD Operation

The timing diagrams for RAD operation are shown in figure 15. During the antenna measurement (Operate mode) the first circulator switch ( $C_1$  of figure 5) of the Dicke switch assembly alternates at a 500 Hz rate between the hot and warm temperature references ( $T_1$  and  $T_2$ ). At the same time the second circulator switch ( $C_2$ ) alternates between  $C_1$  and the antenna input at twice the  $C_1$  rate (1 KHz) to produce the composite video waveform from the square-law detector, shown in Figure 15. The demodulated output of the data synchronous detector is proportional to  $(T_2 + T_1 - 2T_A)$ . This signal is then integrated for 128 milliseconds to produce the time average proportional to radiometer output  $(T_A - (T_1 + T_2)/2)$ . An additional 4 milliseconds are used to A/D convert the output, insert the digital data into a temporary storage register, and then dump the integrators. In the Calibration Mode the radiometer output voltage is proportional to the difference between the two reference load temperatures,  $(T_1 - T_2)$ . The integration time for this mode is 100 milliseconds. The Baseline mode is used to detect DC offset voltages of the integrator. In this mode, the 1 KHz drive for the data synchronous detector is shifted  $180^\circ$  in phase from that for the Calibrate Mode. This produces a demodulated output equal to  $(T_1 + T_2 - (T_1 + T_2))$ . Ideally this voltage is zero; however because of hardware asymmetries, it has a small yet significant value. This voltage is summed with an offset voltage at the input to the integrator and then integrated for 128 ms. The resulting radiometer output voltage is a bias which is present in the Calibrate and Operate Modes and which is subtracted from each during data reduction. In the digital controller the RAD Baseline mode is dominant over all other modes for the RAD processor except calibration.

## Output Data Formats

The digital controller also provides the timing and control logic for collecting and assembling experiment data and diagnostic telemetry data into a suitable format for recording in an analog tape recorder. The output to the recorder consists of two binary PCM 1 KHz clocks (experiment and

telemetry channels). Figure 16 is a pictorial representation of the data format. Note the similarity between the Experiment and Telemetry subframe formats. Each starts with a frame synchronization word composed of three, 10-bit words and is followed by seven, 10-bit words of pertinent data. A detailed description of the output data format is given in Appendix 4.

#### Digital Controller Changes

Two major changes have occurred in the digital controller which affected RADSCAT operation and data recording, and hence must be discussed to allow proper interpretation of measurements taken subsequent to the changes.

a. DFS mode.- The RADSCAT was modified in May 1974 to add a dual-frequency scatterometer (DFS) mode. In this mode, the amplitude of the received signal from two slightly different transmitted frequencies is correlated and used to determine rms wave height (see Ref. 3 for description). This system is not discussed here, but the resulting modifications to RADSCAT are.

First, the Alternating Scan angle mode identification parameters were utilized to identify the DFS mode. As a result, the identification of Alternating Scan Angle Mode was identical thereafter to the Fixed Scan Angle Mode.

b. Calibration Mode.- The sequence of periodic calibration of the RADSCAT was updated January 15, 1975 and is shown in Figure 17. The revised sequence consists of 14 sets of measurements, with each set composed of four Scat and one Rad calibration. The first set are Scat noise measurements (to be discussed in a later section) plus a regular Rad cal. The next 3 sets each consist of four Scat cal's plus a Rad cal. Sets 5 thru 8 repeat the first four sets. Sets 8 through 12 again repeat except the Rad measurement is now baseline. The final two sets repeat frame 9 and 10. The integration time of each cal measurement is 126 msec, for a total CAL time of 9.52 sec.

### Power Subsystem

The power subsystem consists of the direct current supplies shown in figure 18. The unregulated power is supplied by the aircraft 28 Volt bus and is used for the gimbal linear actuator and the base plate heaters. All other electrical power is supplied by well regulated modular and laboratory type power supplies.

### Temperature Controller/Monitor Subsystem

The temperature of the following subsystems/components are controlled by individual analog controllers: the gimballed tray, the radiometer hot load, the radiometer warm load, the signal processor chassis, the two 10 MHz crystal oscillators, and the 100 MHz crystal filters. In addition to the controlled temperature units, the temperature of 19 subsystems/components are monitored by thermistors and are recorded in the Telemetry data channel. The location of the thermistor monitors is given in Appendix 4.

### RADSCAT Analog Outputs

The outputs of the Rad and Scat processors are conditioned by sample and hold and buffer amplifier circuits and displayed on a panel meter and an analog strip chart recorder. These and other selected analog outputs are provided for a real-time assessment of instrument operation. A sample strip chart recording was shown in figure 12(b).

### CALIBRATION TESTS

Since its delivery to NASA Langley, the RADSCAT instrument has undergone extensive tests to determine its operating characteristics and to obtain the necessary instrument characteristics to allow reduction of measured data.

These calibrations have been conducted in the laboratory, in aircraft ground tests, and in flight. This section and Tables IV thru VII document results of the laboratory tests through approximately March 1976. RADSCAT instrument characteristics required for use of the University of Kansas data reduction program (Ref. 1) are tabulated by flight mission in table VIII for Scat and table IX for Rad. Since many changes occurred during this period, data reduction should not be undertaken without first consulting these test results for the proper instrument transfer function.

#### Scatterometer Testing

##### Channel Linearity

During Scat operation, the backscattered power is square law detected and then integrated for a specified time, depending on mode and angle position, as described previously. Laboratory tests were performed to measure the linearity of the Scat receiver and processor over the integration times used in the various modes. These tests were accomplished by operating the instrument first in Continuous Cal Mode, then in Short Scat mode, and finally sequentially in Fixed Angle modes 1 through 6 (a variation in integration time from .1 to .925 sec) with a constant microwave input power. Figure 19 shows typical plots of the scatterometer output voltage vs. integration time at 13.9 GHz and 9.3 GHz, along with linear regression fits of the data. The SCAT linearity is generally good except in Short Scat mode for the 13.9 GHz data at -45, -50 and -70 dBm (not shown) input powers. The reason for this is unknown, but the test method is suspected (for SS data only).

The effect of integrating detected system noise and other dc biases with no signal present is shown in figure 20. During a Scat measurement,

the appropriate integrator offset voltage (for the corresponding integration time) must be subtracted to yield the true value of the integrated signal without noise. This offset is known as the integrator zero-bias. For these tests, the operating mode was the same as described above, except with no signal input. A family of curves was generated by adjusting the integrator offset voltage (note that the slope of a curve depends upon the magnitude of this voltage.) The integrator output generally shows good linearity with integration time.

#### Channel Overlap

Tests were conducted to measure the stability and magnitude of the overlap between Scat channels. The procedure consisted of inserting a sample of the transmit CFS signal into the receiver at such a power that Scat 1 and Scat 2 were both on scale. Scat channels 1 and 2 were selected because their gains differ only by a passive attenuator. Slight parametric changes in the power level were made, and the Scat 1 to Scat 2 voltage ratio for these tests determined as a function of Scat 2 voltage. These data are plotted in Figure 21, along with overlap measurements made in a previous flight test. The laboratory data (SS mode) agree fairly well with the Short Scat flight data, and show that the Scat voltage ratio tends to increase as Scat 2 voltage decreases. This trend is especially noticeable at the higher integration times. A suggested cause is zero-bias precision errors, which exaggerate the overlap ratio in the same manner.

#### IF Passband Response

In the SCAT processor, the received power is passed through a narrow band (8 KHz) crystal filter at the 100 MHz If frequency. Accurate measurement

of the Scat channel frequency response is necessary to properly correct for Scat processor gain changes caused by doppler shifts in the frequency of the received signal. This doppler is caused by aircraft velocity and can be quite significant. (For example, a doppler shift of approximately 4 kHz is provided by an aircraft velocity of 87.5 m/sec and an aft incidence angle of about 30°).

The passband response curve was measured in the laboratory by inserting a signal at the 300 MHz IF input to the signal processor and subsequently varying the second local oscillator frequency while keeping both input power levels constant. The frequency of the second local oscillator 200 MHz was varied by substituting a frequency synthesizer for the 10 MHz crystal oscillator. The signal amplitude was selected such that a single scat channel was sensitive throughout the test (usually Scat 2).

Measurements of the passband response have been made in the laboratory many times during the period preceding this report. Figure 22a shows the comb filter frequency response over a range of 70 KHz, while Figure 22b shows a typical single passband response curve. The curves are normalized to the signal level at 300 MHz center frequency before being used to correct for doppler.

A comparison of the characteristics of some of the single bandpass curves taken during the checkout phase of the instrument is given in the following table.

Bandpass Filter Characteristics

Test Data	<u>1st Peak</u>		<u>2nd Peak</u>		<u>3 db points</u>	
	Freq., KHz	Mag.	Freq., KHz	Mag.	- doppler	+ doppler
9/10/72	-.7	1.35	-4.5	1.55	-6.1	+1.0
3/29/73	-1.0	1.4	-4.7	1.45	-6.4	+ .95
1/26/74	-.7	1.1	-4.1	1.15	-5.8	+1.3

The data of 3/29/73 shows good correlation in frequency (within 0.2 KHz) and magnitude with the data of 9/10/72. However, the test data of 1/26/74 show an apparent change of the center frequency of the characteristic. During testing in March through May 1974, it was discovered that the crystal filter center frequency varies with temperature. Figure 23 shows the effect of changing ambient temperature from laboratory conditions (68°F) to 95°F.

Because the crystal filters used were temperature sensitive, they were placed in controlled ovens in March 1974 to keep the temperature a constant 95°F. In May 1974 it was shown that 95°F was not high enough to stabilize the temperature. For this reason, thermistor monitors were installed on the crystal filters and the temperature was increased to 105°F in late May 1974. Subsequently this temperature was raised to 110°F in August 1974. Figure 24 shows bandpass characteristics appropriate for crystal filter temperatures of 95°F, 105°F and 110°F.

Prior to installation of the thermistors, no measurement of the crystal filter temperature is readily available, so that the bandpass characteristics used were arrived at by an estimate of the RADSCAT temperature environment from ambient conditions. Based on these estimates, previous flight mission data have been reduced, using the following bandpass characteristics:

<u>Mission/Flight</u>	<u>Date of Flight</u>	<u>Characteristic</u> /	<u>Temp.</u>
230/FCF	3/11/73	May 1974	105°F
238/20	6/5/73	3/19/75 (0 Hz offset)	110°F
238/27	6/11/73	3/19/75 (0 Hz offset)	110°F
247/FCF	7/26/73	April 1973	70°F outside ambient
247/37	9/12/73	May 1974	105°F
258/All	Dec. '73 to Feb. '74	May 1974	105°F

Since the actual filter temperature during these flights is unknown an analysis was conducted to estimate the bounds of the error in IF gain for a reasonable temperature range. This error was estimated from the ratio of bandpass characteristic levels at the controlled high-temperature case (110°F at the crystal filters) to those for a lower temperature case (70°F ambient outside temperature). The temperature of the crystal filters during the 70°F ambient test was probably over 90°F due to internal heating, so the above ratios may not represent the most extreme case. The gain errors were estimated at the doppler frequencies experienced in three representative flights, and the results are shown in Figure 25, as a function of incidence angle. The maximum error of approximately 5.5 dB occurs at the larger incidence angles for these flights, but at other angles, the error is 3 dB or less. The nadir value is unchanged.

Another instrument adjustment which affected the bandpass characteristic was the frequency offset of the 10 MHz reference source for the 200 MHz local oscillator by approximately +50 Hz, in July 1974. The effect of this offset frequency adjustment was to change the center frequency of the filter to (100 MHz - 1 KHz) and hence the frequency range of the flat portion of the passband has shifted + 1 KHz. This bandpass characteristic at an oven temperature of 110°F (shown in figure 26(a)) is the correct data to be used from August 1974 on for the instrument in the aft scanning configuration.

In March of 1975 when the instrument was adapted to permit side scanning, a large passband was no longer required since doppler shifts for side scanning are near 0 Hz. For this reason, the center frequency was moved more nearly to the center of the passband, so that large doppler correction factors would no longer be required. Figure 26(b) shows a plot of the passband for side scanning, which is valid from June, 1975 on.



### System Dynamic Range

The scatterometer linearity over its dynamic range was measured using the test configuration shown in figure 27. A sample of the CW signal from the transmit CFS was passed through a precision microwave attenuator and then injected at known power level into one of the ports of the polarization switch. During the test, the polarization switch was alternated between the two ports to yield both a measurement of signal voltage and integrator offset voltage (scat zero). Tests of this type were conducted with the RADSCAT in a normal operating mode, in continuous Cal mode, and with the 10 db pad "in" at high received powers. These tests and the data obtained are discussed in the following.

a. Normal operating mode tests.- These tests were conducted with the RADSCAT in Short Scat or Fixed Angle mode. A chronological listing of the tests is given in table IV. A typical plot of the scatterometer output voltage as a function of input power are given in figure 28. It is noted that the Scat channel output voltage follows a square law, as expected, except for Scat 1 at high input power levels. At these levels, the system is slightly saturating, and compression of the output is observed.

A square law equation,  $V_{SCAT_i} = K_i P_{INPUT}$ , where  $K_i$  is the gain of the  $i$ th scat channel, is fit to the uncompressed data using a least squares regression method. The form of the equation actually used, with  $P_{INPUT}$  expressed in decibels, was  $10 \log_{10} V_{SCAT_i} = 10 \log_{10} K_i + P_{INPUT}$  (dB). Values of  $\log_{10} K_i$  are given in table IV. For the first four tests, the channel separation (difference in channel gains) was quite large (17 to 18 dB between channels). In addition, the channel separation showed large deviations, particularly  $S_1$  to  $S_2$  and  $S_3$  to  $S_4$ . Subsequent to these tests the channel separation (and thus the dynamic range) was reduced.

The next group of dynamic range tests (see table IV) were conducted during the April '73 system calibration, just prior to flight mission 230. The first three tests (tests 11, 26, and 27) were at 13.9 GHz, and the next four (tests 28-2, 29, 43, and 44) were at 9.3 GHz. As stated earlier, the magnitude of the  $S_1$  to  $S_2$  and  $S_2$  to  $S_3$  channel separation is reduced. The channel separations were considerably more stable than for the prior tests, probably due to better calibration procedures and techniques. The data from the regression analysis indicate that system gains at 13.9 GHz increases with altitude (range gate) setting, whereas, the gain is quite stable with range gate setting at 9.3.

The reason for this change in sensitivity at 13.9 GHz is not understood, although a probable cause is the difference in the area under each range gate pulse. More important, regardless of the reason for this system gain change, its effect is compensated for by the regular Scat calibration. For example, tests 28-2 and 29 show the effect of integration time on the square law coefficients. The FA mode test (29) should be  $10 \log_{10} \frac{0.58}{0.30} = 2.86$  dB lower in power than the SS Mode Test (24-2), and the constants show a difference of about 2.2 dB (which is probably within the drift of the system).

The remaining tests in this table were conducted during the October 73 system calibration. Prior to these tests, the Scat channel separation  $S_3$  to  $S_4$  was reduced to provide more overlap. All tests were at 13.9 GHz SS mode. The measurements show that the channel separation was quite stable.

The next table (Table V) shows all normal operating mode tests conducted since October '73. The tests are divided into four groups with the same Mode

and 10 dB attenuator status for ease of comparisons. Generally, the channel separation is quite consistent, especially for the first 3 Scat channels. It is also noted that the separation does not appear to vary with the status of the 10 dB attenuator. The square law constants show a significant but repeatable change starting with the 6/18/75 tests. This indicates the gain of some system component caused is changed; ie, a different system power level is required to produce a given output voltage. Since the system is again stable, no problem is encountered. Comparison of the channel separations with earlier (Oct. '73) measurements indicates very good agreement for  $S_1 - S_2$  and  $S_2 - S_3$ , but a 2 dB mean difference for  $S_3 - S_4$ . The precision of the later tests is considered superior to the earlier measurements, and is probably the true channel separation that existed during the October '73 tests.

b. Continuous calibration mode tests.- These tests were conducted with the TWTA off and using the transmit CFS similar to the dynamic range tests above except that the RADSCAT was continuously cycling through the calibrate mode. In this mode, Scat calibrate attenuators are periodically switched into the Scat processor circuit, providing a reference power for each scat channel. A typical plot of scat channel voltage versus power for a continuous cal dynamic range test is given in Figure 29.

A chronological listing of the tests of this type is given in table VI, along with the mean square law coefficients for all Scat channels with attenuator  $A_1$ , (0 dB ie: no attenuation) and for each Scat channel calibrated with its corresponding calibrate attenuator ( $A_2 S_2$ ,  $A_3 S_3$ , and  $A_4 S_4$ ). The absolute value of the mean square law coefficients depends on the absolute input power level, which was not recorded for the following tests: Post M 218 tests, April tests 99 A and B, and the October Weinschel tests.

Hence, data from these tests can be compared only in a relative sense.

Pre-mission 230 tests (Table VIa) - The channel separations observed on these Post M218 tests and the April 73 tests were about the same level as those measured earlier during corresponding tests. As mentioned, the  $S_1 - S_2$  separation was reduced for this set of tests.

The continuous cal test data are used to measure the cal attenuator attenuation levels. The calibration attenuator level for a given Scat channel is equal to the change in power level which occurs when the attenuator is inserted. The cal attenuators are thus (since  $A_1$  is 0 attenuation),

$$A_2 = P_{A1 S2} - P_{A2 S2} \quad \text{at } V_{S2} = \text{constant},$$

$$A_3 = P_{A1 S3} - P_{A3 S3} \quad \text{at } V_{S3} = \text{constant}, \text{ and}$$

$$A_4 = P_{A1 S4} - P_{A4 S4} \quad \text{at } V_{S4} = \text{constant}.$$

These attenuator levels were evaluated using the square law fit constants (K, defined earlier). It can be shown that  $10 \log_{10} K$  corresponds to the power level at 1 volt on the Scat channel. The cal attenuator values obtained substituting the K values in the above equations are also listed in table VIa. Since any error in the cal attenuator value is a direct error in  $\sigma^0$ , the large variations in the cal attenuator values measured in the pre-mission 230 tests, especially in the  $A_4$  value, were investigated at length in subsequent tests.

October tests - Just prior to those tests, the channel separation between Scat 3 and Scat 4 was reduced as described earlier. The continuous cal dynamic range testing was done primarily to determine the cal attenuator

values to better precision. These tests are analyzed by others\*, but the following data analyses was done using mean square law fits on the computer, and are felt to be slightly more precise than the graphical fit method employed earlier.

Table VI b. shows the channel separation and cal attenuator values determined during the October tests. The precision of these data was improved by taking data as rapidly as possible to avoid power level drifts. The mean values of cal attenuators listed in this table were used in the RADSCAT data conversion program (supplied by the University of Kansas) to compute updated Scat science data, and the first set are valid for flight data taken in all missions prior to M 258 (Skylab 4) while the second set are valid for M 258 only.

Table VIc show channel separation and cal attenuator measurements with the 10 dB IF attenuator "in". This mode is used when Scat return is so strong that saturation of Scat 1 would result. Mean channel separation data and Cal attenuator data are available for all but  $A_4$ , but data are not often expected in  $A_4$  with the 10 dB pad "in". These mean cal attenuator values are used in processing all flight data having the 10 dB pad "in".

Table VI d shows the change in power for a given Scat channel with and without the 10 dB pad in. There is a general decrease in attenuation observed with scat channel used in these measurements.

---

\*Anonymous: Calibration Data Report for the Advanced Applications Flight Experiment (AAFE) Composite Radiometer - Scatterometer (RADSCAT) GE Report 74SD 4206, February 1, 1974.

Table VI e show test results obtained on the C-130 Aircraft using a precision coaxial attenuator in the 300 MHz IF. These cal attenuator and channel separation values are comparable with earlier data.

Post October '73 Tests - The results of all continuous calibration tests conducted since the October '73 tests are given in Table VII. These data have been separated into two groups depending on the status of the 10 dB attenuator. The channel separation for these data are quite consistent for both sets of data and show no trend as a function of pad status. The standard deviation is .52 dB in the worst cases. Cal attenuator data calculations shown in the last three columns for 10 dB pad out show a standard deviation increasing with attenuator magnitude.  $A_2$  and  $A_3$  values are .14 and .43 dB respectively, but  $A_4$  is 1.15 dB. This trend is expected since  $A_4$  requires an extremely wide dynamic range of inputs to be measured. (45 dB  $\approx$  31,600 in ratio). The number of accurate samples of attenuator data with the 10 dB pad "in" is quite limited, especially for  $A_4$ , such that a trend is hard to determine. However, the attenuator levels compare favorably with and without the pad. The reason that pad "in" tests are often inaccurate is that the input signal into the system has to be increased by 10 dB to compensate for the drop across this pad; the increased input signal causes saturation of some components which are upstream of the pad.

For pad out, all present attenuator measurements are larger than those of October '73, but for the pad in, the October '73 values were larger in one case and smaller in another. The reason for the differences is not known; however, since the present data do seem to be independent of the pad status, they are probably more accurate.

Saturated to unsaturated tests

Tests were conducted with the scatterometer input power increased so that the Scat channel output was compressed. These data were obtained during the April 1973 calibrations during tests 87 through 92, in Continuous Calibration, Short Scat, and Fixed Angle modes with the 10 db IF pad "in" and "out". The results are plotted in figure 30. In this plot the Scat voltage is normalized by the integration time, so that Cont. Cal, SS, and FA mode data can be plotted together. The results show 2 traces, one with the pad "in", and one with the pad "out", with the lower parts linear and described by square law, and the upper part compressed. The square law constants for the uncompressed parts are indicated on the plot, and the separation between the trace means is 10.37 dB. The maximum linear region of the scat channel is indicated also. About this level, a regression analysis was fit to the compression curve which is shown in figure 30 and for the 10 dB pad "out" and "in" respectively. This equation was at one time used to reduce data above the linear region.

However, it was discovered later that this compression curve was not unique for the scatterometer for all time. Thus, a method of synthesizing a "non-compressed" scat channel 1 calibrate voltage was developed, since the only data in Scat 1 which is compressed is generally the calibration.

The Scat 1 cal synthesis was based on the relationship between linear Scat 1  $A_1$  and Scat 2  $A_2$  square law curves. A calibration signal on Scat 1  $A_1$  is related to that on Scat 2  $A_2$  by the following (in dB):

$$10 \log_{10} V_{cal} S_1 A_1 + (S_1 - S_2) - A_2 = 10 \log_{10} V_{cal} S_2 A_2 ;$$

or

$$10 \log_{10} \frac{V_{\text{cal } S_1 A_1}}{V_{\text{cal } S_2 A_2}} = - (S_1 - S_2) + A_2 ;$$

or

$$V_{\text{cal } S_1 A_1} = 10^{\frac{A_2 - (S_1 - S_2)}{10}} \times V_{\text{cal } S_2 A_2} .$$

Using the mean value of channel separation ( $S_1 - S_2$ ) of 11.377 dB and Scat 2 attenuator of -14.527 dB from the October '73 tests for example, the ratio above is

$$\frac{V_{\text{cal } S_1 A_1}}{V_{\text{cal } S_2 A_2}} = 10^{-\frac{(11.377 - 14.527)}{10}} = 2.0654$$

This method was used to synthesize scat 1 cals for all data with the 10 dB pad not "in". For the data with the pad "in" the system power was low enough in flight such that no compression occurred, so that actual uncorrected calibration voltage and data were used.

#### Calibration stability

The stability of the calibration voltages on the scat channels was tested by placing the RADSCAT in continuous-cal for a sustained period of time. The scat cal voltages were then sampled periodically, and a plot of Scat Cal voltage vs. time was made, and is shown in Figure 31(a). This plot shows stability over the two minute period between cals which is good in this case. However, tests over a longer period of time show large drifts in the cal voltages. (See figure 31(b)). These drifts are correlated on Scat 1 and 2 but not scat 3 and 4.



In May 1974 it was found that much of the long term instability could be eliminated by the insertion of a second 10 MHz oscillator. (See earlier discussion under RF Processor Subsystem section). A plot of stability subsequent to this change is shown in figure 31(c).

#### Calibration loop attenuation tests

Measurements were made to determine precisely the level of attenuation experienced by the power transmitted when passing through the "calibration loop". This attenuation is required so that the transmitted power can be reproduced during experiment operation.

Measurements of the value of this attenuation were obtained periodically by measurement and inference of losses of components in the "cal loop". These values are shown in Table VIII, SPAR item 17.

#### Sphere test factor

Since component insertion losses and antenna gains cannot be measured without some error, a series of tests designed to compare end-to-end scatterometer measurements with theory were designed. These tests consisted of comparing the measured backscatter from a precision sphere with the theoretical scattering coefficient. The difference between the scatterometer measured  $\sigma^0$  and the theoretical value was interpreted as a lumped-constant adjustment (multiplicative constant in radar equation) to the RADSCAT measurement. This technique is described in Ref. 4, where values of -2.407 dB for 13.9 GHz and -4.340 dB for 9.3 GHz were obtained.

### Radiometer Testing

The RADSCAT radiometer is a modified Dicke radiometer which utilizes dual temperature references and an automatic gain control to maintain constant system gain. During operation the input to the receiver is alternately switched between the antenna and the two different-temperature loads in such a way that a continuous calibration signal (proportional to the differential load temperature) is produced. The long-term stability of this technique is typically more than one order of magnitude better than the usual Dicke radiometer and therefore requires infrequent laboratory calibrations.

#### Radiometer Response to Fixed Temperature Loads

This section presents results from those laboratory calibrations which were used to evaluate the radiometer transfer function and measurement accuracy. These tests consisted of operating the radiometer with loads of known temperature and comparing the measurements with that predicted from the theoretical models of Appendix A2. By connecting the loads to the antenna ports of the polarization switch, two different-temperature loads could be monitored by changing the polarization switch. For these tests, a variable temperature load and a constant ambient temperature load were connected. The variable temperature reference load was obtained by immersing a low VSWR waveguide load in a bath containing different liquids. The temperature of the load material and feed waveguide were carefully measured to provide a corrected radiometric temperature at the input to the receiver. The laboratory equipment set-up used for these tests are given in figure 32. Typical input temperatures used were:

Bath	$T_{load}$	$T_{input}$
Liquid Nitrogen	78K	82K
Acetone/Dry Ice	195K	200K
Water/Ice	278K	279K
Ambient	295K	295K
Hot Water	307K	309K

Calibrations were performed with the gimbaled tray at both ambient temperature and at a controlled temperature (approximately 96°F).

The normal test sequence consisted of first 10 seconds of Continuous Cal, then 10 seconds of Baseline, followed by a period of measurements in the RAD ONLY mode which were interrupted periodically for short Continuous Cal and Baseline checks. The RAD Only data was obtained with the polarization switch alternating between the variable temperature load and the ambient temperature load (approximately every 30 seconds). The output was recorded and averaged for several minutes to reduce the radiometer variance to a small fraction of 1K.

Additional measurements were also made with one port of the polarization switch shorted to determine the radiometer output temperature  $T_{RAD}$ . This quantity which is required to compute the correct antenna temperature, was typically 311K.

During the CONT CAL and BASELINE modes, the radiometer AGC voltages were slightly different from that during regular operation. This produced different system gains (increased over operate) which were compensated for during the data reduction. From fixed AGC voltage tests, the following effective voltages were empirically determined.

$V_{OP}$  = radiometer voltage during operate mode

$V_{cal} = .927 V_{Cont\ Cal\ Mode} = .98 V_{Reg\ Cal\ Mode}$

$V_{BL} = .88 \times V_{Baseline\ Mode}$

Typical results of these tests are illustrated in a plot of normalized radiometer voltage  $\xi = \frac{V_{OP} - V_{BL}}{1.28 V_{Cal} - B_L}$  versus  $T_{IN}$  given in Figure 33; also shown is a least squares linear regression fit to the data. A summary of calibration results is given in Table X.  $T_{IN}$  (Model) is from the radiometer transfer equation given in Appendix A2 (using the thermistor temperatures measured during the given test) and  $T_{IN}$  (REGRESSION) is the equation for the least mean squares linear fit to the data ( $\xi$  vs.  $T_{IN}$ ).

During flight operations, the performance of the radiometer was frequently degraded over that obtained under laboratory calibrations. Typically the radiometer output experienced slowly time varying bias of approximately  $\pm 5$  K and  $\Delta T$ 's of  $2^\circ - 4$  K for 128 ms integration time. For reduction of the aircraft ocean data, the radiometer transfer equation (equation A2-26, Appendix 2) was used. For this case the temperature  $T_{IN}$  becomes the antenna temperature. The ocean surface brightness temperature is determined by correcting  $T_{IN}$  for antenna VSWR, losses, and pattern effects.

#### Additional Radiometric Testing

Other radiometer evaluation tests were conducted by a contractor\* in October and November, 1973. Since this document is not readily available, the radiometer results are presented in this section. The material presented are direct quotations except for renumbering of tables and figures to be consecutive with those given in this report.

---

\*General Electric Technical Report 74SD4206 February 1, 1974.

a. Radiometer linearity - The Radiometer linearity test was performed by using a cryogenically cooled load with a heating option and stabilizing the radiometric temperature at eight discrete points. Sufficient data was taken at each point to adequately determine the mean values for Data, AGC, CAL and BASELINE using the computer averaging program.

Table XI lists the VTR (variable temperature reference) temperatures, as read from the monitors on the cryogenic load controller, and the actual radiometric temperature presented to the V-port on the gimbal mounted equipment.

Figure 34 shows a curve of the Rad voltage, corrected for the baseline measurements, versus the actual radiometric temperatures. The equation for the curve was found to be:

$$T(^{\circ}\text{K}) = \frac{10.0 - (V_{\text{Data}} - V_{\text{Baseline}})}{0.026434}$$

$$\text{Rad sensitivity} = 26.434 \text{ Millivolts}/\text{K}$$

---

b. Radiometer stability (Rad only mode) - The radiometer stability tests were performed with the VTR set to 100K. This corresponds to an actual radiometric temperature of about 114.65 K as shown in Table XI. Test No. 4, performed at Langley Research Center (LaRC) and Test No. 42, performed at Ellington AFB on the flight line with aircraft power show excellent correlation. The values plotted are the mean values of the one minute Rad average data for each five minute time slot. Table XII illustrates the correlation obtained from two distinct tests greatly removed in time, location and environment. It should be noted that the standard deviation of the one minute means is less than 1.25 K over a long term.

At the conclusion of Test No. 42, the polarization was switched to H to allow the radiometer to look at the 13.9 GHz circulator termination. A RAD data value of 1.78 volts and a  $V_{BL}$  of -0.150 volts was obtained along with 4.71 volts for the thermistor at this termination site ( $T_{11}$ ). The following calculations show how correlation was determined.

Calculations for equivalent radiometric temperature.

$$T(^{\circ}K) = \frac{10.0 - (V_{Data} - V_{BL})}{0.026434}$$

where:

$$V_{Data} = 1.78 \text{ volts}$$

$$V_{BL} = -0.150 \text{ volts.}$$

$$\text{Thus } T(^{\circ}K) = \frac{10.0 - (1.78 + 0.150)}{0.026434} = 305.29$$

Calculations for the actual measured temperature.

$$T_{11}(^{\circ}C) = 72.96 - 6.12759 TM - 0.23561 TM^2$$

where:

$$TM = 4.71 \text{ volts (thermistor } T_{11} \text{ voltage).}$$

$$\text{Thus } T_{11}(^{\circ}C) = 72.96 - 28.86 - 5.23 = 38.87.$$

$$\text{Or } T_{11}(\text{K}) = 38.87^{\circ}\text{C} + 273.16 = 312.03^{\circ}\text{K}.$$

Here again, excellent correlation is shown especially when one considers the losses in the polarization switch and the thermal gradient between the termination housing and the absorber tip.

Figures 35 and 36 are the plotted average values for the two long term stability tests.

c. Radiometer stability (Continuous Cal Mode) - Functional check flight tests No. 46 and No. 50 were performed to determine the long term variation of Rad Cal and Rad AGC as well as for Scat Cal purposes. The plots in Figures 37 and 38 show the typical range of variation for the above listed parameters over a 1-1/2 hour continuous operating period. The mean of ten consecutive data points was taken every five minutes to obtain the data plotted.

#### Other Calibrations

---

##### Thermistor calibrations

Tests were conducted to determine the voltage output versus temperature of the thermistors in the electronics package and antenna system. These calibrations were obtained by monitoring the thermistor output voltage as the thermistor temperature was varied from  $50^{\circ}$  to  $10^{\circ}\text{C}$ . The temperatures monitored by these thermistors are used as input data to the Radiometer temperature correction model, and a high degree of precision is required. A typical voltage-temperature plot of the points obtained, along with a regression fit to the data is given in figure 39. The remaining regression coefficients are given in table VIII. A second order regression fit was necessary to describe the slight nonlinearity at lower temperature.

### AGC calibrations

Tests were conducted to determine the relative gain versus output voltage of the AGC system. These tests were conducted in March 1973 and the results are shown in figures 40(a) and 40(b). The useful range of AGC data is described by the third order regression shown.

### Antenna gimbal angle

Calibrations of output voltage versus antenna gimbal angle were obtained with the instrument mounted in the aircraft. First, telemetry output voltage versus antenna pitch angle  $\theta$  (relative to vertical) was obtained. Next the angle  $\phi$  between the reference plate (on the A/C) and the horizontal, and the angle  $\gamma$  between the reference plate and the aircraft pitch axis (LTN-51) was obtained. The correct nadir angle during flight is obtained from the above by

$$\xi = \theta + \gamma + \phi .$$

The plot of voltage versus  $\xi$  is shown in figure 41.



## CONCLUDING REMARKS

The AAFE RADiometer/SCATterometer (RADSCAT) instrument, which is described in this report, was developed to measure ocean surface brightness temperature and radar backscatter coefficient from an aircraft. A brief description of the electrical and mechanical instrument configuration, followed by an extensive discussion of laboratory tests and results are contained herein. This information is required to provide parameters for data reduction, and a basis for analysis of the measurement errors of data taken with this instrument.

REFERENCE LIST

1. Claassen, John P.: AAFE RADSCAT Data Reduction Program User's Guide.  
NASA CR-144992, May 1976.
2. Cross, A. E.; Jones, W. L., Jr.; and Jones, A. L.: Experimental  
Measurements of RADSCAT Antenna Characteristics. NASA TMX in editing.
3. Johnson, J. W., Jones, W. L., Swift, C. T., Grantham, W. L., and Weissman,  
D. E.: Dual Frequency Scatterometer Measurement of Ocean Wave Height.  
1974 USNC/URSI Meeting, Boulder, Colorado October 1974.
4. Grantham, W. L., Schroeder, L. C., and Mitchell, J. L.: Absolute  
Calibration of the RADSCAT Scatterometer using Precision Spheres.  
NASA TN D-8259, 1976.
5. Moore, J. H.: The Radiometer Transfer Function for the AAFE Composite  
Two-Frequency Radiometer Scatterometer. NASA CR-2343, 1973.

List of Tables

- I. Summary of Antenna Characteristics
- II. Alternate Scan Angle Mode Timing Values
- III. RADSCAT Calibration Timing
- IV. Normal Operation Mode Scat Dynamic Range Tests
- V. Normal Operation Mode Scat Dynamic Range Tests  
(Tests subsequent to October '73)
- VI. Continuous Cal Dynamic Range Tests
  - (a) Pre-Mission 230 (~April 11, 1973)
  - (b) October 1973, 10 dB attenuator out
  - (c) October 1973, 10 dB attenuator in
  - (d) October 1973,  $\Delta$  dB, pad in and pad out
  - (e) Weinschel Tests
- VII. Continuous Cal Dynamic Range Tests - post October '73
  - (a) 10 dB pad out
  - (b) 10 dB pad in
- VIII. Scatterometer Parameters (SPAR)
- IX. Radiometer Parameters (RPAR)
- X. Summary of Radiometer Calibration Results
- XI. VTR/Actual Temperature Correlation Data
- XII. Radiometer Correlation
- XIII. Thermistor Regression Coefficients

TABLE I  
ANTENNA CHARACTERISTICS

a. Original Antenna, used till Jan. 1975 (Data from Appendix A3).

	9.3 GHz		13.9 GHz	
	<u>E-Plane (H-pol)</u>	<u>H-Plane (V-pol)</u>	<u>E-Plane (H-pol)</u>	<u>H-Plane (V-pol)</u>
3 dB beamwidth, deg (in line)	2.10	2.38	1.40	1.63
3 dB beamwidth, deg (side arm)	2.05	2.45	1.42	1.66
Equivalent beamwidth, deg*	1.94		1.29	
Antenna gain, dB (in line)	37.95		41.5	
Antenna gain, dB (side arm)	37.85		41.5	
Efficiency, per cent	90		88.5	

b. Replacement Antenna, used from January 1975 until Aug. 16, 1975.

(Data from Reference 2.) 13.9 GHz in line port pattern data only -  
other options were not used.

	<u>E-Plane (H-pol)</u>	<u>H-Plane (V-pol)</u>
3 dB beamwidth, deg	1.28	1.44
Equivalent beamwidth, deg*	1.15	
Antenna gain, dB	41.7	

c. Replacement Antenna, used from Aug. 20, 1975 until present.

(Data from Reference 2.) 13.9 GHz inline port pattern data  
only - other options were not used.

	<u>E-Plane (V-pol)</u>	<u>H-Plane (H-pol)</u>
3 dB beamwidth, deg	1.45	1.25
Equivalent beamwidth, deg*	1.15	
Antenna Gain <sup>†</sup>	41.7	

\*For definition, see Ref. 1.

†Not measured, but assumed from previous test.

TABLE II. Alternating Scan Angle Mode Timing Values

Antenna Position	Incidence Angle Degrees	Dwell Time Sec	Each SCAT Meas. Time Sec	Each RAD Meas. Time Sec
1	Nadir	8.86	0.58	0.128
2	12.7	9.04	0.60	0.128
3	24.5	9.55	0.64	0.128
4	34.8	10.38	0.71	0.128
5	43.7	11.52	0.80	0.128
6	51.1	12.98	0.92	0.128

Table III RADSCAT Calibration Timing

<u>SCAT Calibration</u>	<u>Time</u>
ATTN 1 (0 dB)	100 ms
Conversion & Readout	8 ms
Dump Integrators	2 ms
ATTN 2 (20 dB)	100 ms
Conversion & Readout	8 ms
Dump Integrators	2 ms
ATTN 3 (35 dB)	100 ms
Conversion & Readout	8 ms
Dump Integrators	2 ms
ATTN 4 (55 dB)	100 ms
Conversion & Readout	8 ms
Dump Integrators	2 ms
<u>RAD Calibration</u>	
RAD Calibration	100 ms
Conversion & Readout	2 ms
Dump Integrators	<u>2 ms</u>
	544 ms x 3 calibration cycles
	= 1632 milliseconds
	or 1.632 seconds

TABLE IV. NORMAL OPERATING MODE DYNAMIC RANGE TESTS

TEST	DATE	MODE RANGE GATE	FREQ.	CURVE FIT CONSTANTS				CHANNEL SEPARATION		
				S <sub>1</sub>	S <sub>2</sub>	S <sub>3</sub>	S <sub>4</sub>	S <sub>1</sub> -S <sub>2</sub>	S <sub>2</sub> -S <sub>3</sub>	S <sub>3</sub> -S <sub>4</sub>
PreM203	6/4/72		300MHz	4.3252	6.2544	7.968	9.5772	19.292	17.137	16.091
GE	9/19/72		300MHz	2.2749	4.0042	5.6710	7.5064	17.293	16.668	18.354
M218 <sup>Inc.</sup> Dec.	10/13/72	SS-5K	13.9	4.1474 4.1970	5.890 5.9718	7.5524 7.5965	9.1473 9.1661	17.426 17.748	16.624 16.627	16.449 15.696
Post M218	11/21/72	SS-2K	300Mhz	1.2949	3.0769	4.7067	6.5204	17.820	16.298	18.137
Mean								17.9158	16.5948	16.9454
Stan.Dev.								.79985	.3568	1.2188
<u>April Tests</u>										
11	3/28/73	SS-2K	13.9	4.739	5.863	7.442	9.364	11.24	15.79	19.22
26	3/28/73	SS-5K	13.9	4.9454	6.064	7.5545	9.4143	11.186	14.905	18.598
27	3/28/73	SS-10K	13.9	5.0437	6.154	6.6649	9.4968	11.103	15.109	18.319
Mean				4.9094	6.027	7.5538	9.425	11.1763	15.268	18.712
Stand.Dev.				.1555	.1490	.1114	.0671	.0690	.4634	.4612
<u>April Tests</u>										
28-2	3/28/73	SS-2K	9.3	4.8173	5.9031	7.4193	9.2767	10.858	15.162	18.574
29	3/28/73	FA1-2K	9.3	5.0235	6.1334	7.6250	9.5142	11.099	14.916	18.892
43	3/28/73	SS-5K	9.3	4.7766	5.8865	7.3780	9.1931	11.099	14.915	18.151
44	3/28/73	SS-10K	9.3	4.7784	5.8797	7.4048	9.2263	11.013	15.251	18.215
Mean				4.8490	5.9507	7.4568	9.3026	11.0172	15.061	18.458
Stand.Dev.				.1179	.1222	.1134	.1452	.1136	.1719	.3440
<u>Oct. Tests</u>										
1 (INC)	10/1/73		13.9	4.7088	5.8173	7.4014	8.7379	11.085	15.841	13.365
1 (Dec)	10/1/73		13.9	4.8139	5.9359	7.5237	8.9926	11.220	15.878	14.489
1 5dBSteps	10/1/73		13.9	4.6968	5.7951	7.3799	8.6953	10.983	15.848	13.154
5 (Inc)	10/3/73	SS-10K	13.9	4.6517	5.7528	7.3268	8.4598	11.011	15.740	11.330
5 (Dec)	10/3/73	SS-10K	13.9	4.8223	5.9372	7.4785	8.6037	11.149	15.413	11.252
6 (Inc)	10/3/73	SS-10K	13.9	4.8103	5.9488	7.4420	8.7365	11.385	14.923	12.945
6 (Dec)	10/3/73	SS-10K	13.9	4.8296	5.9465	7.4913	8.8698	11.169	15.448	13.785
Mean				4.7619	5.8762	7.4348	8.7279	11.1431	15.5857	12.9314
Stand.Dev.				.0736	.0844	.0693	.1726	.1364	.3462	1.2543

TABLE V - NORMAL OPERATING MODE DYNAMIC RANGE TESTS

Subsequent to October 1973

Test Date	Test No.	Mode	Range Gate	Square Law Constants				Channel Separations		
				S <sub>1</sub>	S <sub>2</sub>	S <sub>3</sub>	S <sub>4</sub>	S <sub>1</sub> -S <sub>2</sub>	S <sub>2</sub> -S <sub>3</sub>	S <sub>3</sub> -S <sub>4</sub>
a. <u>Short Scat tests with No 10 dB Pad</u>										
5/16/74	2	SS	2K	4.8680/ .016	5.7788/ .027	7.3300/ .023	8.6900*/ .051	10.92	15.52	13.60*
10/28/74		SS	2K	4.4715/ .030	5.5767/ .011	7.1026/ .010	8.6171/ .022	11.05	15.26	15.14
11/22/74	1	SS	10K	4.4612/ .019	5.575/ .011	7.1118/ .006	8.6685/ .034	11.14	15.37	15.57
3/13/75	1	SS	10K	4.3228/ .022	5.4388/ .009	6.9665/ .010	8.5006/ .018	11.16	15.28	15.34
6/18/75	1	SS	10K	5.0859/ .0312	6.1774/ .011	7.7476/ .009	9.2061/ .036	10.92	15.70	14.58
8/6/75	1	SS	10K	5.1402/ .032	6.2680/ .014	7.8226/ .020	9.2196/ .021	11.28	15.55	13.97
10/15/75	1	SS	10K	5.1560/ .046	6.3024/ .013	7.8207/ .009	9.3201/ .018	11.46	15.18	14.99
12/10/75	1	SS	10K	5.1150/ .025	6.2450/ .013	7.7682/ .010	9.3043/ .015	11.30	15.23	15.36
2/27/76	1	SS	10K	5.0984/ .027	6.2325/ .020	7.7429/ .009	9.2566/ .015	11.34	15.10	15.14
							Mean	11.17	15.35	15.01
							δ	.188	.197	.513
							#pts	9	9	8
b. <u>Short Scat tests with 10 dB Pad "in"</u>										
5/16/74	3	SS	2K	3.663*/ .031	4.807/ .034	6.396/ .024	7.8234/ .017	11.44*	15.89	14.27
10/28/74		SS	2K	3.4393/ .036	4.5473/ .008	-	-	11.08	-	-
11/22/74	2	SS	10K	3.4237/ .043	4.5438/ .006	-	-	11.20	-	-
3/13/75	2	SS	10K	2.5146/ .025	3.6148/ .022	5.1639/ .040	-	11.00	15.49	-
6/18/75	2	SS	10K	4.0342/ .036	5.1453/ .021	6.7224/ .012	8.1734/ .016	11.11	15.78	14.50
8/6/75	2	SS	10K	4.0939/ .023	5.2301/ .011	-	-	11.36	-	-
10/15/75	2	SS	10K	4.1425/ .033	5.2488/ .013	6.7795/ .007	-	11.06	15.31	-
12/10/75	2	SS	10K	4.1231/ .032	5.2213/ .013	-	-	10.98	-	-
2/27/76	2	SS	10K	4.0515/ .025	5.1652/ .022	6.7219/ .008	-	11.14	15.57	
							Mean	11.12	15.61	14.38
							δ	.122	.231	.163
							# pts.	8	5	2

\*Considered inaccurate - mean and δ calculation does not include.



TABLE V - Continued.

Test Date	Test No.	Mode	Range Gate	<u>Square Law Constants</u>				<u>Channel Separations</u>		
				S <sub>1</sub>	S <sub>2</sub>	S <sub>3</sub>	S <sub>4</sub>	S <sub>1</sub> -S <sub>2</sub>	S <sub>2</sub> -S <sub>3</sub>	S <sub>3</sub> -S <sub>4</sub>
c. <u>FAI tests with no 10 dB pad</u>										
6/18/75	3	FAI	10K	5.3776/ .024	6.4740/ .023	8.0358/ .019	9.5263/ .030	10.96	15.62	14.90
8/6/75	4	FAI	10K	5.4475/ .056	6.5512/ .042	-	-	11.04	-	-
10/15/75	3	FAI	10K	5.4166/ .025	6.5293/ .010	-	-	11.13	-	-
12/9/75	3	FAI	10K	5.4569/ .034	6.5277/ .010	-	-	10.71	-	-
2/27/76	3	FAI	10K	5.4166/ .021	6.4563/ .012	-	-	10.40	-	-
							Mean	10.85	-	-
							δ	.295	-	-
							# pts	5		
d. <u>FAI tests with 10 dB pad "in"</u>										
10/24/74		FAI	2K	3.7660/ .034	4.8406/ .013	-	-	10.75	-	-
11/22/74	3	FAI	10K	3.7438/ .042	4.8194/ .005	-	-	10.76	-	-
3/13/75	3	FAI	10K	3.8184/ .037	4.9068/ .026	-	-	10.88	-	-
6/18/75	No test run									
8/6/75	3	FAI	10K	4.4435/ .038	5.5324/ .010	-	-	10.99	-	-
10/15/75	4	FAI	10K	4.4219/ .040	5.5210/ .019	-	-	10.99	-	-
12/10/75	4	FAI	10K	4.4120/ .054	5.5103/ .014	-	-	10.98	-	-
2/27/76	4	FAI	10K	4.2986/ .026	5.4264/ .012	-	-	11.28	-	-
							Mean	10.95	-	-
							δ	.180	-	-
							# pts	7		

TABLE VIa. CONTINUOUS CAL DYNAMIC RANGE TESTS - PRE MISSION 230 (~April 11, 1973)

TEST	DATE	CHANNEL SEPARATION, dB			CAL ATTENUATORS, dB		
		S <sub>1</sub> -S <sub>2</sub>	S <sub>2</sub> -S <sub>3</sub>	S <sub>3</sub> -S <sub>4</sub>	A <sub>2</sub>	A <sub>3</sub>	A <sub>4</sub>
Post M218	11/20/72	17.39	16.665	18.169	13.972	26.811	44.890
Increasing	11/21/72	Sat	16.400	17.424	13.618	26.833	41.981
Decreasing	11/21/72	Sat	16.494	17.718	13.459	26.608	43.192
April Tests							
47	4/1/73	10.95	15.5	18.3	8.9	29.0	36.2
99A	4/6/73	11.14	-	-	15.12	-	-
99B	4/6/73	-	15.9	19.5	-	-	-
100	4/6/73	11.9	15.6	18.5	14.9	29.8	45.6
<u>Scat. Statistics</u>							
Pre-S <sub>1</sub> -S <sub>2</sub> change mean		17.39	16.093	18.2685	13.3282	27.8104	42.3726
dev.		-	.4928	.7207	2.2718	1.4810	3.7309
Post S <sub>1</sub> -S <sub>2</sub> change Man.		11.33					
dev.		.5027					

TABLE VIb - CONTINUOUS CAL DYNAMIC RANGE TESTS - OCTOBER 1973, 10 dB ATTENUATOR OUT

TEST	DATE	CHANNEL SEPARATION, dB			CAL ATTENUATORS, dB			
		S <sub>1</sub> -S <sub>2</sub>	S <sub>2</sub> -S <sub>3</sub>	S <sub>3</sub> -S <sub>4</sub>	A <sub>2</sub>	A <sub>3</sub>	A <sub>4</sub>	
October Tests								
10	10/5/73	11.464	15.665	12.504	14.589	30.683	50.201	
12	10/5/73	11.303	15.848	11.807	14.433	28.907	47.703	
14	10/5/73	11.284	15.551	12.165	14.734	29.488	47.626	
15 +	10/8/73	11.808	16.490	13.170	15.160	30.750	50.650	Excessive Drift
24	10/9/73	11.416	16.078	12.932	14.653	29.338	48.326	
32	10/11/73	11.352	15.670	12.430	14.360	29.540	41.530	Change in A <sub>4</sub> noted.
34	10/11/73	11.354	15.673	12.955	14.302	29.153	41.330	
35	10/11/73	11.466	15.611	12.929	14.620	29.151	41.266	
36 At + Houston	10/26/73	11.400	16.805	15.212	15.072	31.349	45.521	
<u>Scat Statistics</u>								
Pre-A <sub>4</sub> Change - Mean		11.377	15.728	12.5317	14.527	29.466	48.510	
- dev		.0734	.1790	.4412	.1626	.5810	1.465	
Post A <sub>4</sub> Change - Mean					Un- changed	Un- changed	41.375	
- Dev.							.103	

+ Data not included in Statistics

TABLE VIc - CONTINUOUS CAL DYNAMIC RANGE TESTS - OCTOBER (10 dB IF ATTENUATOR IN)

TEST	DATE	CHANNEL SEPARATION, dB			CAL ATTENUATORS, dB			
		S <sub>1</sub> -S <sub>2</sub>	S <sub>2</sub> -S <sub>3</sub>	S <sub>4</sub> -S <sub>4</sub>	A <sub>2</sub>	A <sub>3</sub>	A <sub>4</sub>	
October Tests								
10	10/5/73	11.882	16.284	11.936	15.33	30.584	-	
12	10/5/73	11.782	15.993	12.167	16.78	30.953	-	
14	10/5/73	11.771	16.013	12.090	17.217	30.710	-	
+ 15	10/8/73	11.517	15.881	12.430	17.068	31.619	-	Excess drift
25	10/9/73	11.567	15.969	13.014	16.957	31.736	-	
+ 36 Houston	10/26/73	11.500	16.125	12.971	16.733	30.938	42.670	
Scat. mean		11.750	16.0647	12.3018	16.571	30.906	-	
Statistics dev.		.1321	.1473	.4844	.8466	.5565	-	

+ Data not included in mean

TABLE VIa - CONTINUOUS CAL DYNAMIC RANGE TESTS -  $\Delta$ dB (10 dB pad out - 10 dB pad in)

TEST	DATE	$A_{1S_1}$ $\Delta$ dB	$A_{1S_2}$ $\Delta$ dB	$A_{1S_3}$ $\Delta$ dB	$A_{1S_4}$ $\Delta$ dB
October 10	10/5/73	11.877	11.459	10.840	11.408
12	10/5/73	9.522	9.043	8.898	8.538
14	10/5/73	9.610	9.123	8.661	8.736
25	10/9/73	8.584	8.433	8.537	8.460
Mean		9.8982	9.5145	9.2340	9.2855
Var.		1.9558	1.7754	1.1688	2.0157
Stand. Dev.		1.3985	1.3324	1.0811	1.4198

TABLE VIe - CONTINUOUS CAL DYNAMIC RANGE TESTS - ON C-130 A/C  
 USING 300 MHz COAXIAL ATTENUATOR

TEST	DATE	CHANNEL SEPARATION, dB			CAL ATTENUATORS, dB		
		S <sub>1</sub> -S <sub>2</sub>	S <sub>2</sub> -S <sub>3</sub>	S <sub>3</sub> -S <sub>4</sub>	A <sub>2</sub>	A <sub>3</sub>	A <sub>4</sub>
26	10.9/73	11.1	15.720	12.35	15.207	31.0	48.214
40 Houston	10/26/73	11.1	14.314	11.563	15.253	29.944	40.157
43 Houston	10/10/73	10.8	15.458	12.302	15.519	30.838	42.811
Scat statistics							
	Mean	11.0	15.164	12.0717	15.3263	30.594	43.7273
	dev.	.1732	.7477	.4412	.1684	.5687	4.1059

TABLE VII - CONTINUOUS CALIBRATION TESTS

a. 10 dB Pad Out

TEST	DATE	A <sub>1</sub> VALUES							CHANNEL SEPARATION			CAL ATTENUATORS		
		S <sub>1</sub>	S <sub>2</sub>	S <sub>3</sub>	S <sub>4</sub>	A <sub>2</sub> S <sub>2</sub>	A <sub>3</sub> S <sub>3</sub>	A <sub>4</sub> S <sub>4</sub>	S <sub>1</sub> -S <sub>2</sub>	S <sub>2</sub> -S <sub>3</sub>	S <sub>3</sub> -S <sub>4</sub>	A <sub>2</sub>	A <sub>3</sub>	A <sub>4</sub>
a. Continuous Cal Tests - No 10 dB rad														
4	5/29/74	4.1586/ .012	5.339/ .017	6.9054/ .016	8.3697/ .017	3.7577/ .051	3.6125/ .017	3.7392/ .015	11.80	15.70	14.64	15.81	32.94	46.30
9	5/30/74	4.107/ .020	5.2846/ .009	6.8507/ .027	8.3301/ .030	3.7650/ .036	3.4985/ .627	3.6951/ .023	11.78	15.66	14.79	16.10	33.52	46.35
-	10/28/74	3.9596/ .025	5.0836/ .016	6.6145/ .010	8.1199/ .022	3.6751* .115	3.3661/ .028	3.7088/ .028	11.24	15.31	15.05	14.08*	32.48	44.11
4A	11/22/74	3.9434/ .013	5.0757/ .0135	6.6130/ .010	8.1201/ .022	3.5293* .129	3.3557/ .013	3.6991/ .018	11.32	15.37	15.07	15.46*	32.57	44.21
4	3/13/75	4.1346/ .012	5.2634/ .014	6.8152/ .020	8.3833/ .031	3.8103* .051	3.4527/ .029	3.7557/ .026	11.29	15.52	15.68	14.53*	33.62	46.28
4	6/18/75	4.6562/ .033	5.7923/ .009	7.3675/ .008	8.8109/ .023	4.1956/ .015	4.0630/ .031	4.3575/ .021	11.36	15.75	14.43	15.97	33.04	44.53
5	8/6/75	4.7581/ .019	5.8888/ .0175	7.4749/ .014	8.8804/ .023	4.2768/ .018	4.1774/ .0306	4.4899/ .012	11.31	15.86	14.06	16.12	32.98	43.90
5B	10/15/75	4.7060/ .033	5.8365/ .019	7.3464/ .041	8.8706/ .0084	4.2077/ .024	4.0226/ .024	4.3964/ .019	11.30	15.10	15.24	16.29	33.24	44.74
5	12/9-10/75	4.6848/ .025	5.8487/ .013	7.3794/ .0095	8.9241/ .015	4.3098/ .021	4.2980/ .018	4.7856/ .024	11.64	15.31	15.45	15.39*	30.81*	41.39*
5	2/27/76	4.6132/ .018	5.7697/ .027	7.3013/ .018	8.8300/ .013	4.1029/ .021	3.9460/ .026	4.3103/ .029	11.56	15.32	15.29	16.67	33.53	45.20
								Mean	11.46	15.49	14.97	16.16	33.10	45.07
								δ	.215	.245	.493	.297	.412	1.00
								# Pts	10	10	10	6	9	9

51

## (b) 10 dB Pad in

TEST DATE	A <sub>1</sub> VALUES							CHANNEL SEPARATION			CAL ATTENUATORS		
	S <sub>1</sub>	S <sub>2</sub>	S <sub>3</sub>	S <sub>4</sub>	A <sub>2</sub> S <sub>2</sub>	A <sub>3</sub> S <sub>3</sub>	A <sub>4</sub> S <sub>4</sub>	S <sub>1</sub> -S <sub>2</sub>	S <sub>2</sub> -S <sub>3</sub>	S <sub>3</sub> -S <sub>4</sub>	A <sub>2</sub>	A <sub>3</sub>	A <sub>4</sub>
b. Continuous Cal tests 10 dB pad "in"													
5 5/29/74	3.064/ .034	4.2602/ .022	5.8882/ .007	7.3384/ .041	2.306* 1 pt	2.509* 3 pt	2.6692* 2 pt	11.96	16.28	14.51	-	33.79*	48.88*
8 5/30/74	3.0308/ .019	4.2207/ .008	5.8153/ .011	7.3281/ .017	2.324* 2 pt	-	2.5801* .017 3 pt	11.90	15.94	15.13	-	-	46.68*
- 10/28/74	2.9666/ .027	4.0701/ .024	5.5850/ .008	7.100/ .012	2.5767/ .039	2.3240/ .020	2.6304/ .001	11.04	15.15	15.15	14.93	32.61	44.70
5A 11/22/74	2.9430/ .009	4.0560/ .020	5.5759/ .018	7.0831/ .027	2.5201/ .031	2.2692/ .014	2.6265/ .013	11.13	15.20	15.07	15.36	33.07	44.57
5 3/13/75	3.0743/ .025	4.2199/ .0214	5.7668/ .022	7.2737/ .045	2.4982* .031	2.3155* .021	3.1891* .100	11.46	15.47	15.07	17.22*	34.51*	40.85*
						2 pt							
5 6/18/75	3.6475/ .038	4.7548/ .026	6.3415/ .039	7.7981/ .006	3.1265/ .022	2.9810/ .026	3.3089* .043	11.07	15.87	14.57	16.28	33.60	44.89*
6 8/6/75	3.7191/ .025	4.8438/ .018	6.4690/ .010	7.8840/ .021	3.1660/ .032	3.0454/ .035	3.4038* .046	11.25	16.25	14.15	16.78	34.24	44.80*
6A 10/15/75	3.6383* .058	4.7888/ .051	6.3649/ .026	7.8258/ .093	3.1432* .01	2.9369/ .038	3.3208/ .039	11.50*	15.76	14.61	16.46*	34.28	45.05
6A 12/9-10/75	3.6459/ .024	4.8001/ .011	6.3435/ .026	7.8468/ .010	3.2115/ .021	3.2033/ .017	3.7035/ .019	11.54	15.43	15.04	15.89*	31.40*	41.43*
6A 2/27/76	3.5919/ .013	4.7165/ .010	6.2395/ .025	7.7295/ .009	3.0221/ .025	2.8412/ .018	3.1077/ .033	11.25	15.23	14.90	16.94	33.98	46.22
							Mean	11.40	15.67	14.82	16.06	33.63	45.07
							δ	.343	.423	.339	.881	.674	.668
							# pts	9	10	10	5	6	5

\*Data considered inaccurate - not included in mean and δ





TABLE IX. RADIOMETER PARAMETERS (RPAR)

RPAR Item	Parameter	Symbol	Units	Mission 203(6/72) Mission 207(7/72) Mission 218(10/72)	Mission 230(4/73) and all subsequent *2 missions	RPAR Item	Parameter	Symbol	Units	Mission 203 (6/72) Mission 207 (7/72) Mission 218 (10/72)	Mission 230 (4/73) and all subsequent *2 missions
1	Frequency		GHz	13.9 9.3 *1	13.9	41	Thermal conversion constant	$\beta_6$	$^{\circ}\text{C/volts}$	-5.0174	↑ SAME AS M203 ↓
2	Feed	WG/CIRC		WG	WG	42		$\delta_6$	$^{\circ}\text{C}$	68.434	
3	Aleas. int. time	$\tau$		.128	.128	43		$\alpha_7$	$^{\circ}\text{C/volt}^2$	-1.9433	
4	Cal. int. time			.100	.100	44		$\beta_7$	$^{\circ}\text{C/volt}$	-6.6046	
5	Hot load sens. fac.	$C_6$		1.4123	1.2987	45		$\delta_7$	$^{\circ}\text{C}$	73.272	
6	Warm load factor	$C_5$		1.4367	1.3214	46		$\alpha_8$	$^{\circ}\text{C/volt}^2$	-1.6239	
7	Hot load trip. factor	$C_7$		.0241	.0221	47		$\beta_8$	$^{\circ}\text{C/volt}$	-6.8896	
8	Cutler feed bias	$C_{3H}$		0	.0555	48		$\delta_8$	$^{\circ}\text{C}$	74.288	
9	Cutler feed bias	$C_{3V}$		0	.0509	49		$\alpha_9$	$^{\circ}\text{C/volt}^2$	-1.6973	
10	OMT bias constant	$C_{1H}$		0	.0354	50		$\beta_9$	$^{\circ}\text{C/volt}$	-6.7432	
11	OMT bias constant	$C_{1V}$		0	0	51		$\delta_9$	$^{\circ}\text{C}$	73.286	
12	Pol sw bias constant	$C_{2H}$		0	.0211	52		$\alpha_{10}$	$^{\circ}\text{C/volt}^2$	-1.9238	
13	Pol sw bias constant	$C_{2V}$		0	.0152	53		$\beta_{10}$	$^{\circ}\text{C/volt}$	-6.4966	
14	Input guide bias	$C_8$		.0569	.1758	54		$\delta_{10}$	$^{\circ}\text{C}$	73.169	
15	T/R circ. bias	$C_4$		.3458	.0583	55		$\alpha_{11}$	$^{\circ}\text{C/volt}^2$	-2.23561	
16	Input trip. bias	$C_9$		.0232	.0305	56		$\beta_{11}$	$^{\circ}\text{C/volt}$	-6.1276	
17	Hot load bias	$C_{11}$		.6975	.6365	57		$\delta_{11}$	$^{\circ}\text{C}$	72.957	
18	Warm load bias	$C_{12}$		.7094	.6476	58		$\alpha_{12}$	$^{\circ}\text{C/volt}^2$	-1.13609	
19	Load trip. bias	$C_{10}$		.0364	0	59		$\beta_{12}$	$^{\circ}\text{C/volt}$	-7.1465	
20	Resid. trip. bias	$C_{13}$	K	.0232	0	60		$\delta_{12}$	$^{\circ}\text{C}$	73.386	
21	- Empty					61		$\alpha_{13}$	$^{\circ}\text{C/volt}^2$	-1.5235	
22	- Empty					62		$\beta_{13}$	$^{\circ}\text{C/volt}$	-6.9673	
23	Upper temp. limit		K	325	↑ SAME AS M203 ↓	63		$\delta_{13}$	$^{\circ}\text{C}$	74.459	
24	Lower temp. limit		K	285		64		$\alpha_{14}$	$^{\circ}\text{C/volt}^2$	-1.6745	
25	Thermal conversion constant	$\alpha_1$	$^{\circ}\text{C/volt}^2$	-24134		65		$\beta_{14}$	$^{\circ}\text{C/volt}$	-6.8462	
26		$\beta_1$	$^{\circ}\text{C/volt}$	-6.0348		66		$\delta_{14}$	$^{\circ}\text{C}$	73.607	
27		$\delta_1$	$^{\circ}\text{C}$	72.431		67		$\alpha_{15}$	$^{\circ}\text{C/volt}^2$	-1.8563	
28		$\alpha_2$	$^{\circ}\text{C/volts}^2$	-1.2338		68		$\beta_{15}$	$^{\circ}\text{C/volt}$	-6.5839	
29		$\beta_2$	$^{\circ}\text{C/volt}$	-7.3562		69		$\delta_{15}$	$^{\circ}\text{C}$	73.031	
30		$\delta_2$	$^{\circ}\text{C}$	75.684		70		$\alpha_{16}$	$^{\circ}\text{C/volt}^2$	-2.0172	
31		$\alpha_3$	$^{\circ}\text{C/volt}^2$	-1.13344		71		$\beta_{16}$	$^{\circ}\text{C/volt}$	-6.1414	
32		$\beta_3$	$^{\circ}\text{C/volt}$	-7.2283		72		$\delta_{16}$	$^{\circ}\text{C}$	70.321	
33		$\delta_3$	$^{\circ}\text{C}$	74.620	73	Hot load conv. factor	$\alpha_{17}$	$^{\circ}\text{C/volt}^2$	0	2.672	
34		$\alpha_4$	$^{\circ}\text{C/volt}^2$	-1.14290	74		$\beta_{17}$	$^{\circ}\text{C/volt}$	1.0000	-35.689 *3	
35		$\beta_4$	$^{\circ}\text{C/volts}$	-7.0632	75		$\delta_{17}$	$^{\circ}\text{C}$	-273.18	222.419	
36		$\delta_4$	$^{\circ}\text{C}$	73.578							
37		$\alpha_5$	$^{\circ}\text{C/volts}^2$	-1.14648							
38		$\beta_5$	$^{\circ}\text{C/volt}$	-7.0404							
39		$\delta_5$	$^{\circ}\text{C}$	74.520							
40		$\alpha_6$	$^{\circ}\text{C/volts}^2$	-32135							

\*1 9.3 GHz not used after Mission 230

\*2 Exception - The previous values for RPAR items 1 thru 20 were used on the following flights:

Mission 247 - All flights except 37

Mission 258 - Flights 40 and 41

\*3 These parameters used on Mission 288 (Copenhagen - Nov. 74) and subsequent missions only.

TABLE X. SUMMARY OF RADIOMETER CALIBRATION RESULTS

<u>Date</u>	<u>Baseplate Temp.</u>	<u>T<sub>IN</sub> (Model)</u>	<u>T<sub>IN</sub> (Regression)</u>
10-18-72	96°F	$T_{IN} = \xi[-137.96] + 379.93$	$T_{IN} = \xi[-144.98] + 373.04$
3-26-73	AMBIENT (75°F)	$T_{IN} = \xi[-155.15] + 389.31$	$T_{IN} = \xi[-149.48] + 362.25$
3-27-73	96°F	$T_{IN} = \xi[-136.06] + 387.15$	$T_{IN} = \xi[-135.69] + 373.88$
10-2-73	96°F	$T_{IN} = \xi[-132.33] + 378.71$	$T_{IN} = \xi[-128.61] + 377.26$

TABLE XI. VTR/Actual Temperature Correlation Data

VTR Reference Temperatures			"Actual" Radiometric Temperature, K	Test Ref.
T <sub>L</sub> , K	T <sub>W</sub> , K	T <sub>WG</sub> , K		
38.7	208.8	294.7	58.557	Tape No. 3
78.3	211.0	294.6	94.420	
80.3	212.0	294.7	96.284	
138.0	228.8	295.3	149.530	
140.0	232.1	295.5	151.477	
142.1	234.1	295.8	153.475	
220.1	265.0	296.9	228.601	
300.0	298.5	298.4	303.382	
100.0	221.2	297.2	114.704	Tape No. 4
100.0	220.0	296.2	114.61	Tape No. 12

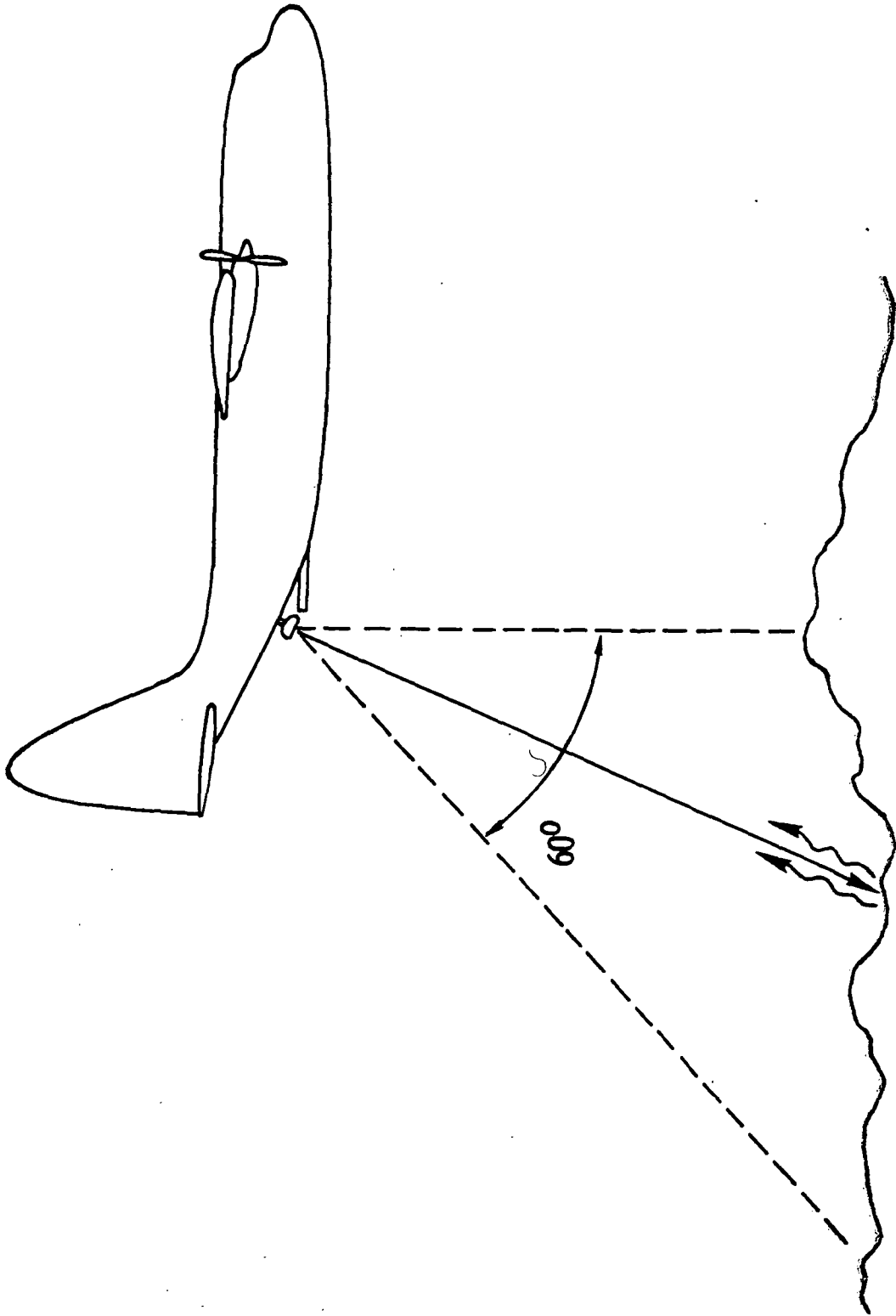
TABLE XII. Radiometer Correlation

Test No.	Rad Mean	V <sub>BL</sub> Mean	σ Volts	σ K	$T(K) = \left( \frac{10.0 - (V_D - V_{BL})}{0.026434} \right)$
4	7.017	+0.160	0.0321	1.21	118.9
42	6.805	-0.149	0.029	1.10	115.23

TABLE XIII. Coefficients of Thermistor Voltage-Temperature Conversion Equations, Obtained From Second Order Regression Fit.

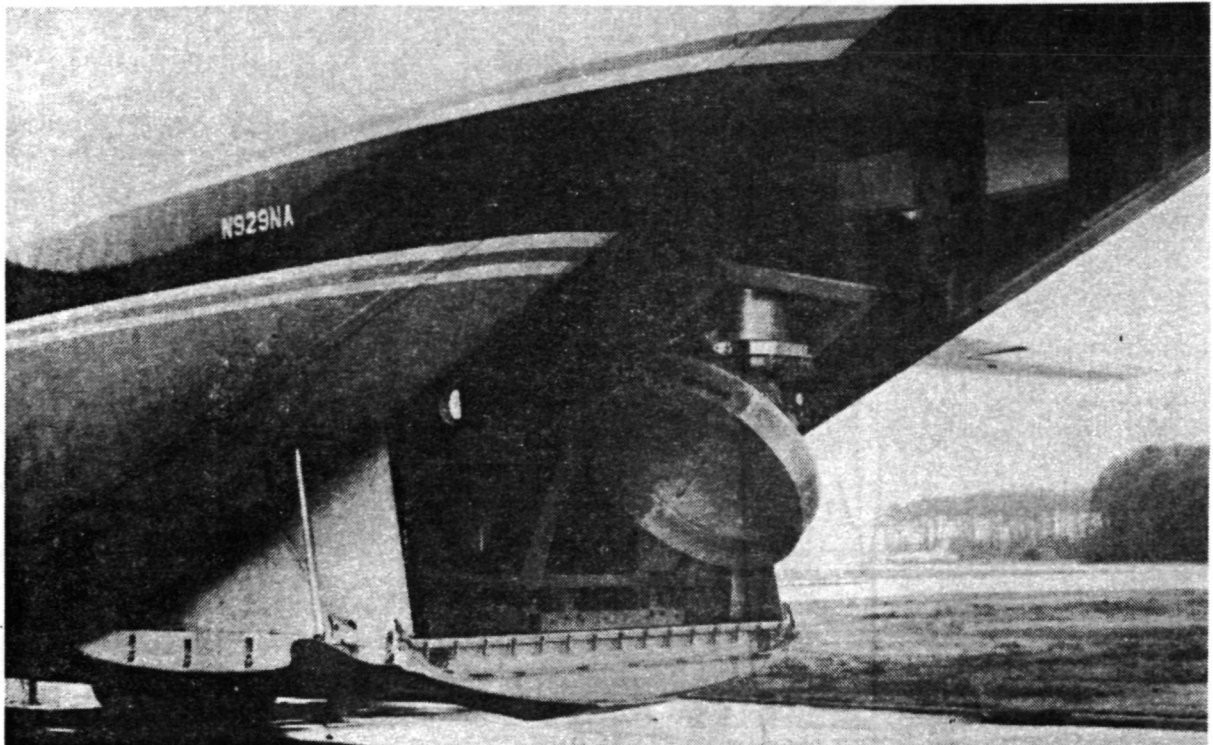
$$\text{Form of equation } \text{Temp}(^{\circ}\text{C}) = b_0 + b_1(\text{TM Voltage}) + b_2(\text{TM Voltage})^2$$

<u>Thermistor</u>	<u>b<sub>0</sub></u>	<u>b<sub>1</sub></u>	<u>b<sub>2</sub></u>
1	72.43083	-6.03483	-.24134
2	75.68447	-7.35625	-.12338
3	74.61968	-7.22831	-.13344
4	73.57793	-7.06315	-.14290
5	74.51987	-7.04041	-.14648
6	68.43424	-5.01740	-.32135
7	73.27249	-6.60464	-.19433
8	74.28770	-6.88957	-.16239
9	73.28622	-6.74318	-.16973
10	73.16915	-6.49663	-.19238
11	72.95750	-6.12759	-.23561
12	73.38603	-7.14653	-.13609
13	74.45938	-6.96731	-.15235
14	73.60741	-6.84623	-.16745
15	73.03071	-6.58393	-.18563
16	70.32149	-6.14136	-.20172
19	89.58324	-5.57183	0.02318
23	89.58324	-5.57183	0.02318
24	222.41936	-35.68917	2.67179

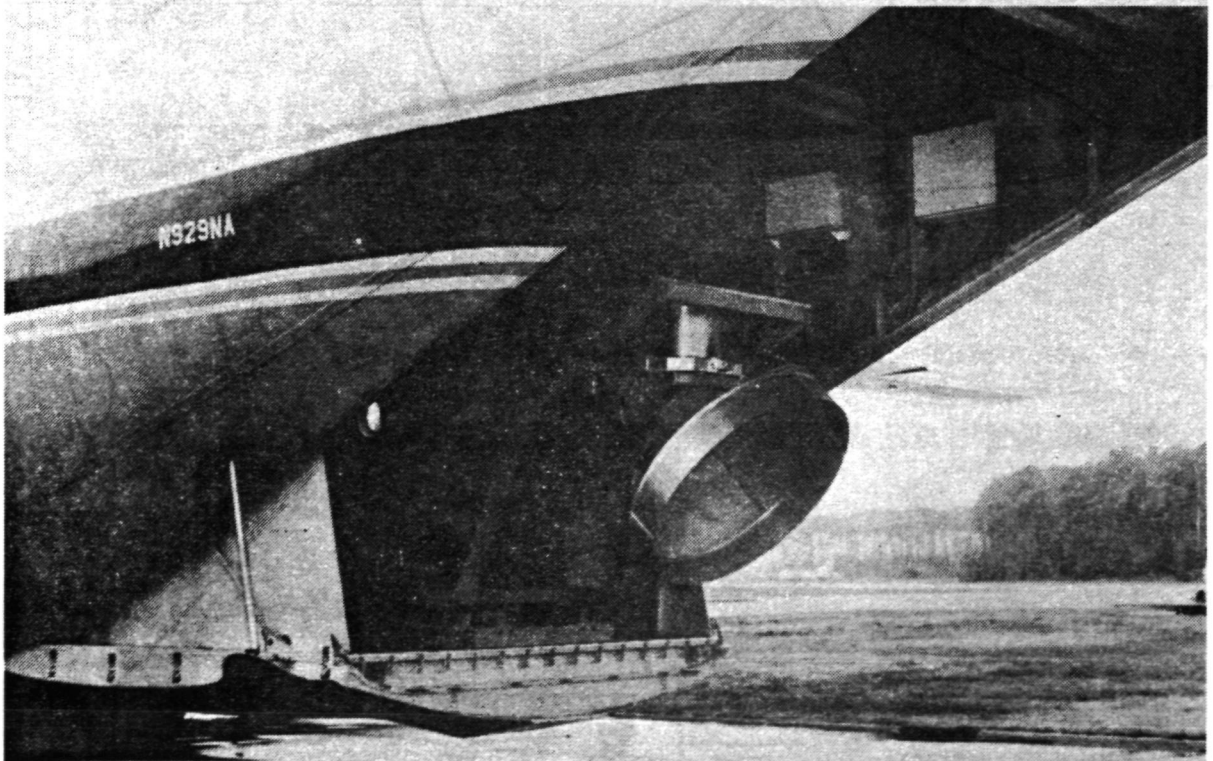


(a). - Conceptual view.

Figure 1. - AAFE RADSCAT in operation on a C-130 aircraft.



(b). - RADSCAT on aircraft in side-scanning configuration.



(c). - RADSCAT on aircraft in aft-scanning configuration.

Figure 1. - (Concluded).

ORIGINAL PAGE IS  
OF POOR QUALITY

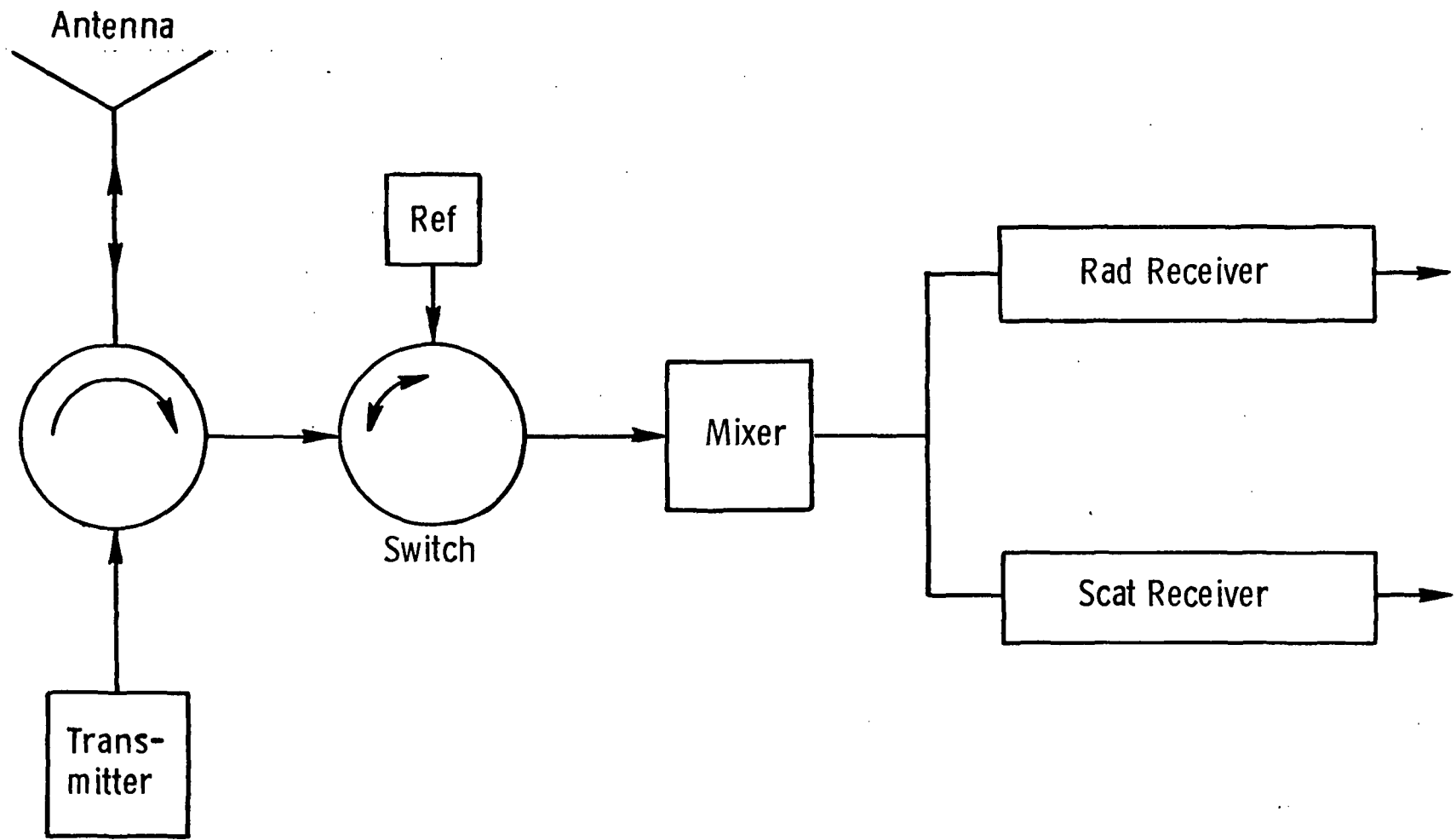


Figure 2. - Simplified Block Diagram of RADSCAT.



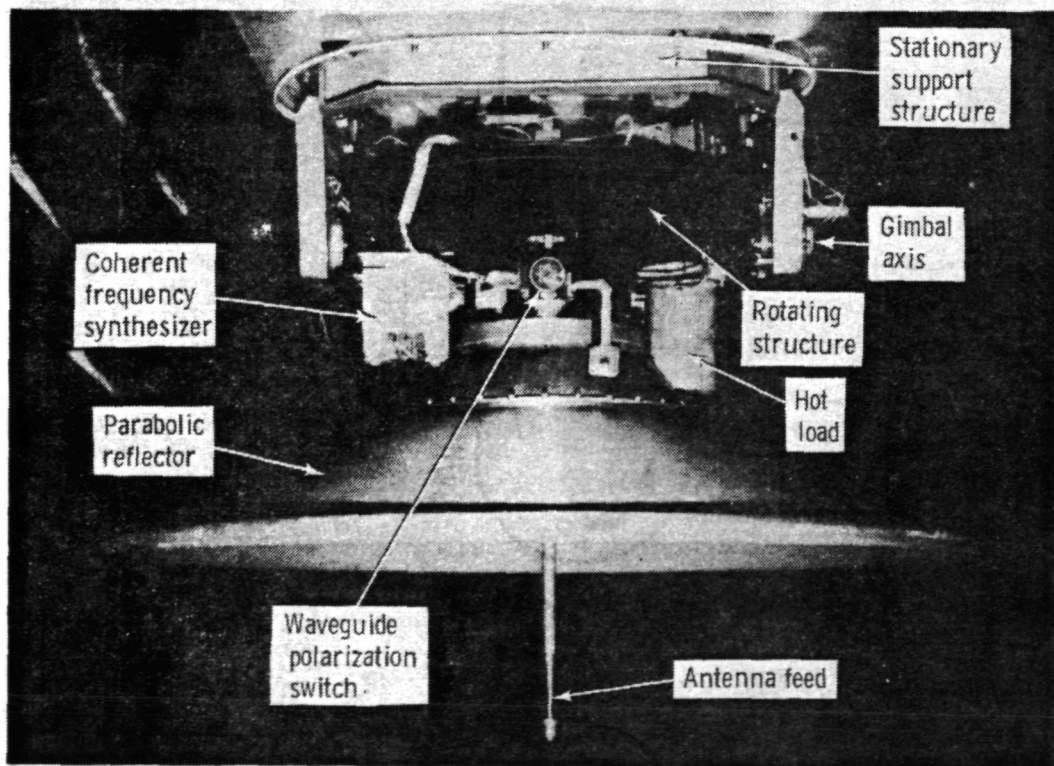
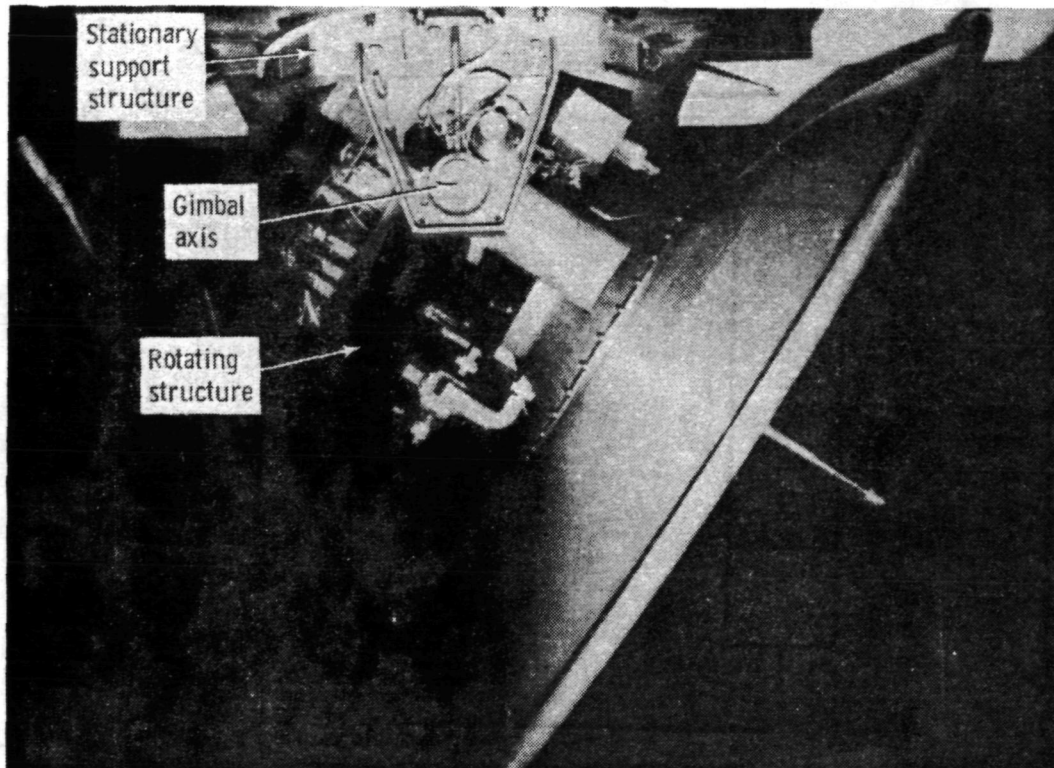


Figure 3. - The antenna gimballed platform - two views.

ORIGINAL PAGE IS  
OF POOR QUALITY

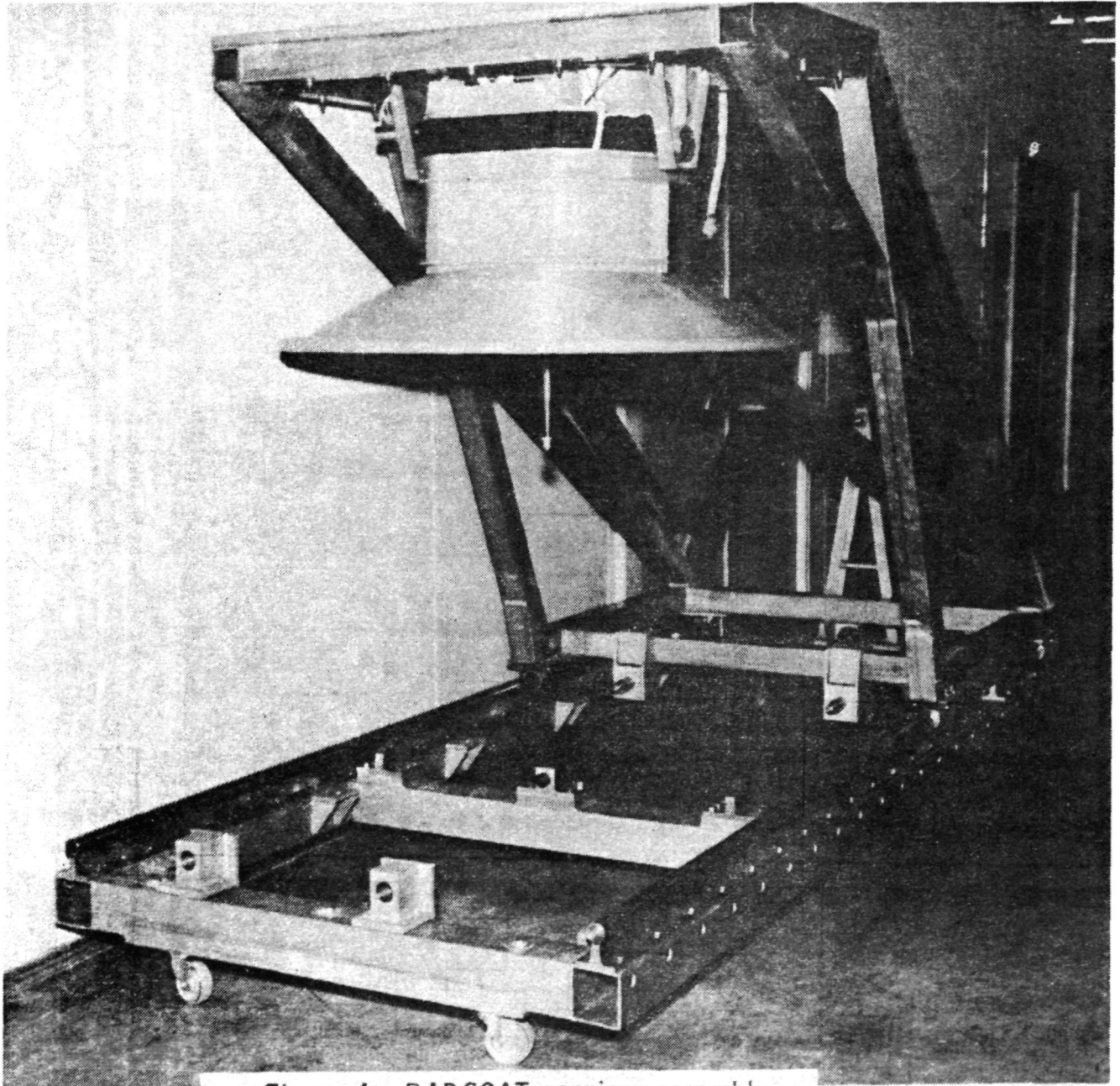


Figure 4. - RADSCAT carriage assembly.

ORIGINAL PAGE IS  
OF POOR QUALITY

ORIGINAL PAGE IS  
OF POOR QUALITY

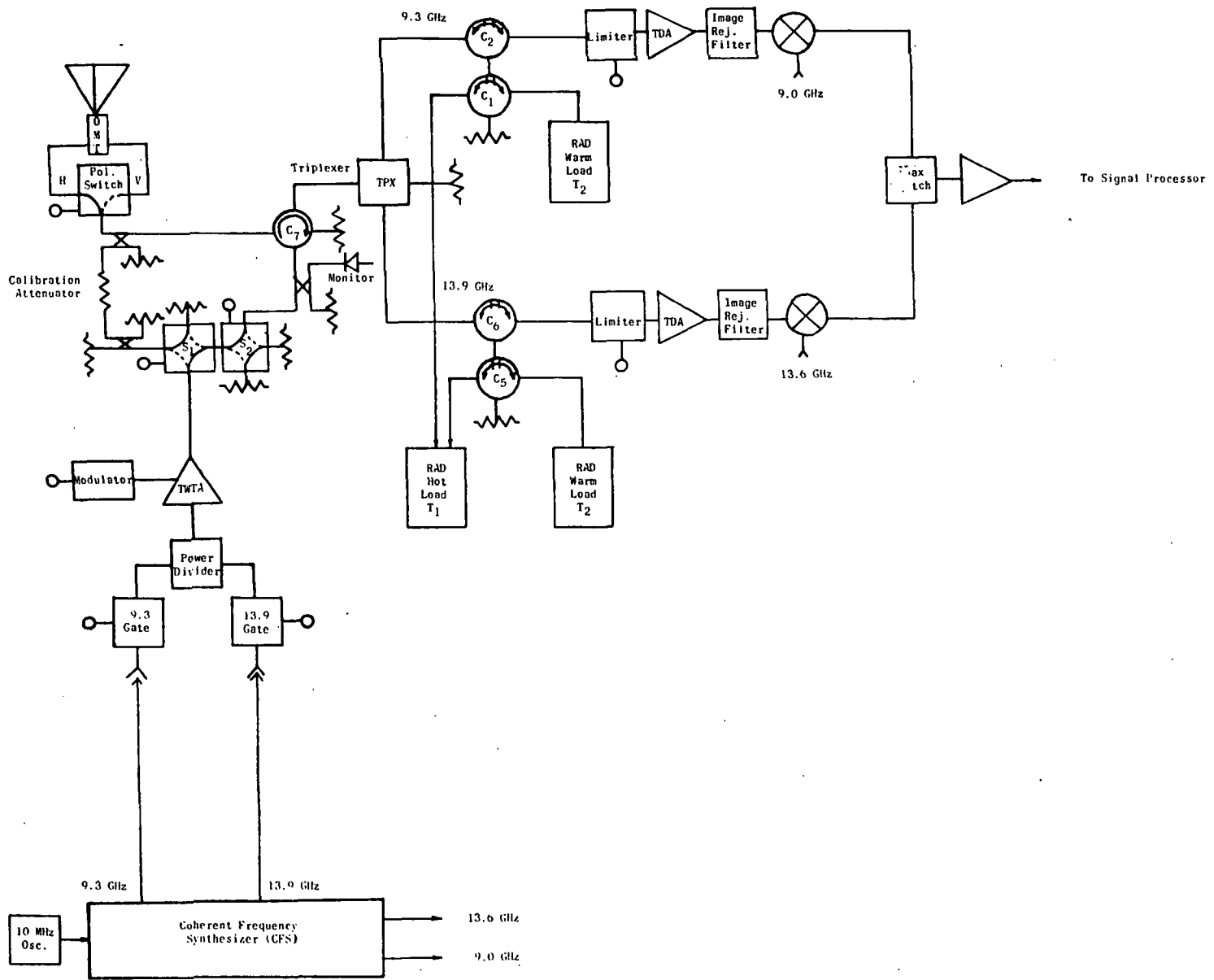


Figure 5. RADSCAT RF system block diagram (antenna-mounted equipment).

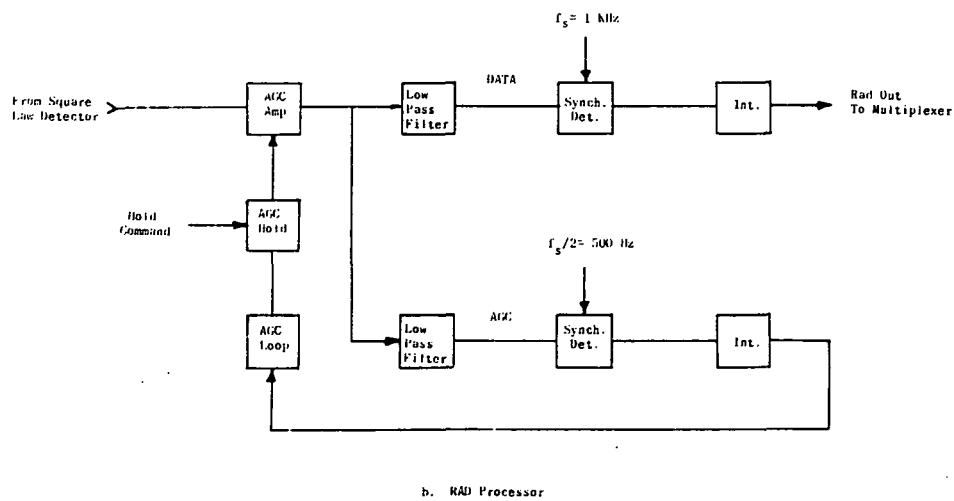
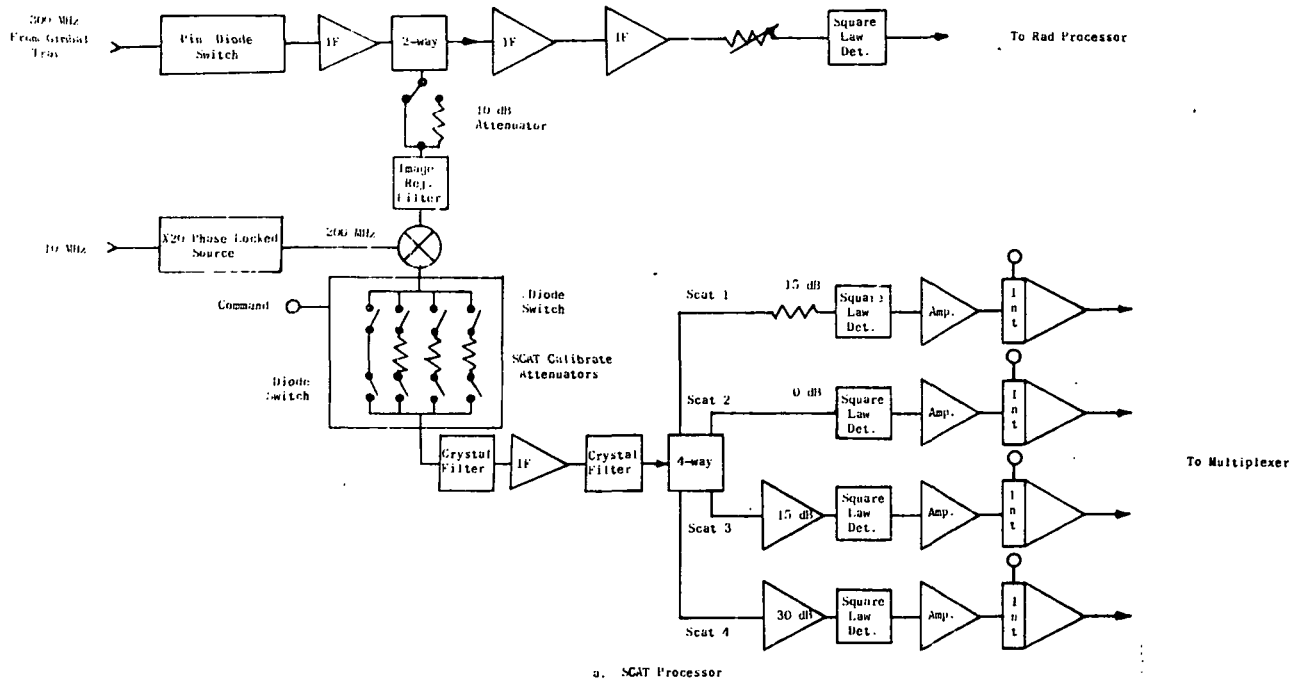


Figure 6. - RADSCAT signal processor block diagram.

ORIGINAL PAGE IS  
OF POOR QUALITY

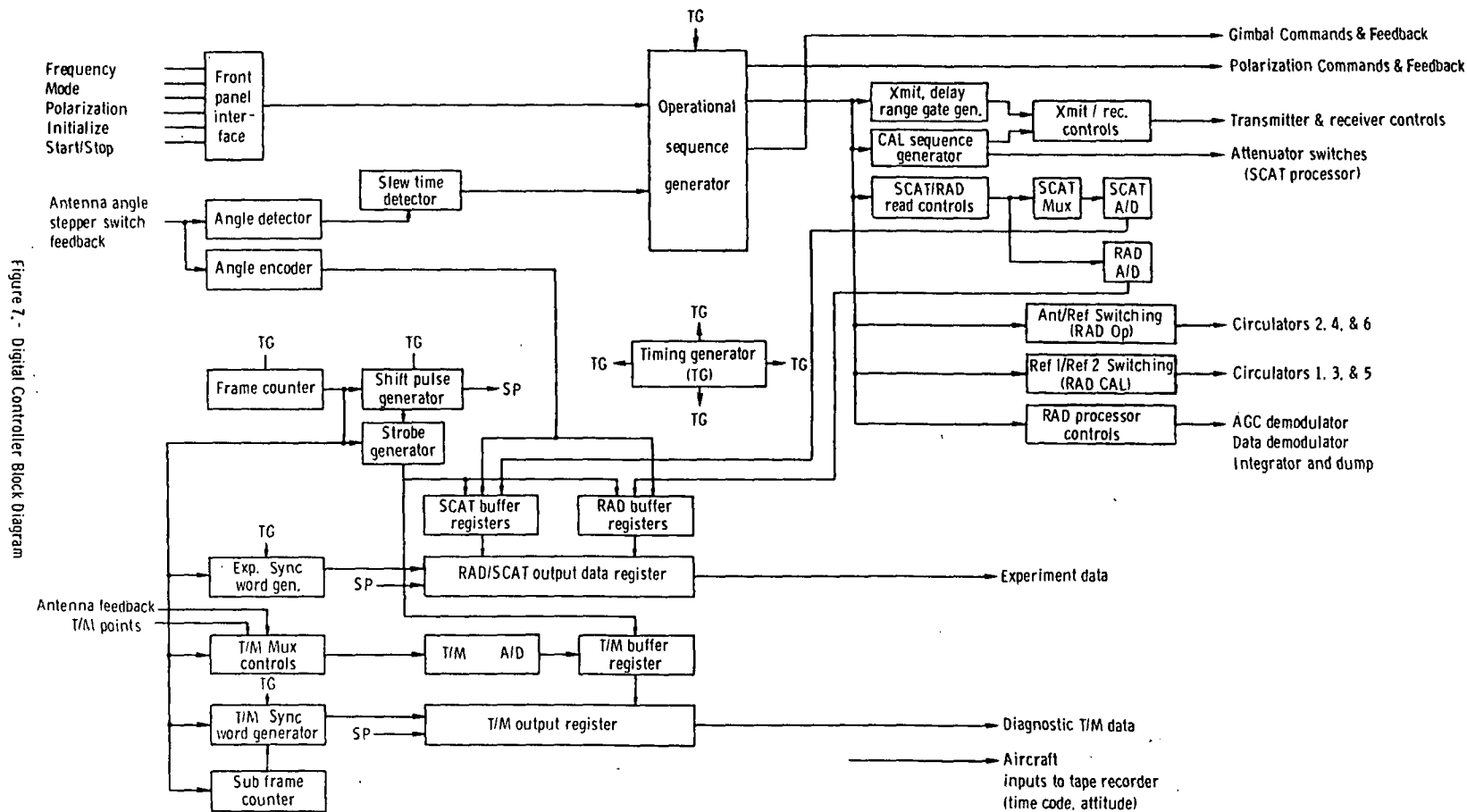


Figure 7 - Digital Controller Block Diagram

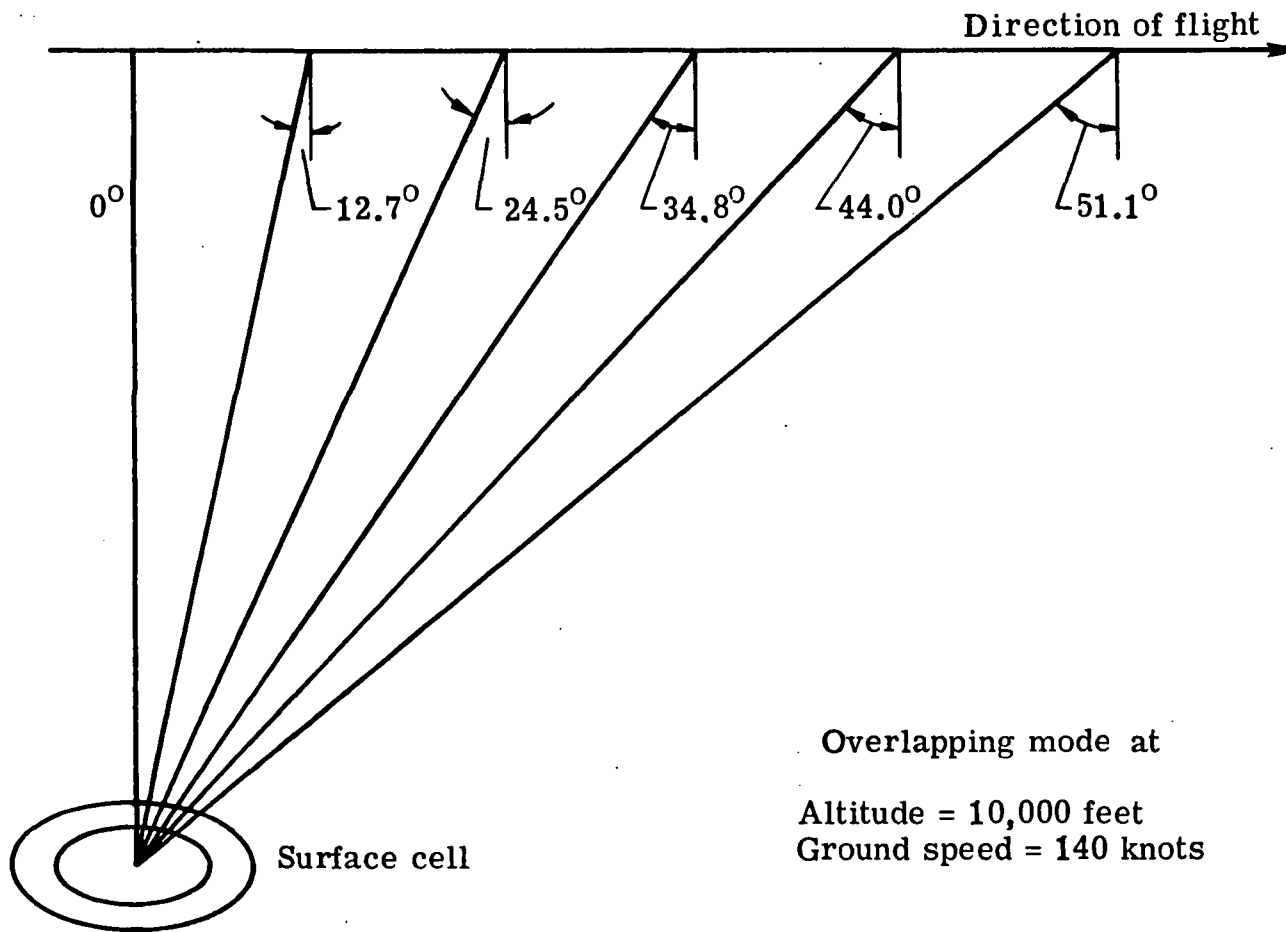


Figure 8.- RADSCAT Alternating Angle Mode Scan Pattern

ORIGINAL PAGE IS  
OF POOR QUALITY

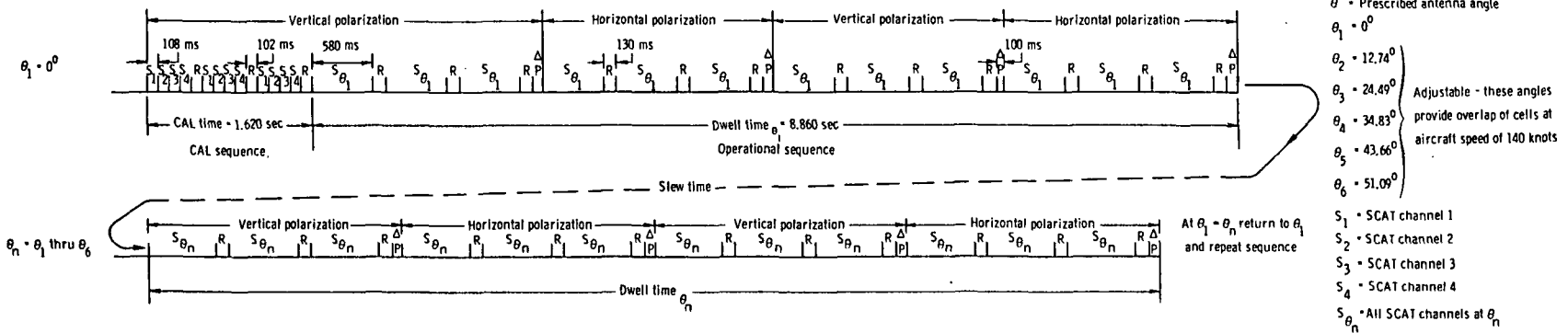


Figure 9.- Alternate Scan Angle Mode

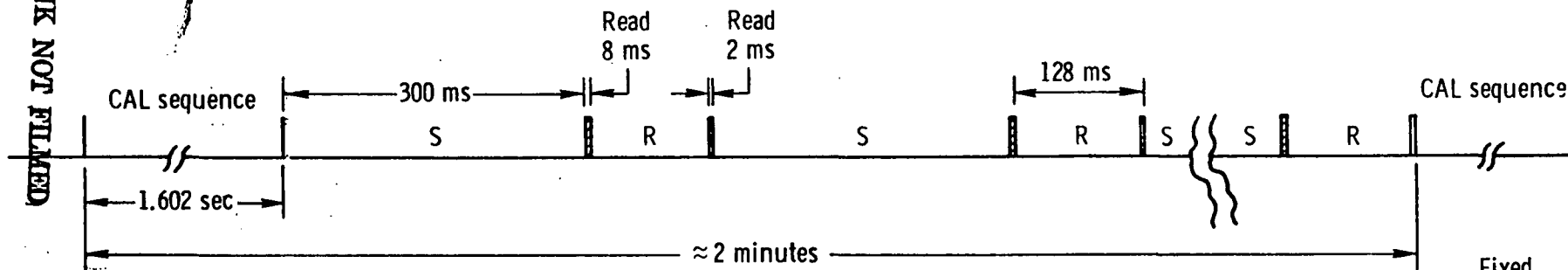


Figure 10.- Fixed Scan Angle Mode - Short Scat Option

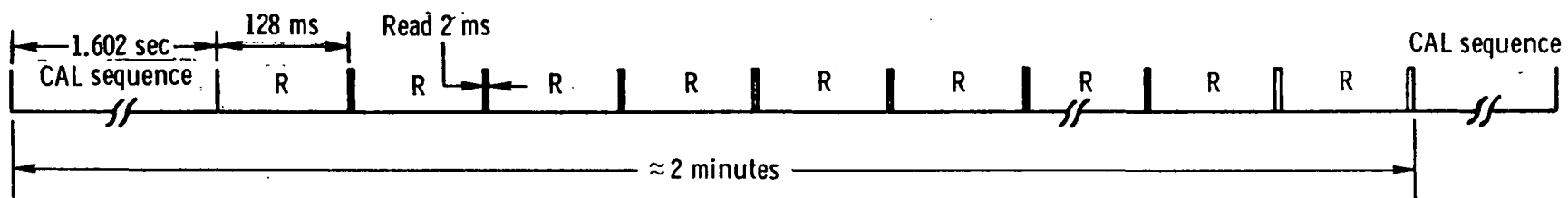
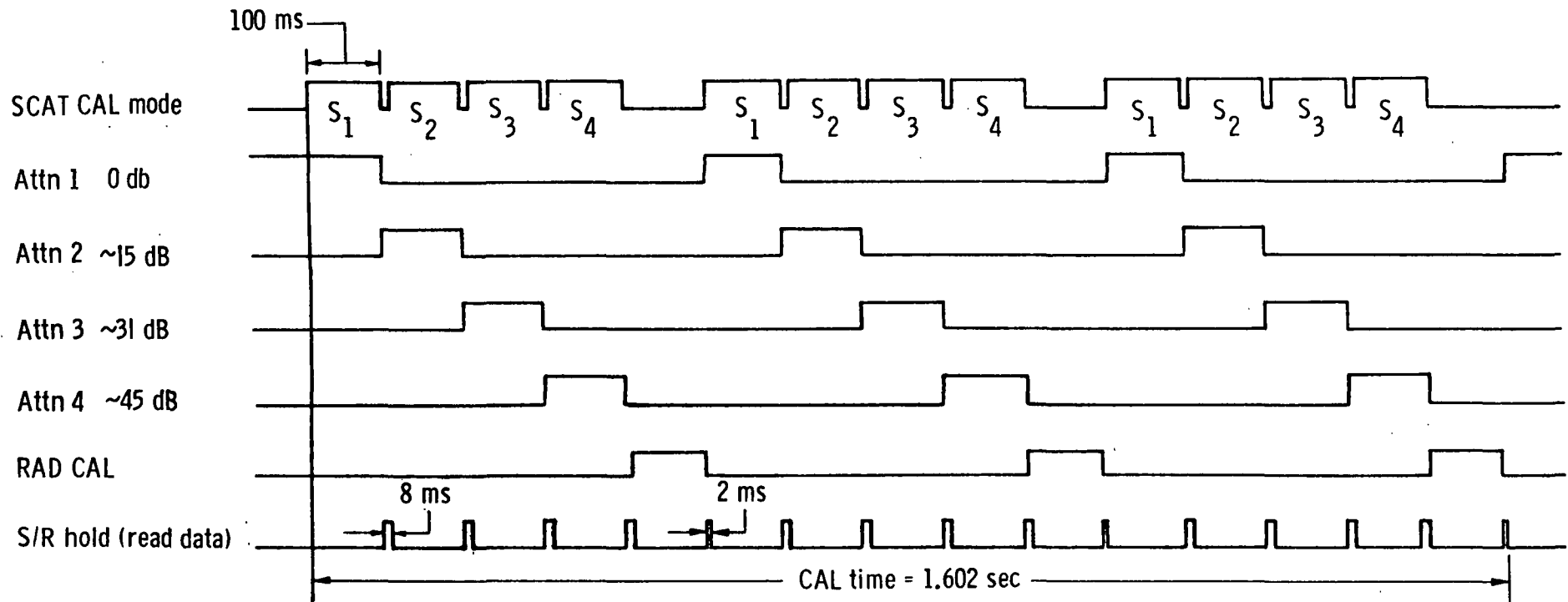


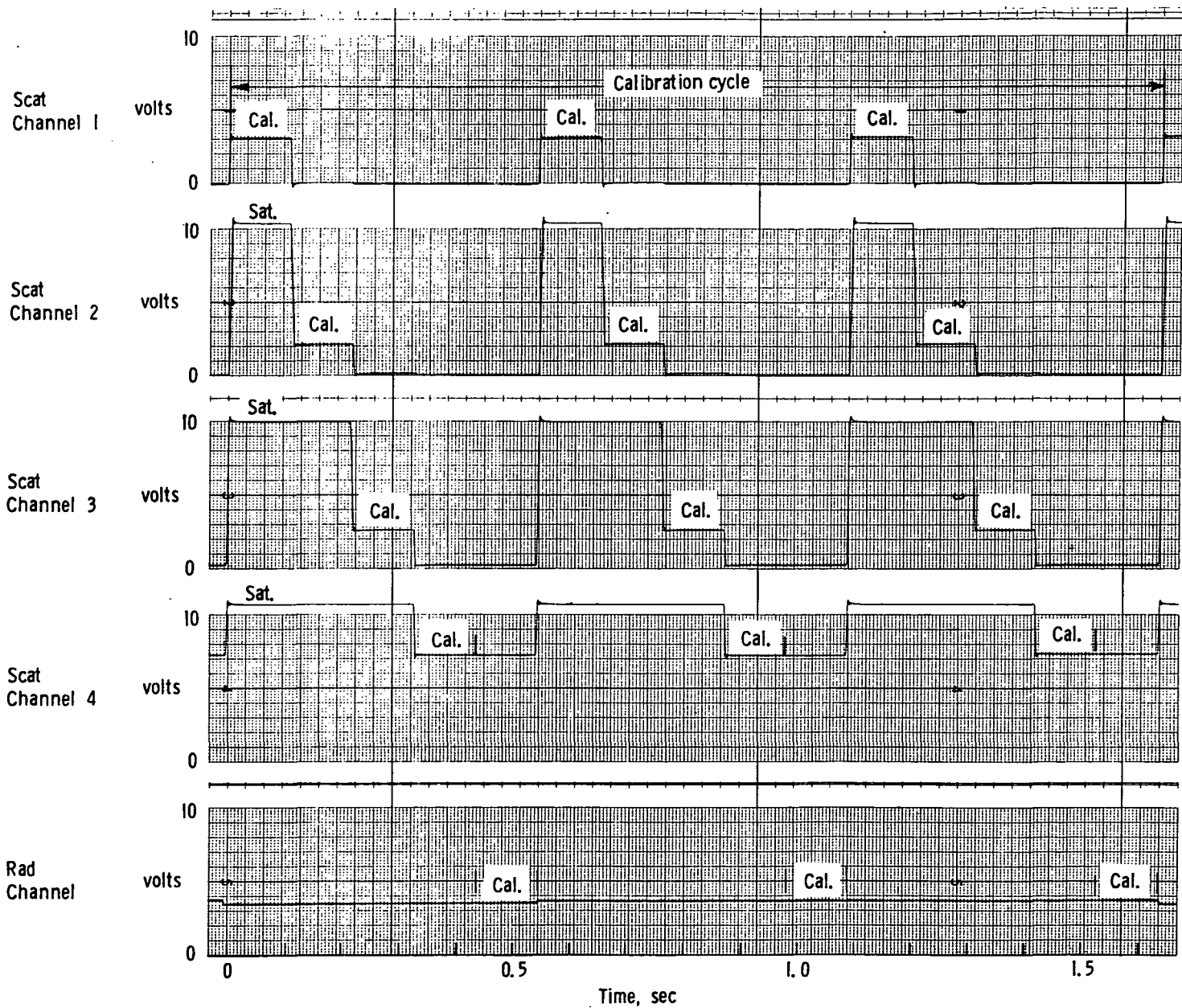
Figure 11.- Fixed Scan Angle Mode - Rad Only Option





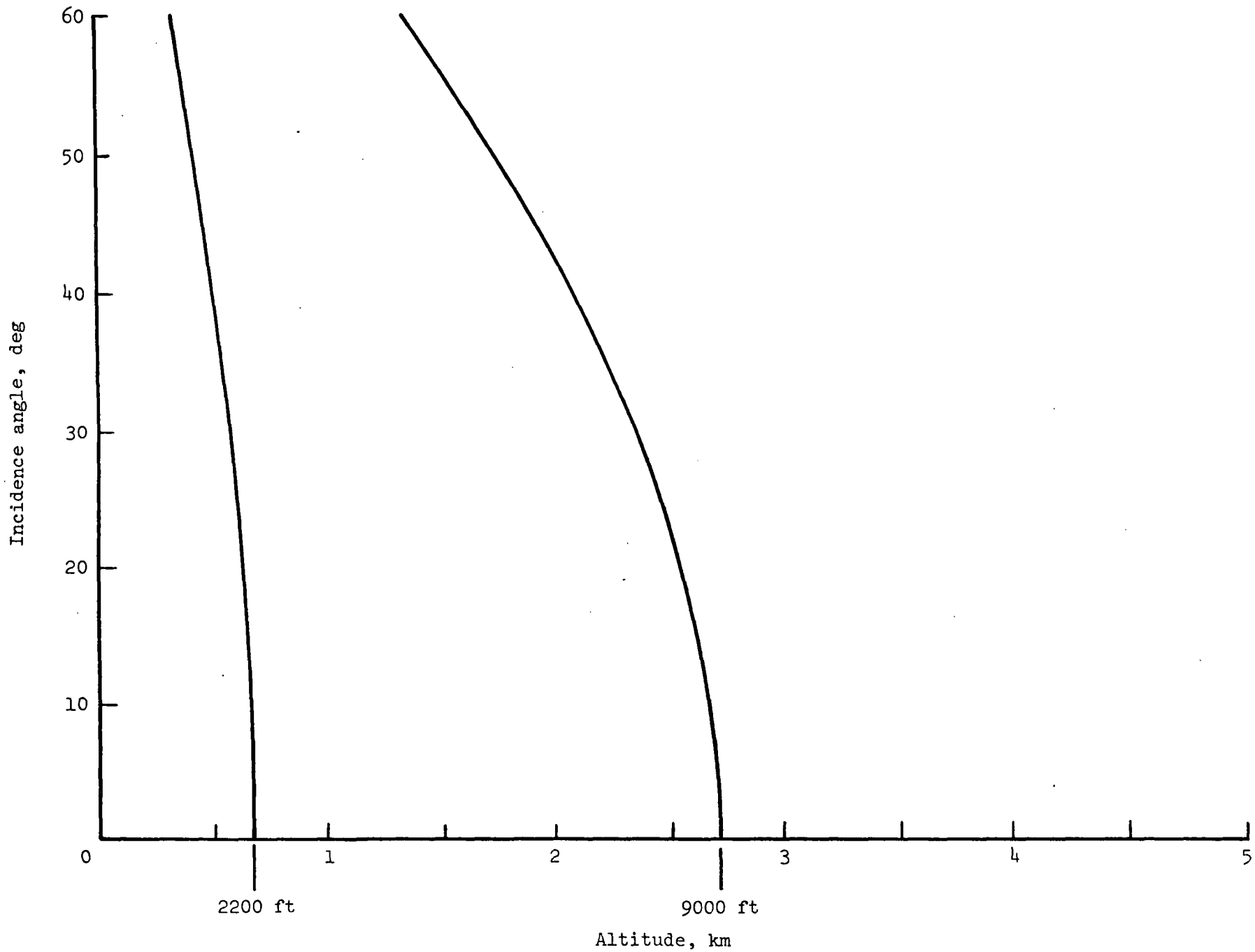
(a) Calibration Sequence

Figure I2. - Regular Calibration



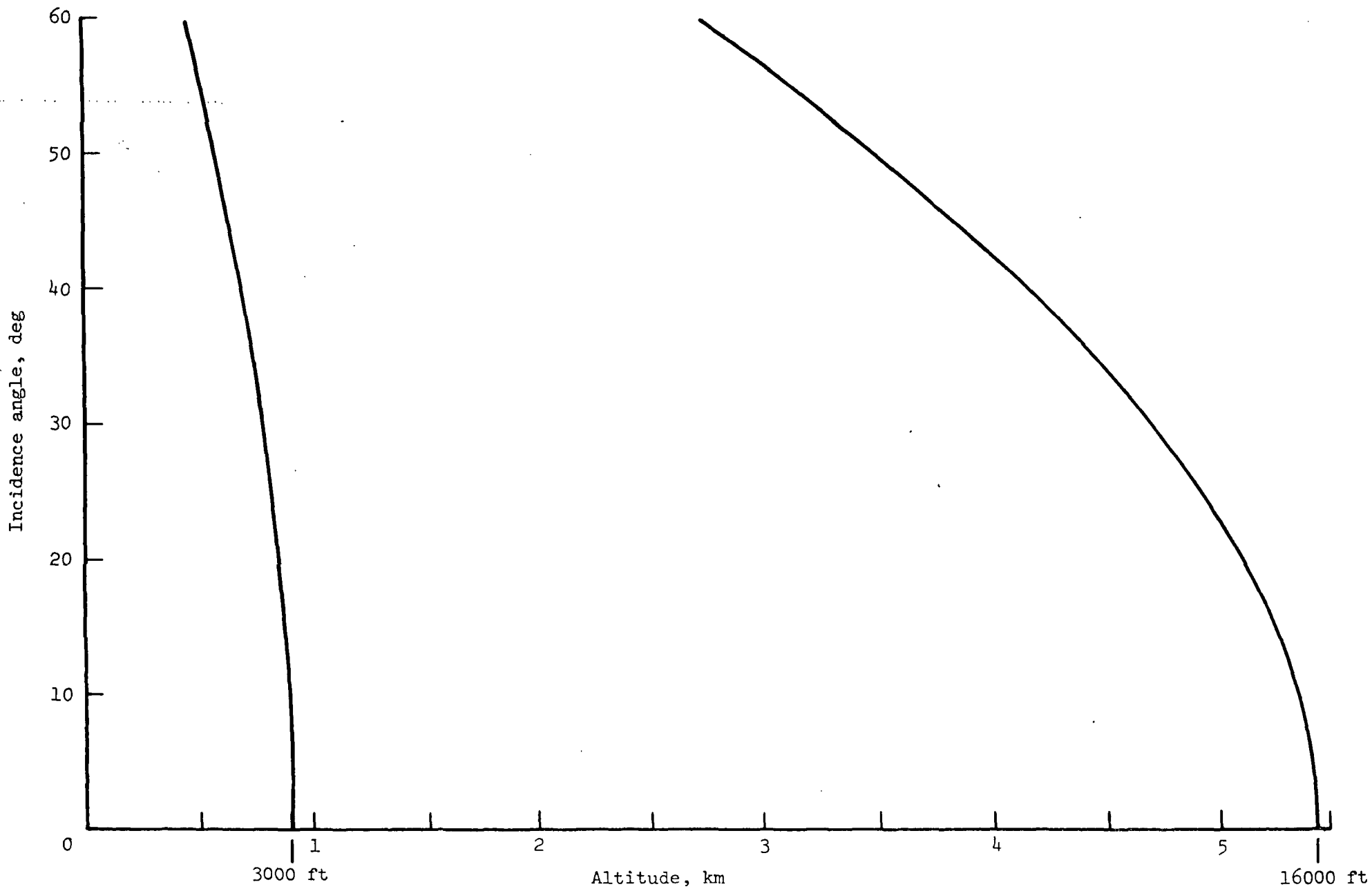
(b) Typical strip chart recording of RADSCAT regular calibration.

Figure 12. - (Concluded).

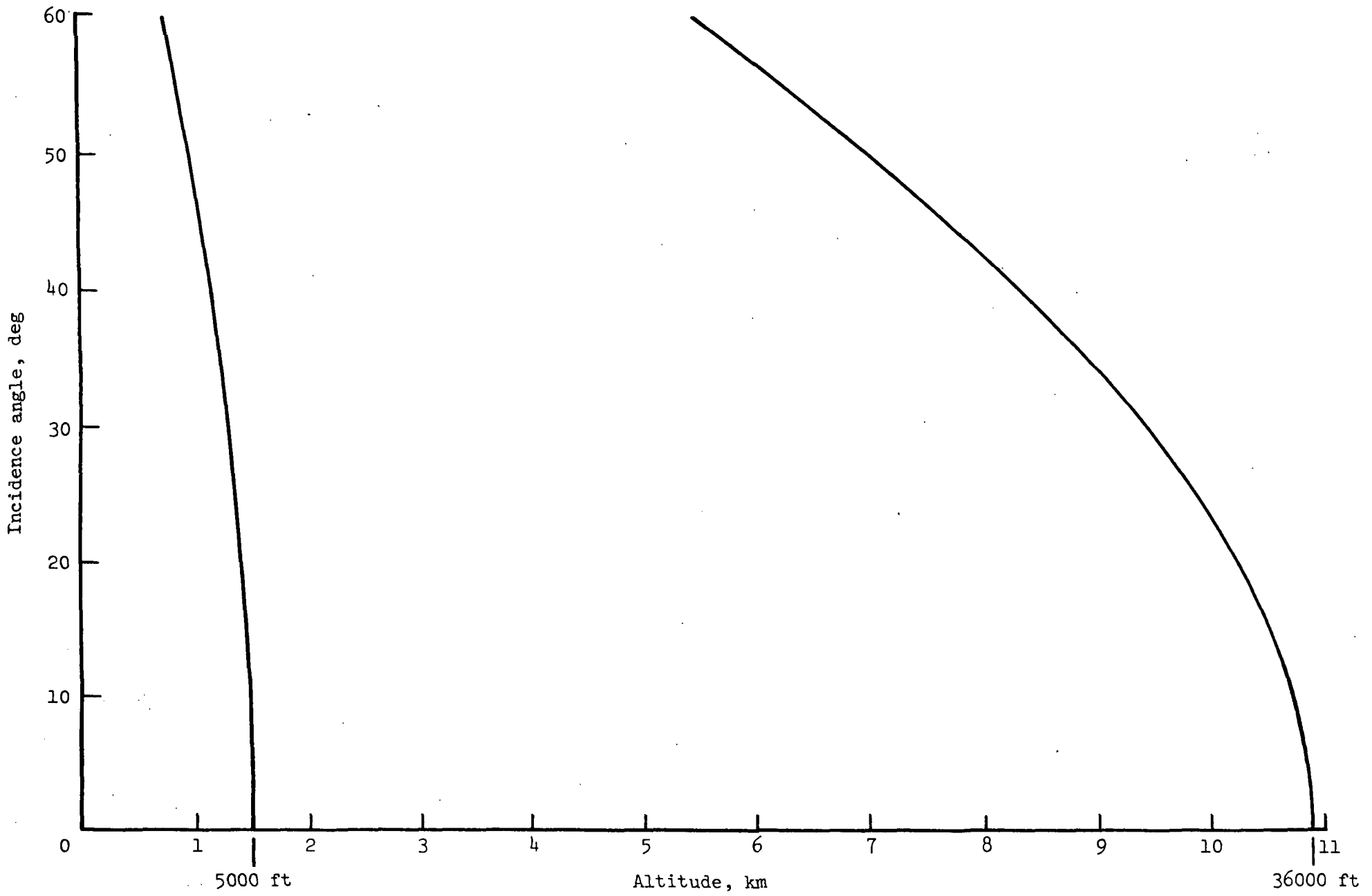


(a) 2K range gate.

Figure 13.- Altitude limits as a function of incidence angle for RADSCAT.



(b) 5K range gate.  
Figure 13.- Continued.



(c) 10K range gate.  
Figure 13.- Concluded.

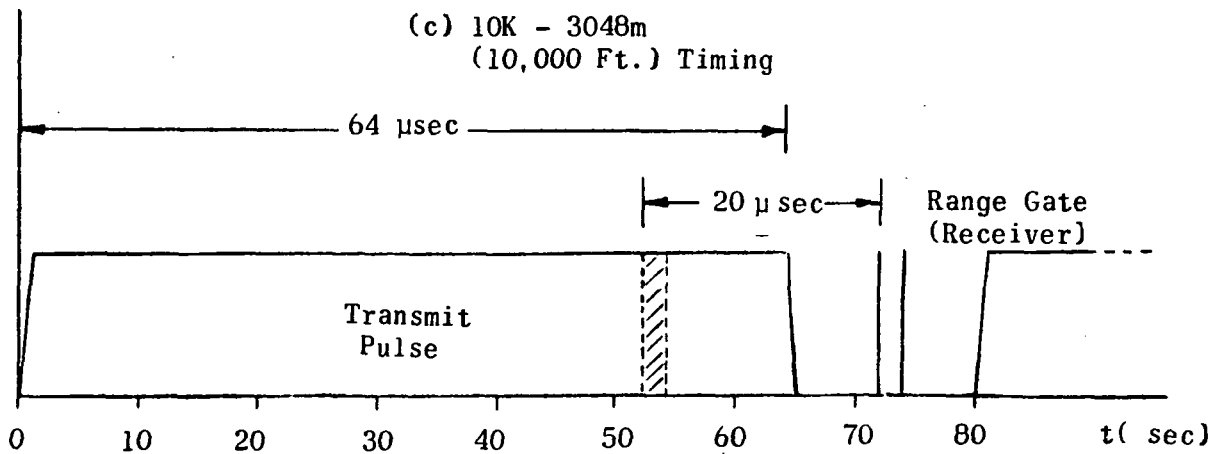
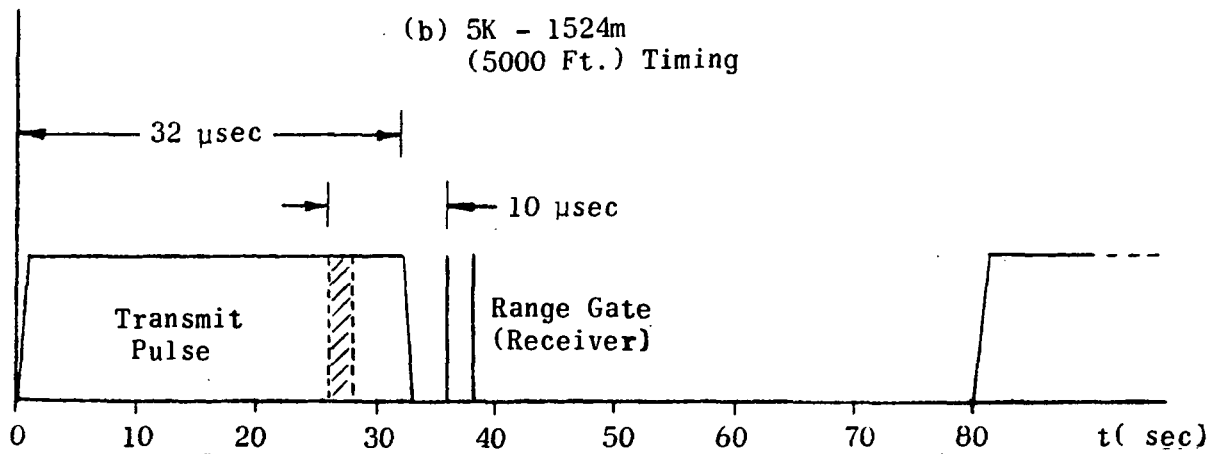
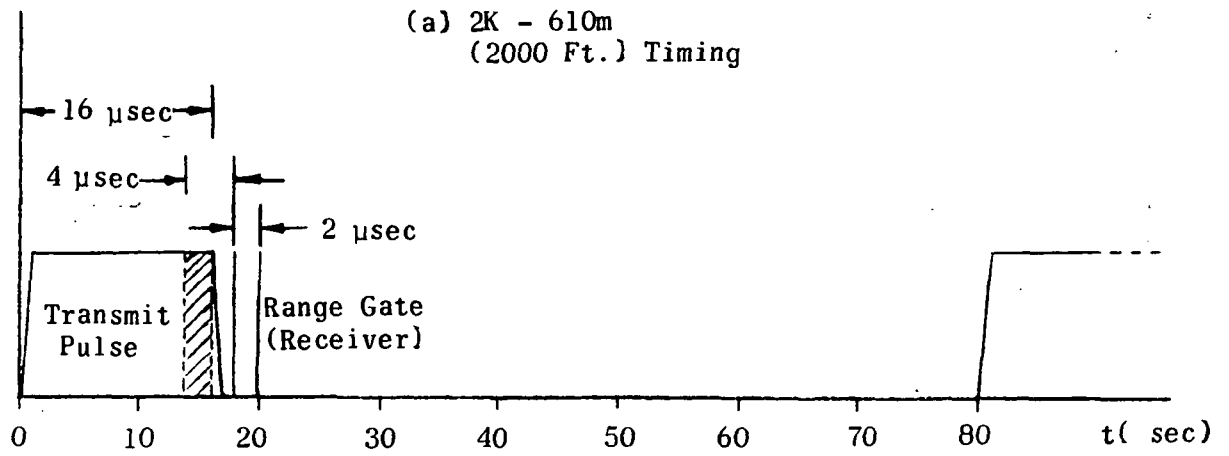


Figure 14. Transmit/Receive timing for RADSCAT operation at 2K, 5K, and 10K range gate settings

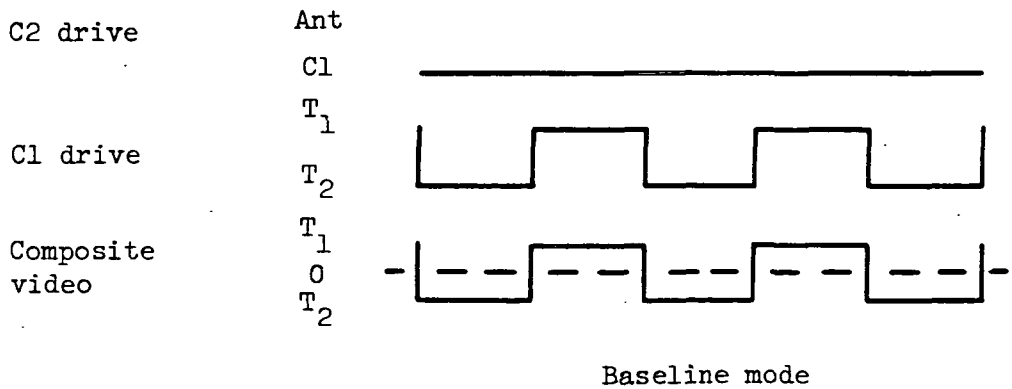
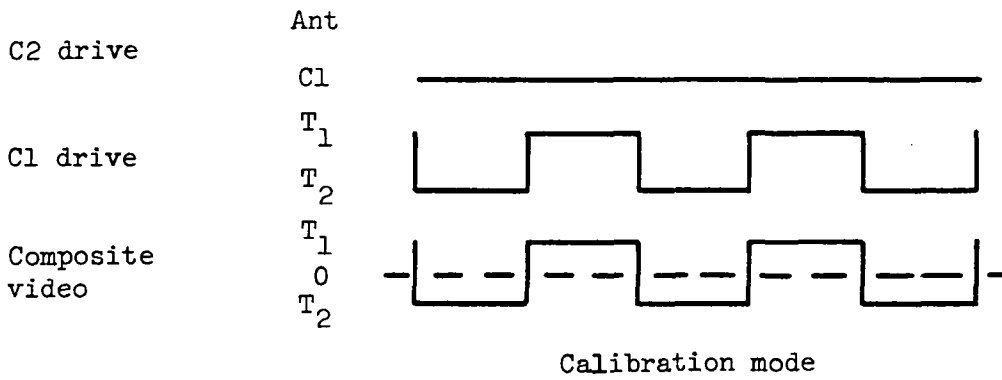
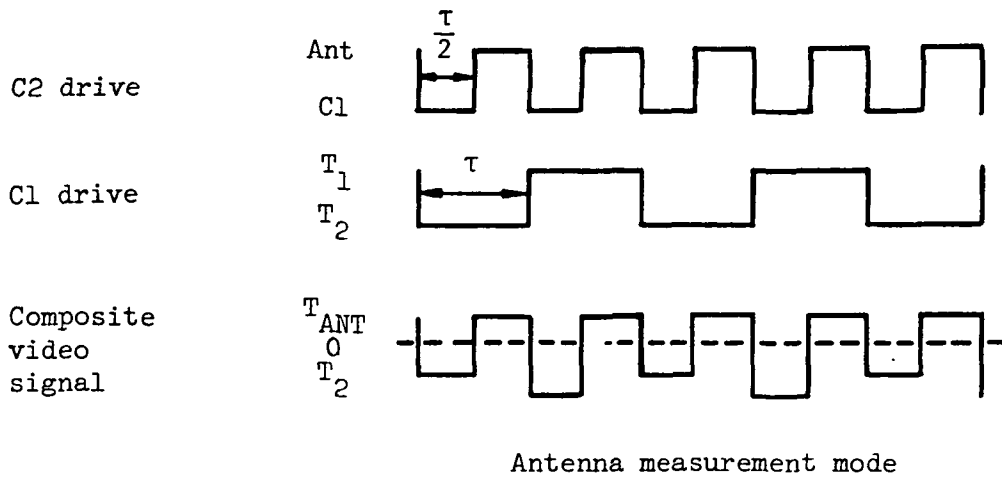
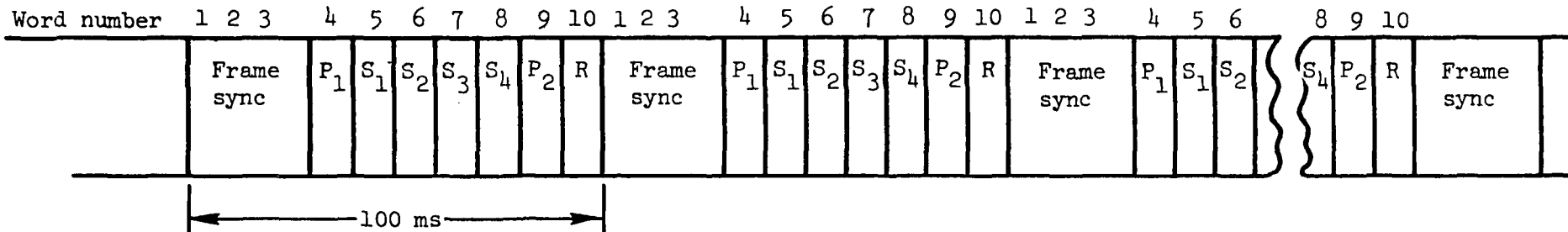
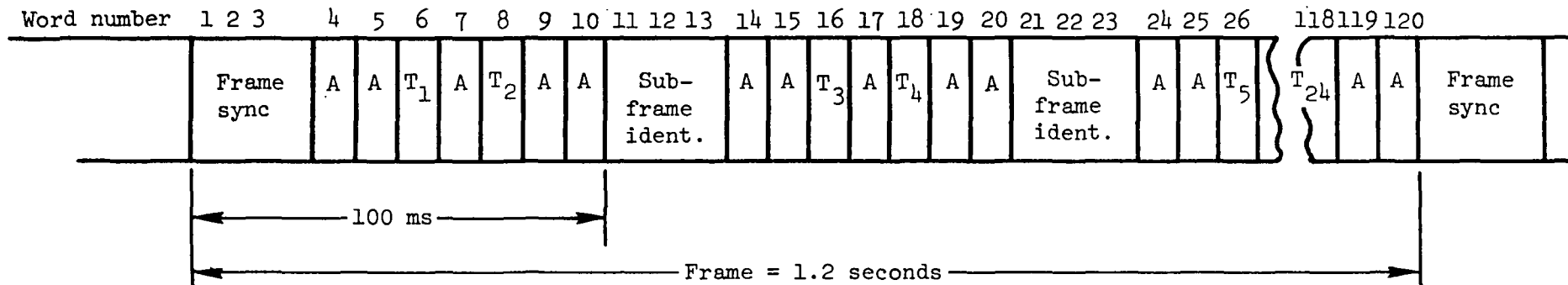


Figure 15.- Timing diagrams for RAD operation.



Experiment information format



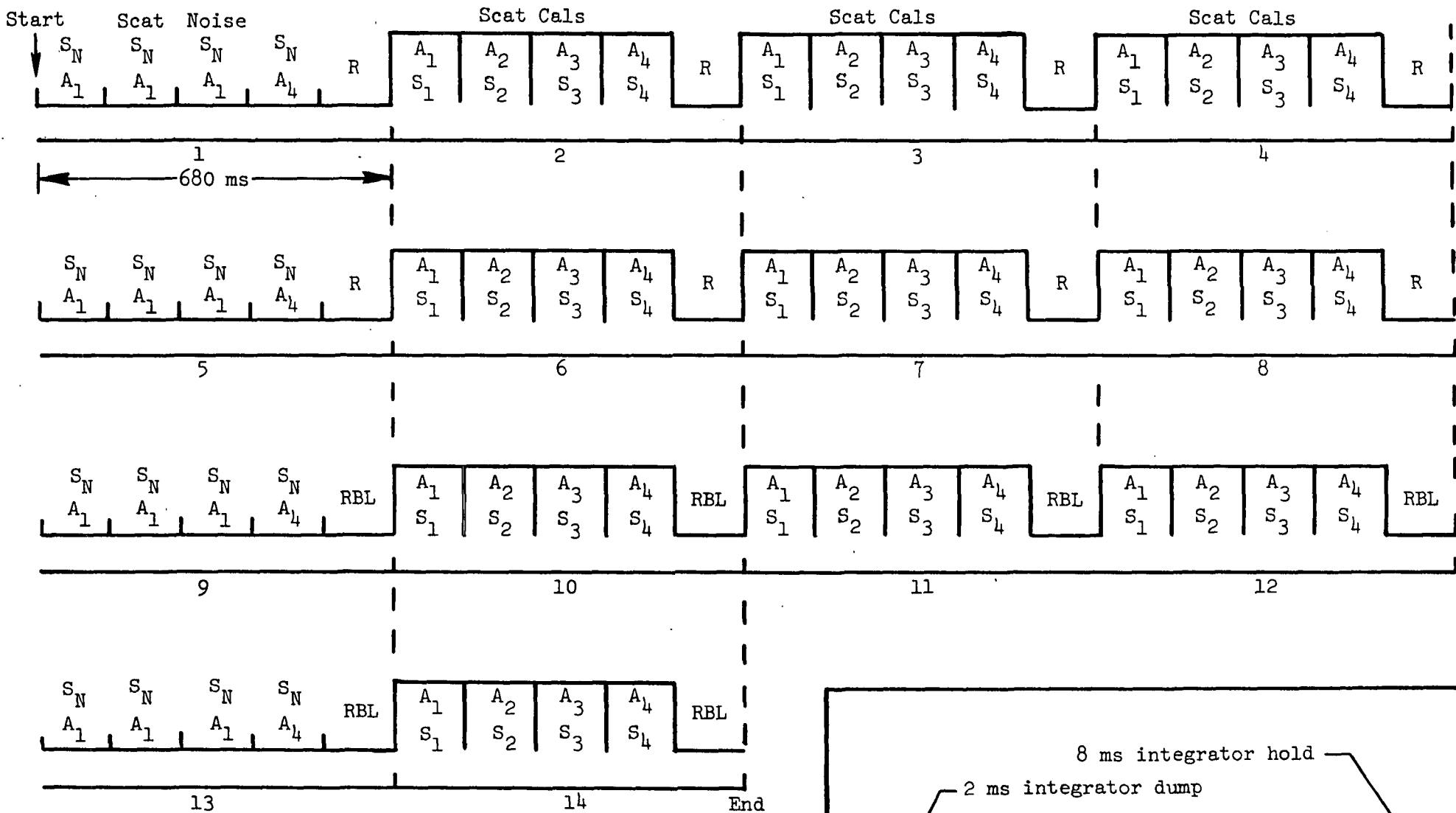
Diagnostic telemetry format

Code:

- P parameter word
- S Scat measurement
- R Rad measurement
- A AGC measurement
- T Temp measurement

Figure 16.- Data formats.





Total period of sequence = 9.52 sec

Key  
 R = Rad cal  
 SN = Scat noise  
 A<sub>i</sub> = Scat attenuator  
 S<sub>i</sub> = Scat channel  
 RBL = Rad baseline

Figure 17.- Revised calibration sequence for RADSCAT.  
 (Modification occurred Jan. 15, 1975).

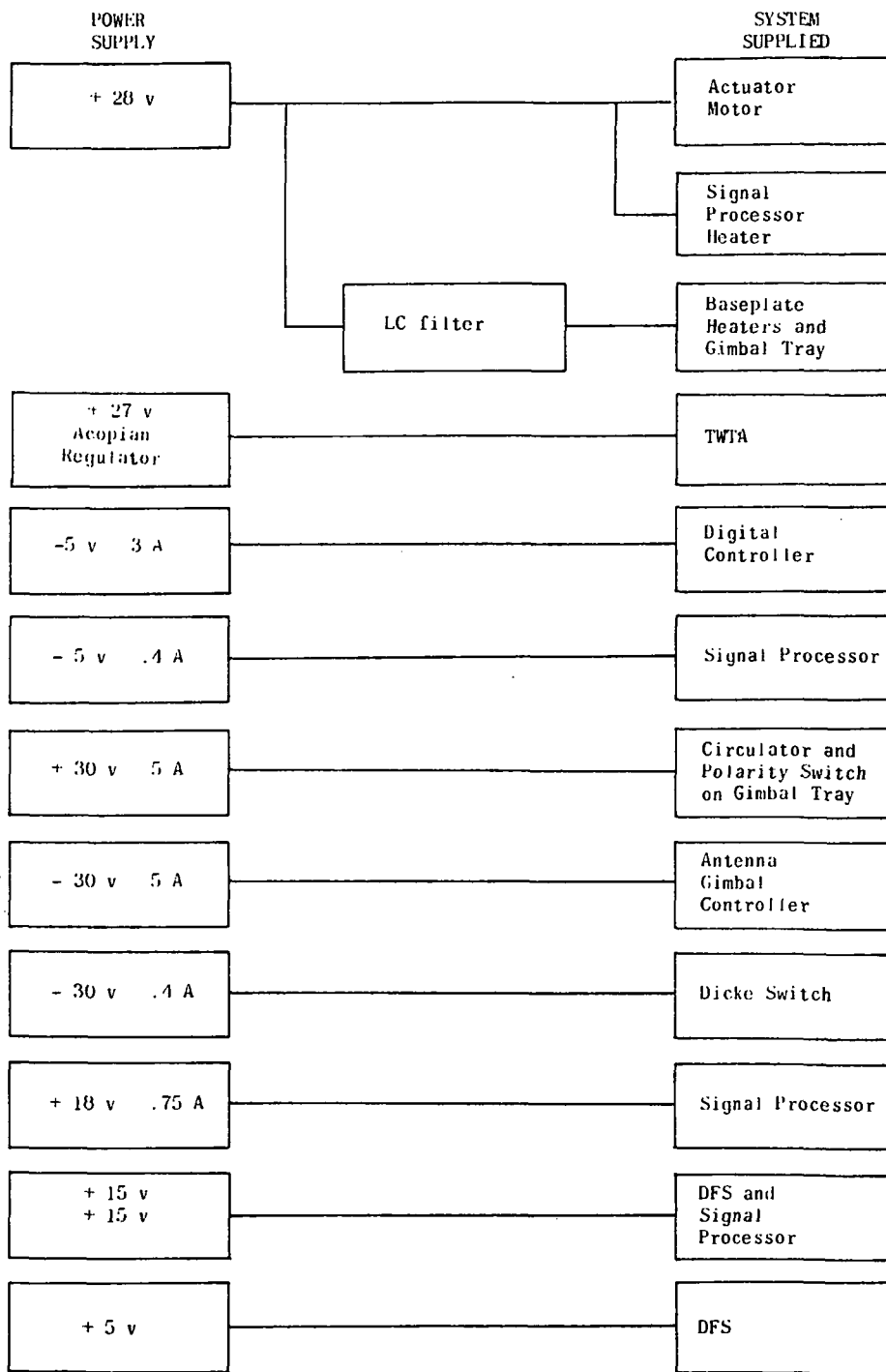
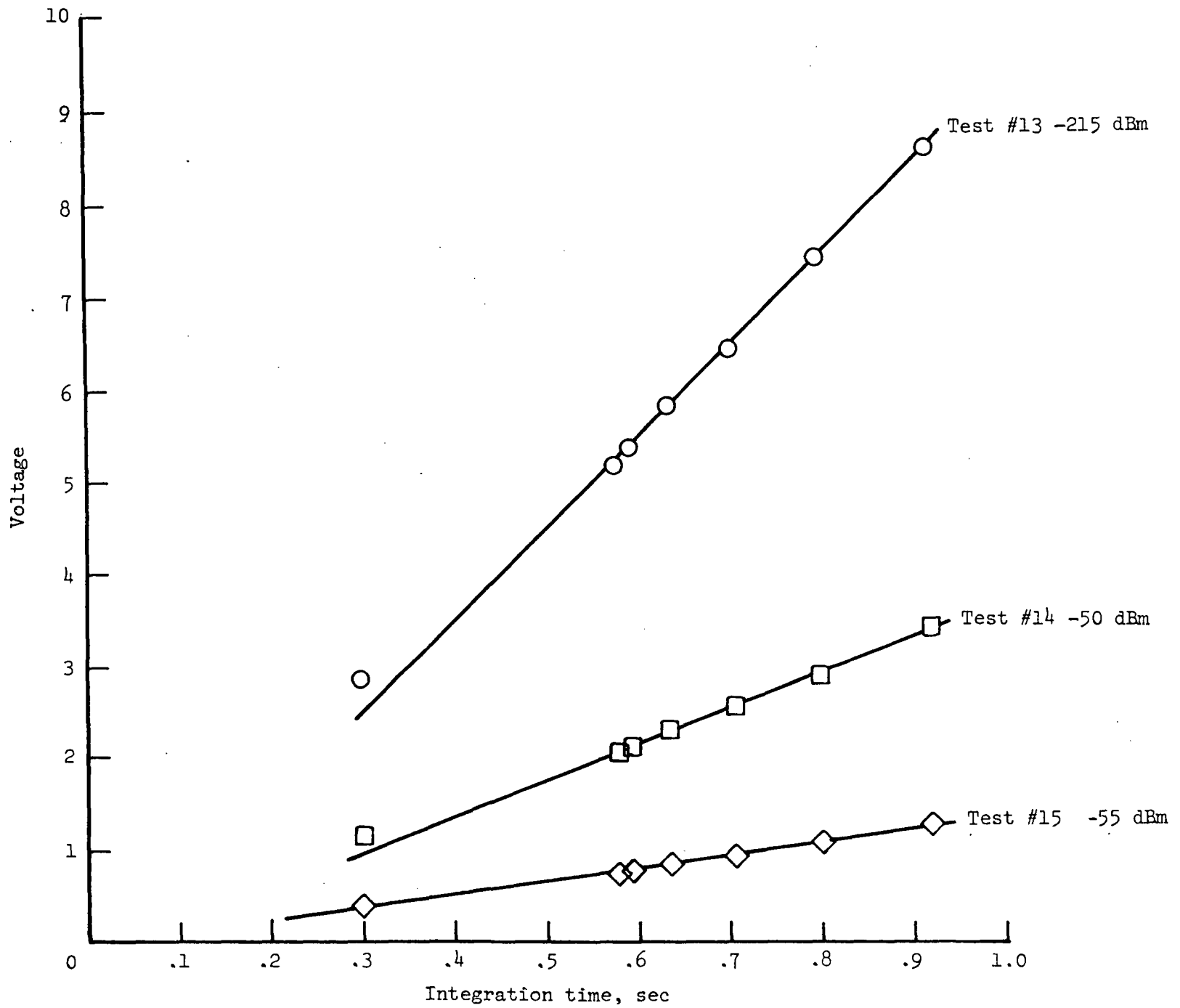


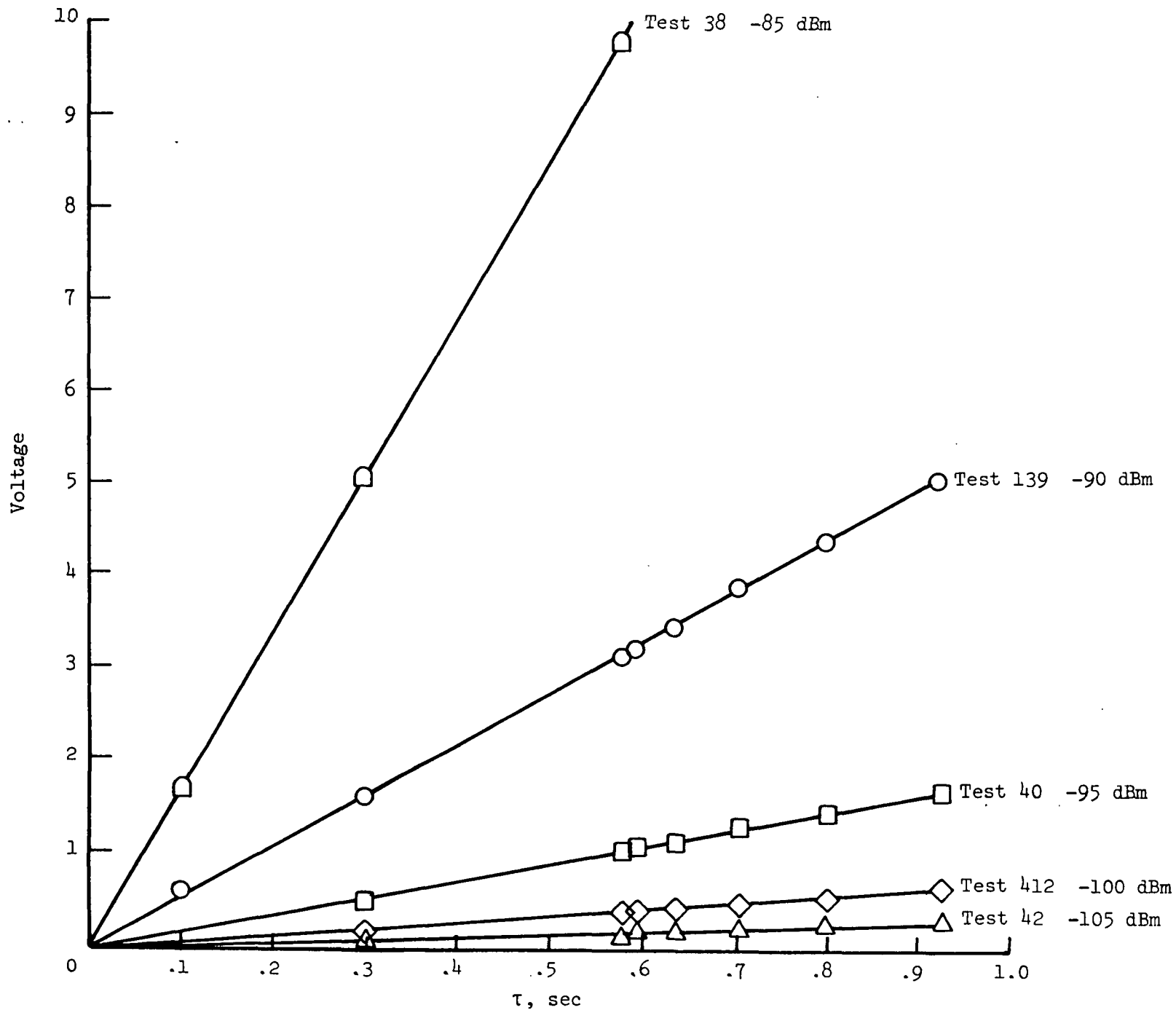
Figure 18. - Power supply block diagram.

ORIGINAL PAGE IS  
OF POOR QUALITY



a. 13.9 GHz (April 73), Scat 1.

Figure 19.- Scat voltage vs. integration time as a function of input power.



b. 9.3 GHz (April 11, 75), Scat 4.

Figure 19.- Concluded.

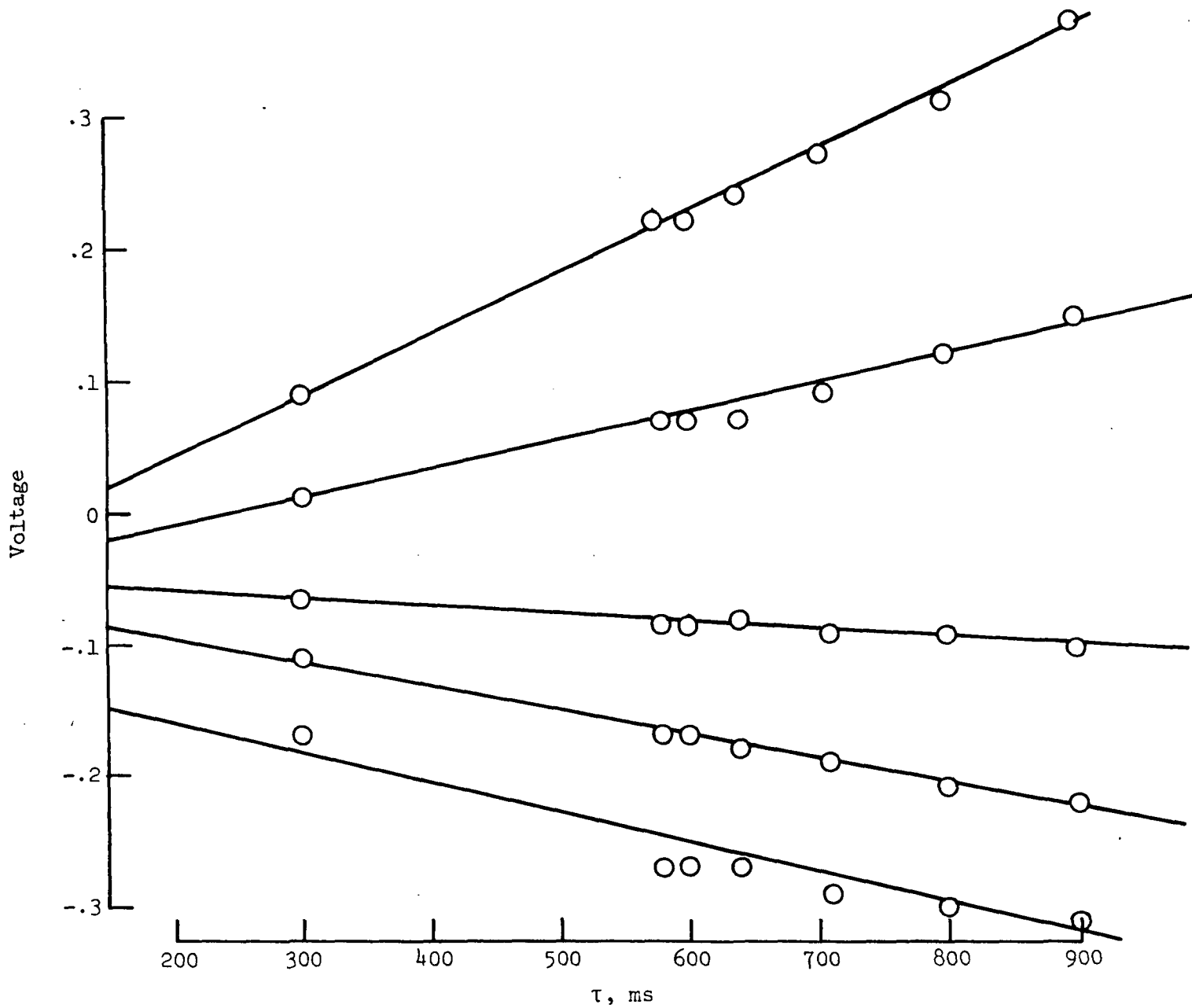


Figure 20.- Scat zeros vs. integration time  $\tau$ , for no input signal.

Flight data from M230 FCF Line 2-6

- Short scat
- ◻ Angle 1
- ◻ Angle 3
- ◻ Angle 4
- ◻ Angle 5

● Lab data from Test Tape #2  
10/1/73

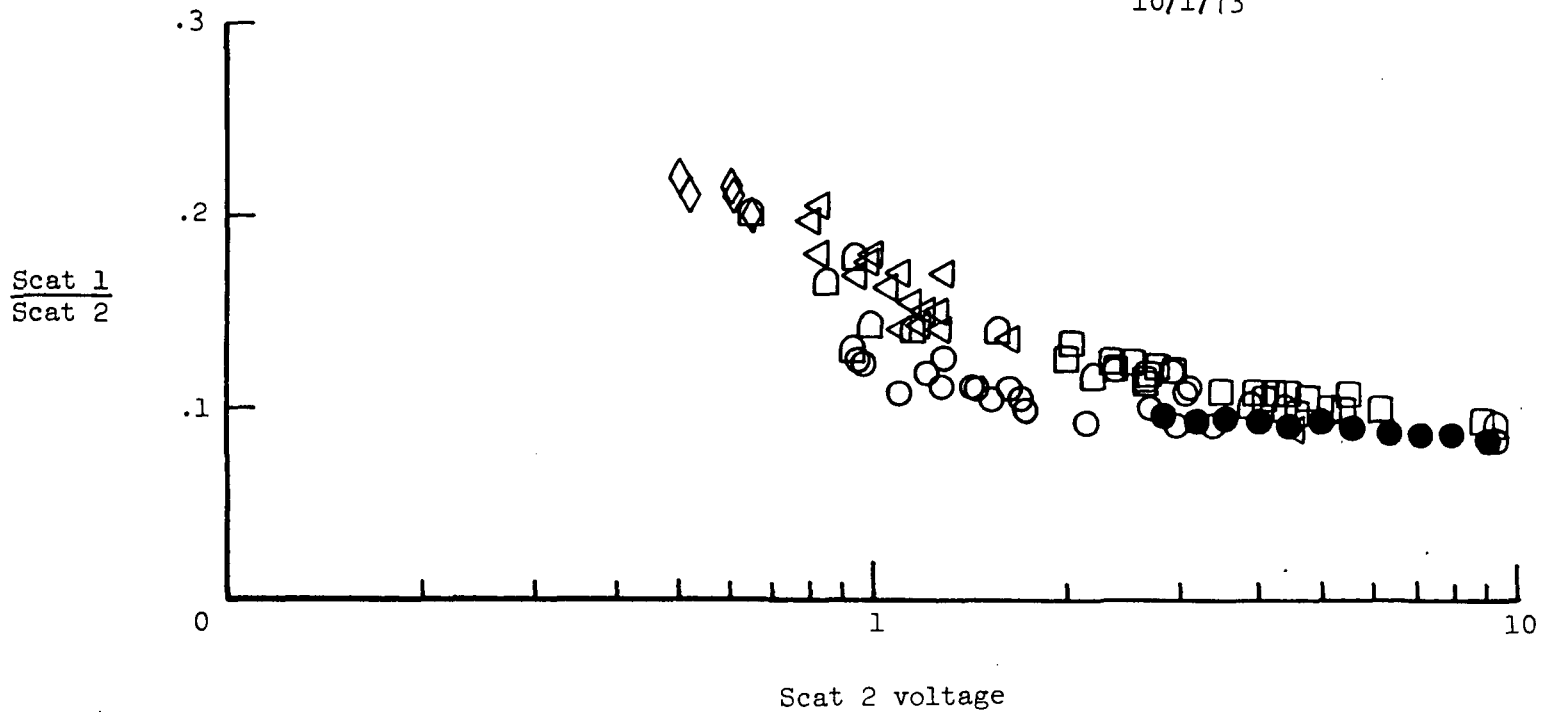
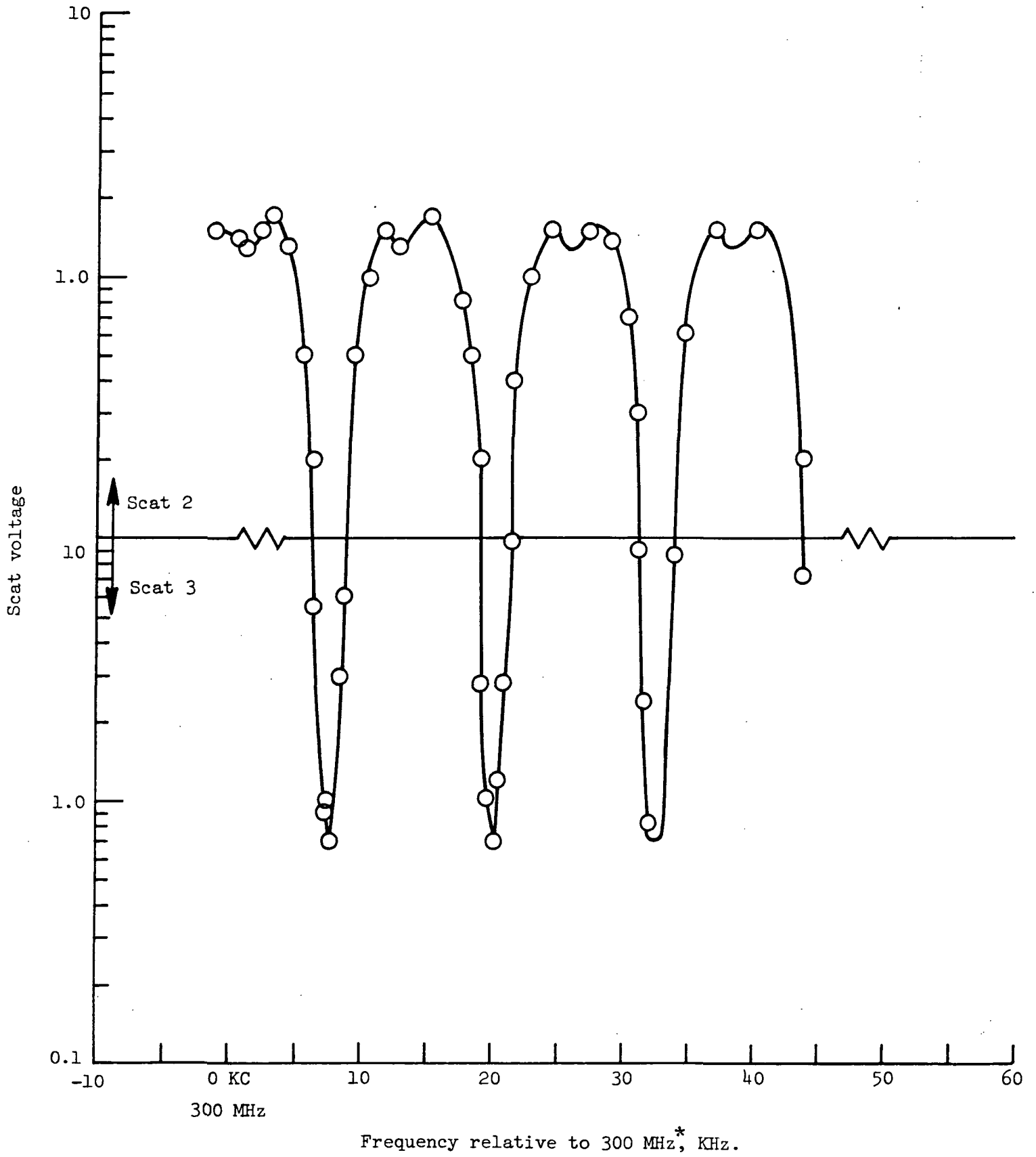


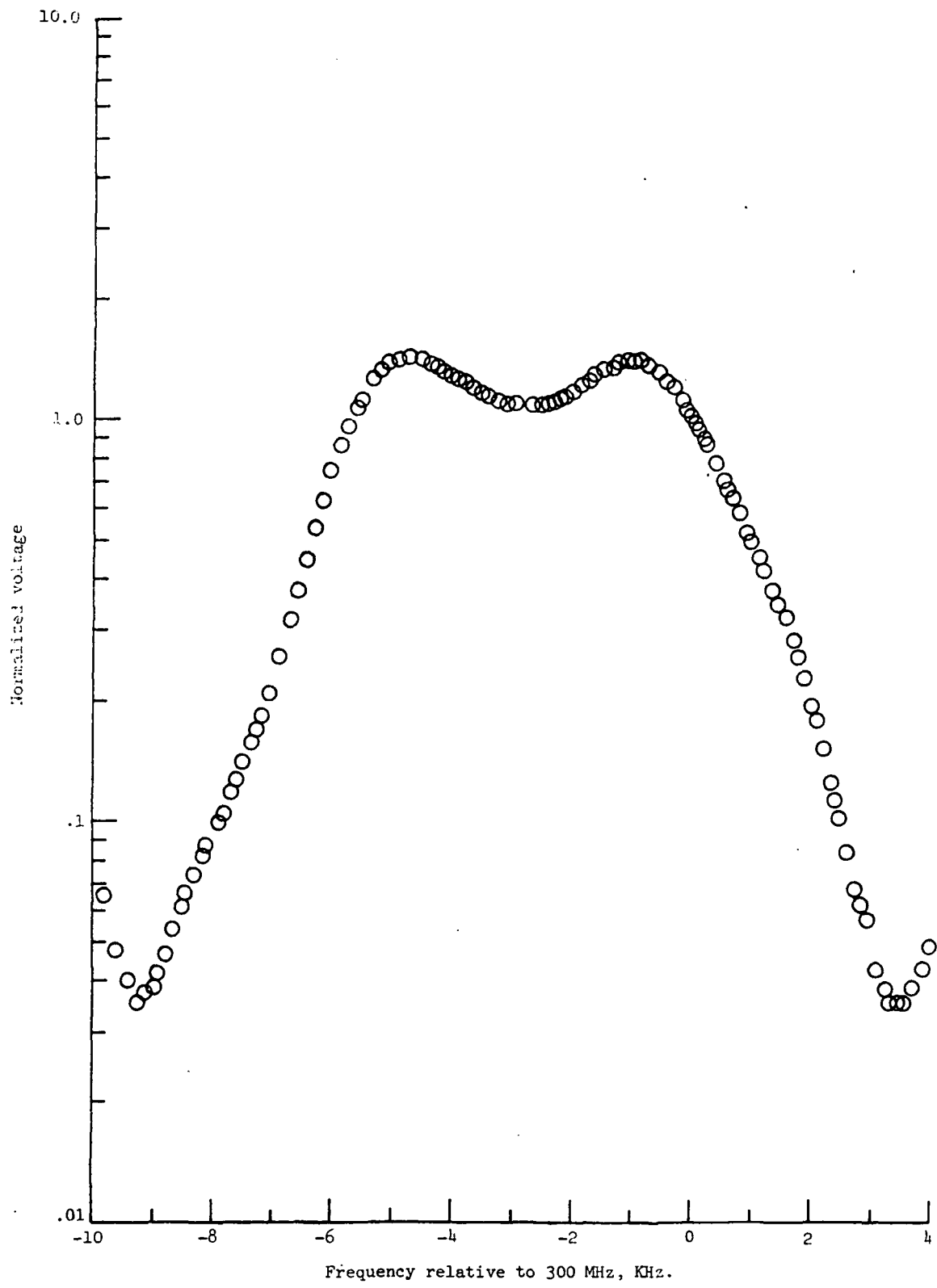
Figure 21.- Comparison of lab and flight overlaps.



a. 70 KHz test, 6/4/72.

Figure 22.- 300 MHz\* IF passband response.

\* Response at 100 and 300 MHz is identical.



b. Single passband, 3/29/73, Test 45.

Figure 22.- Concluded.



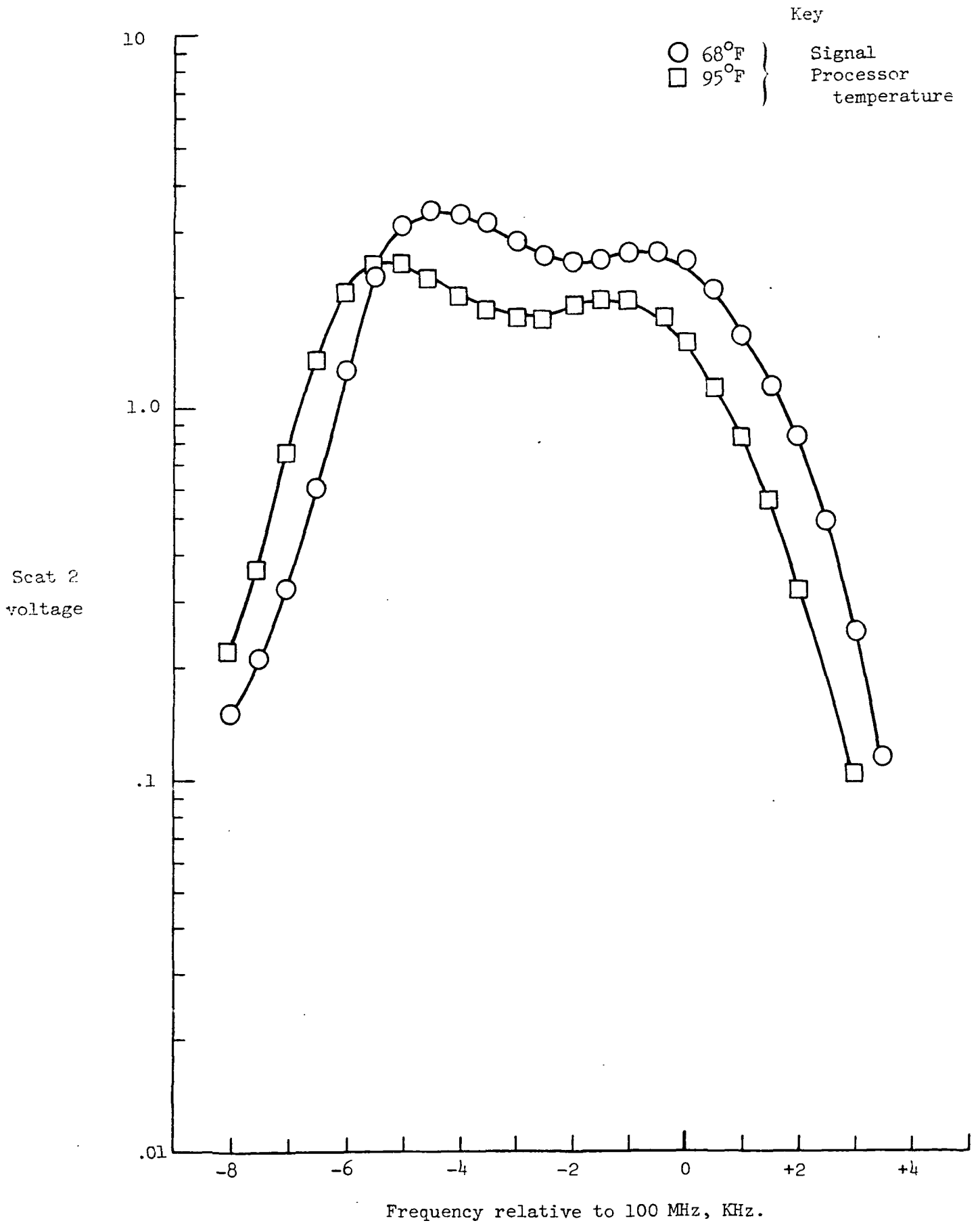


Figure 23.- 100 MHz passband response as a function of temperature.

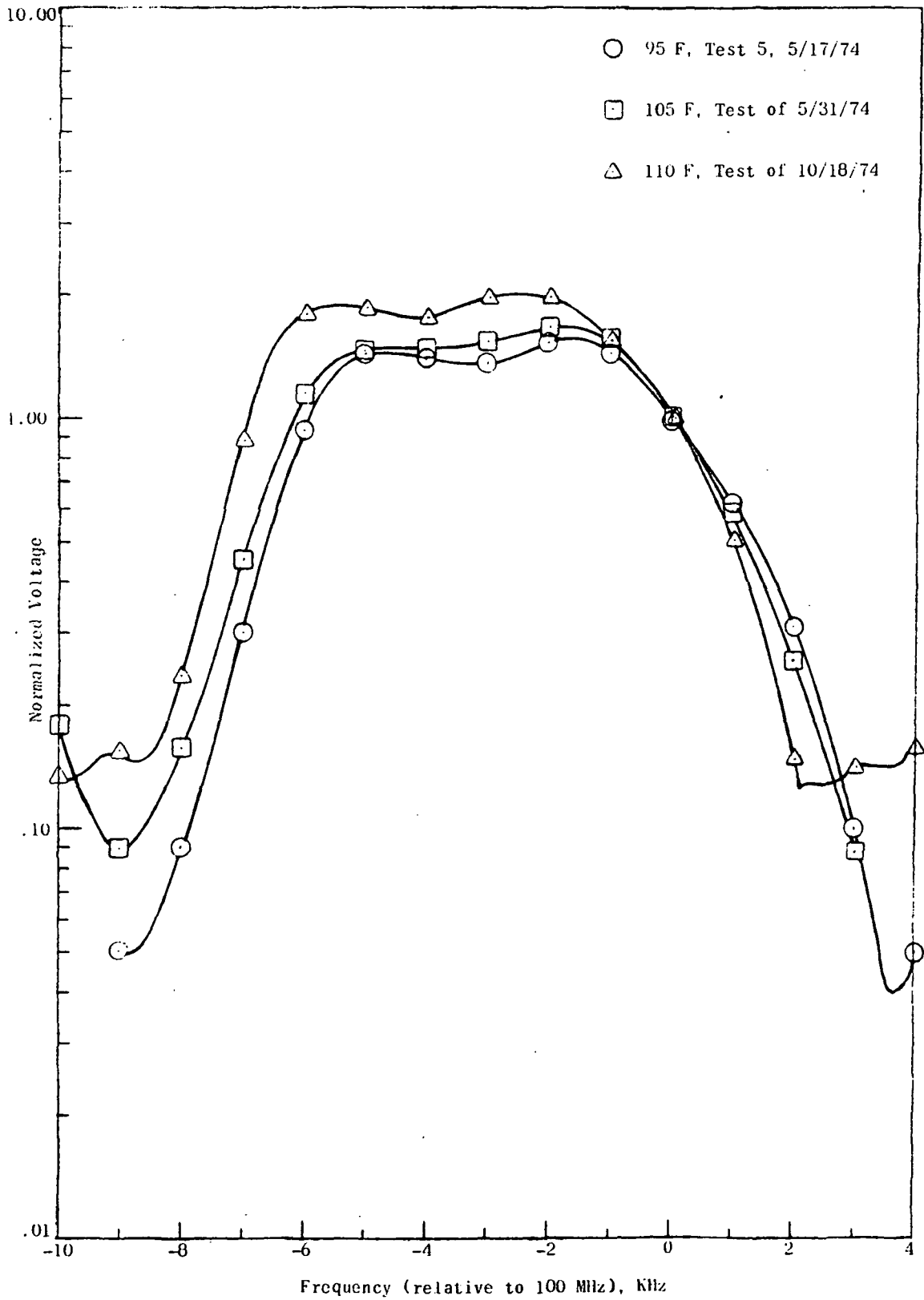


Figure 24. - Passband response with heaters installed to control the crystal filter environment

$\sigma^{\circ}T_2$  is based on 110°F at  
crystal filter, Bandpass  
cal (Figure 29c).

$\sigma^{\circ}T_1$  is based on 70°F ambient  
(Figure 22b) Apr. '73.

Symbol	Flight	Key Direction	Aircraft Ground Speed
○	M230 FCF	Upwind	190 knts
○	M230 FCF	Downwind	120 knts
□	M238/20	Upwind	170 knts
□	M238/20	Downwind	132 knts
◇	M238/27	Upwind	170 knts
◇	M238/27	Downwind	155 knts

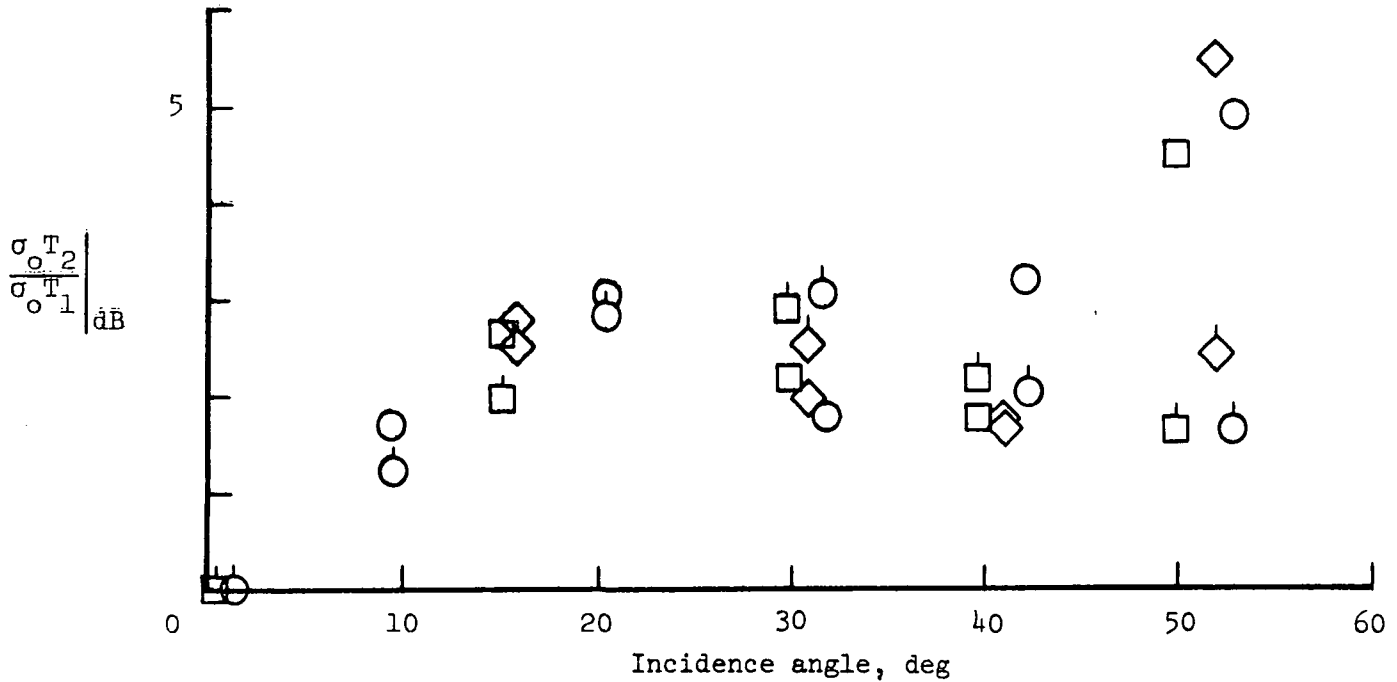
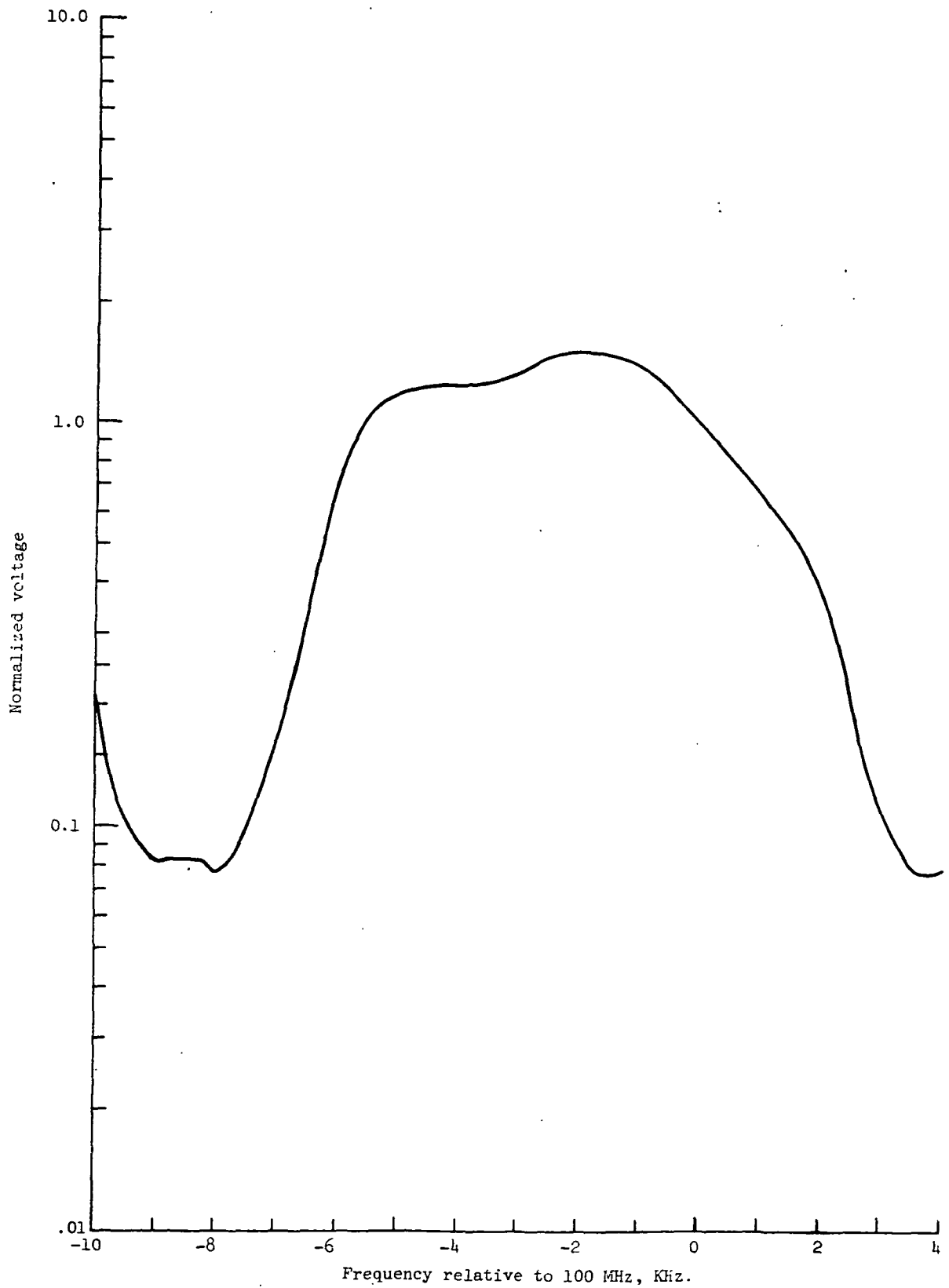


Figure 25.- Deviation in  $\sigma^{\circ}$  if temperature varies from 70°F outside ambient to 110°F at crystal filters for flight tests listed, where temp. was not monitored.



a. Passband for aft scanning, with 200 MHz local oscillator offset by 50 Hz.

Figure 26.- Current passband response.

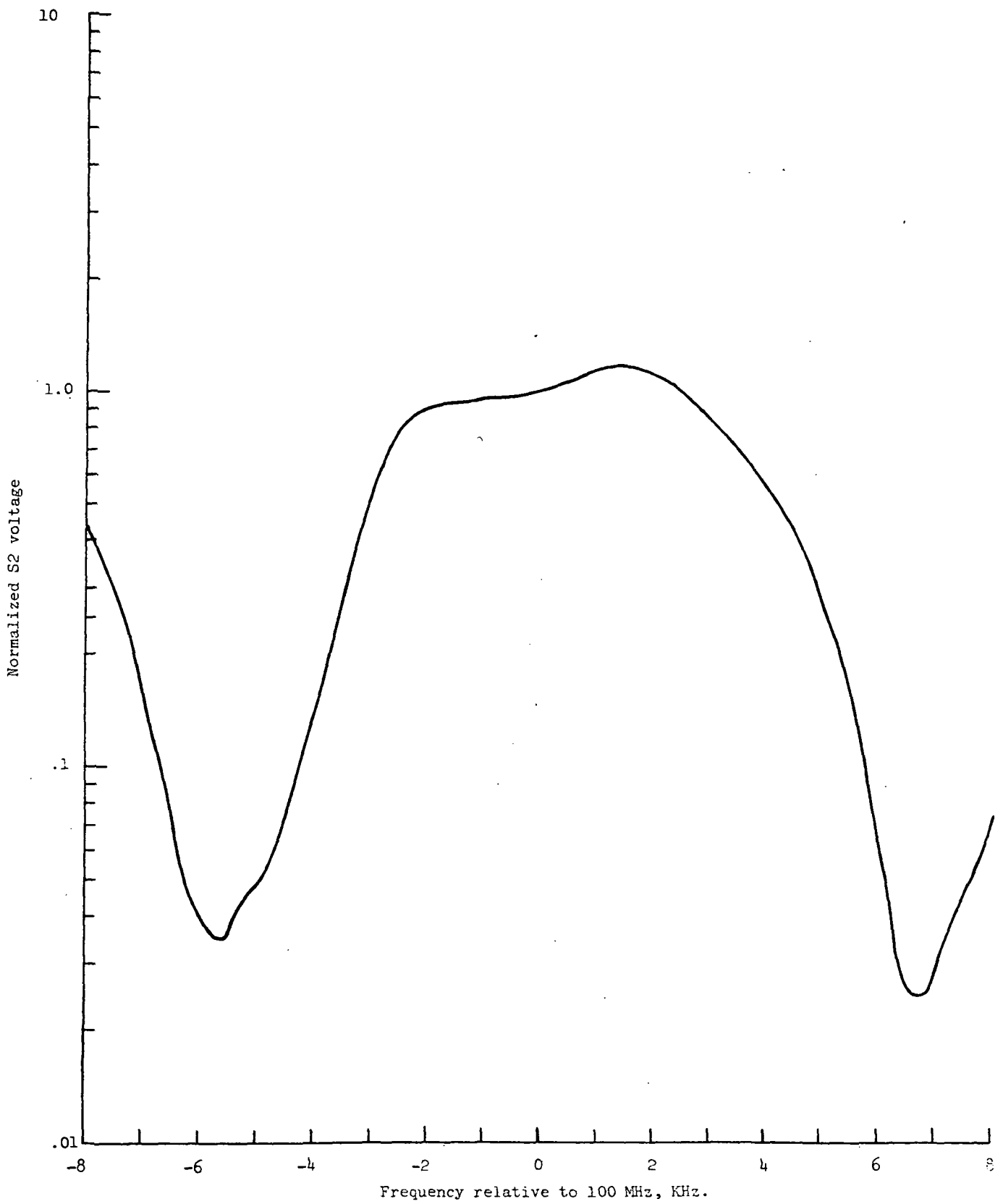


Figure 26.- Concluded.

b. Passband for side scanning.

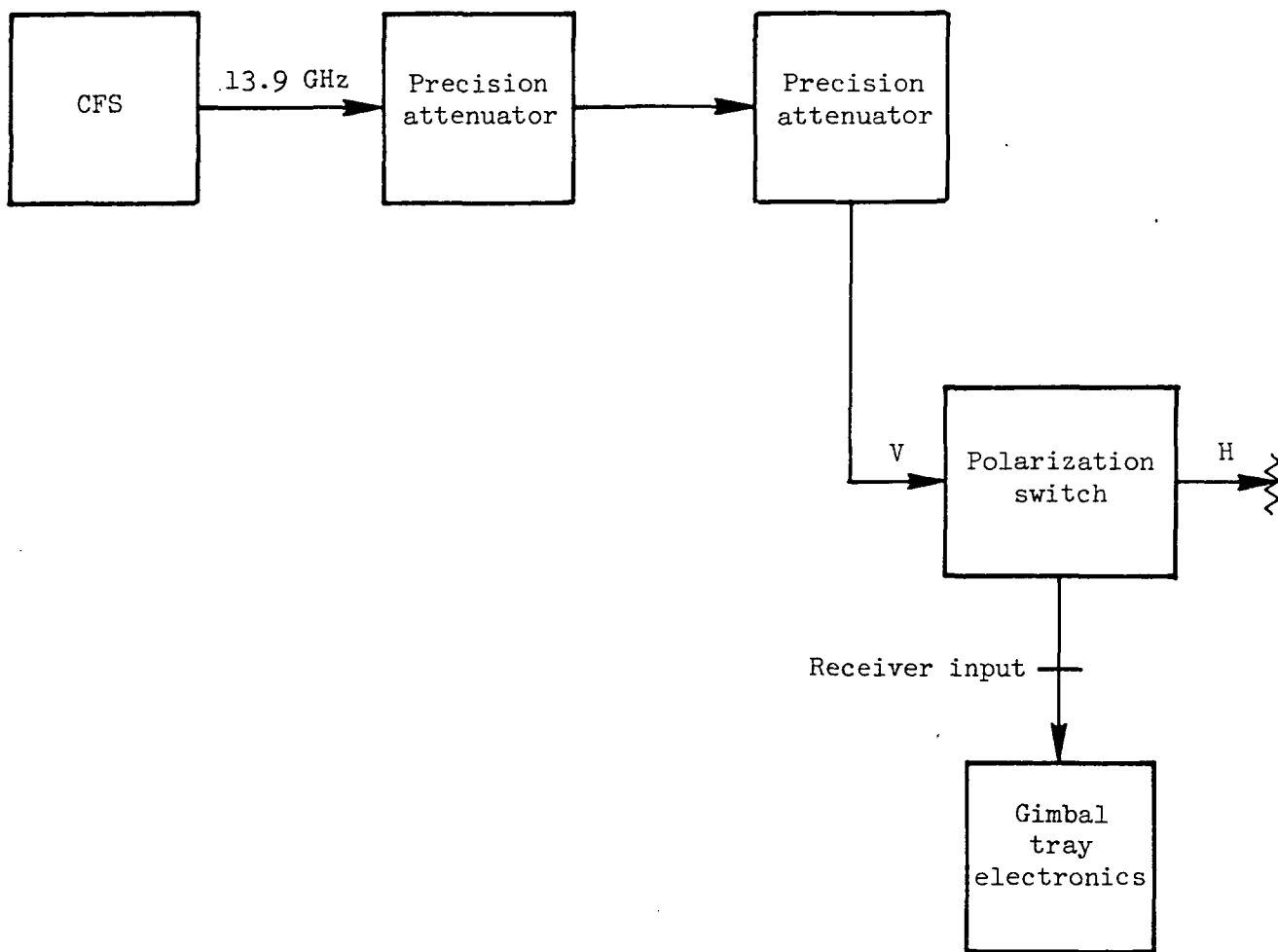


Figure 27.- Configuration used to measure scatterometer system dynamic range.

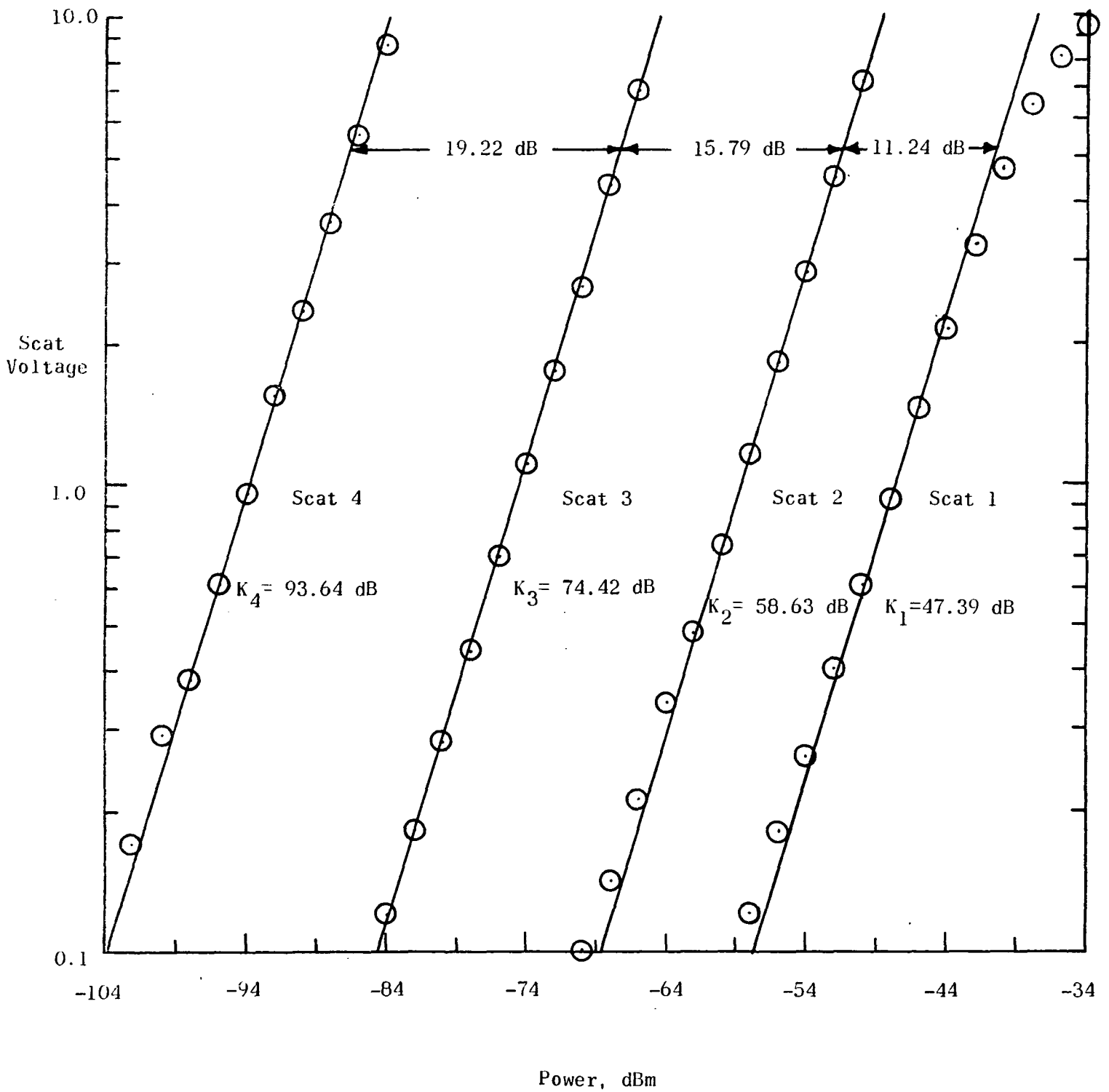
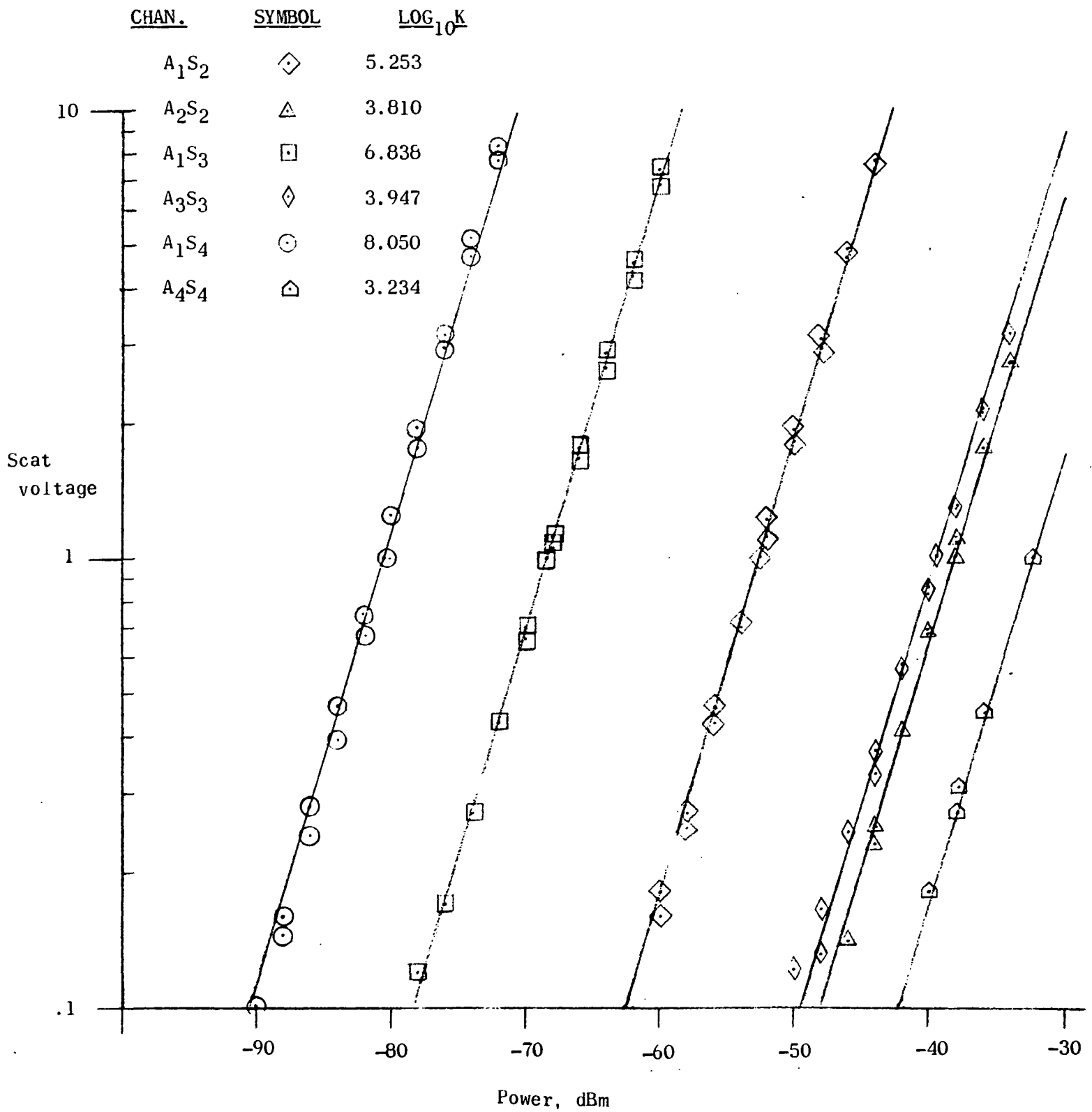


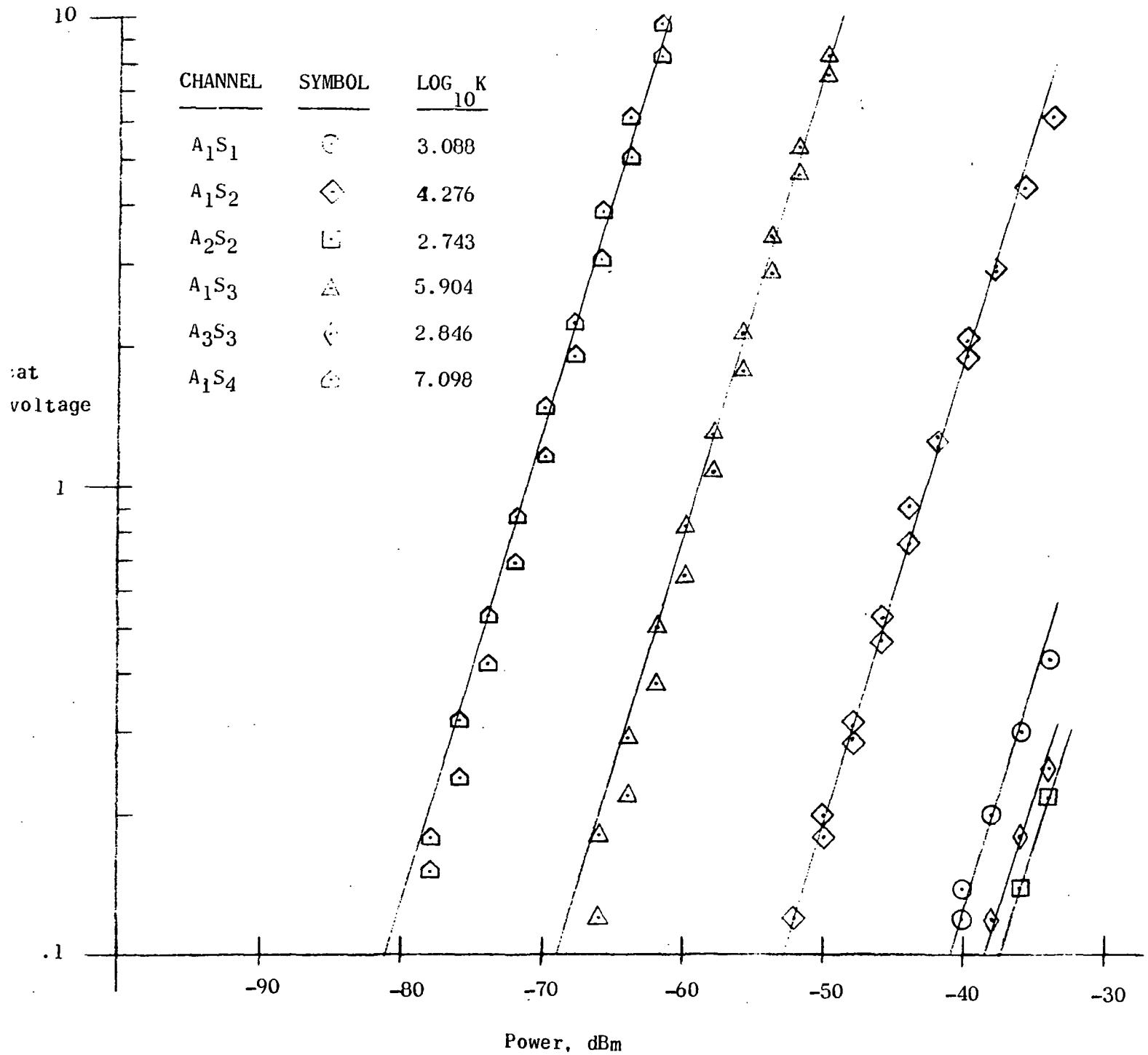
Figure 28. - Scat dynamic range test in a normal operation mode - data from April test 11, 13.9 GHz, 3/28/73



(a) 10 dB pad out, October Test I2, 10/5/73.

Figure 29. - Continuous cal. dynamic range test data.





(b) 10 dB pad in, October Test 10, 10/5/73.

Figure 29. - (Concluded).

REGRESSION FITS

PAD OUT

$$P(\text{dBm}) = -55.077 + 6.363 Y$$

$$+ 15.101 Y^2 - 16.636 Y^3$$

$$+ 5.614 Y^4$$

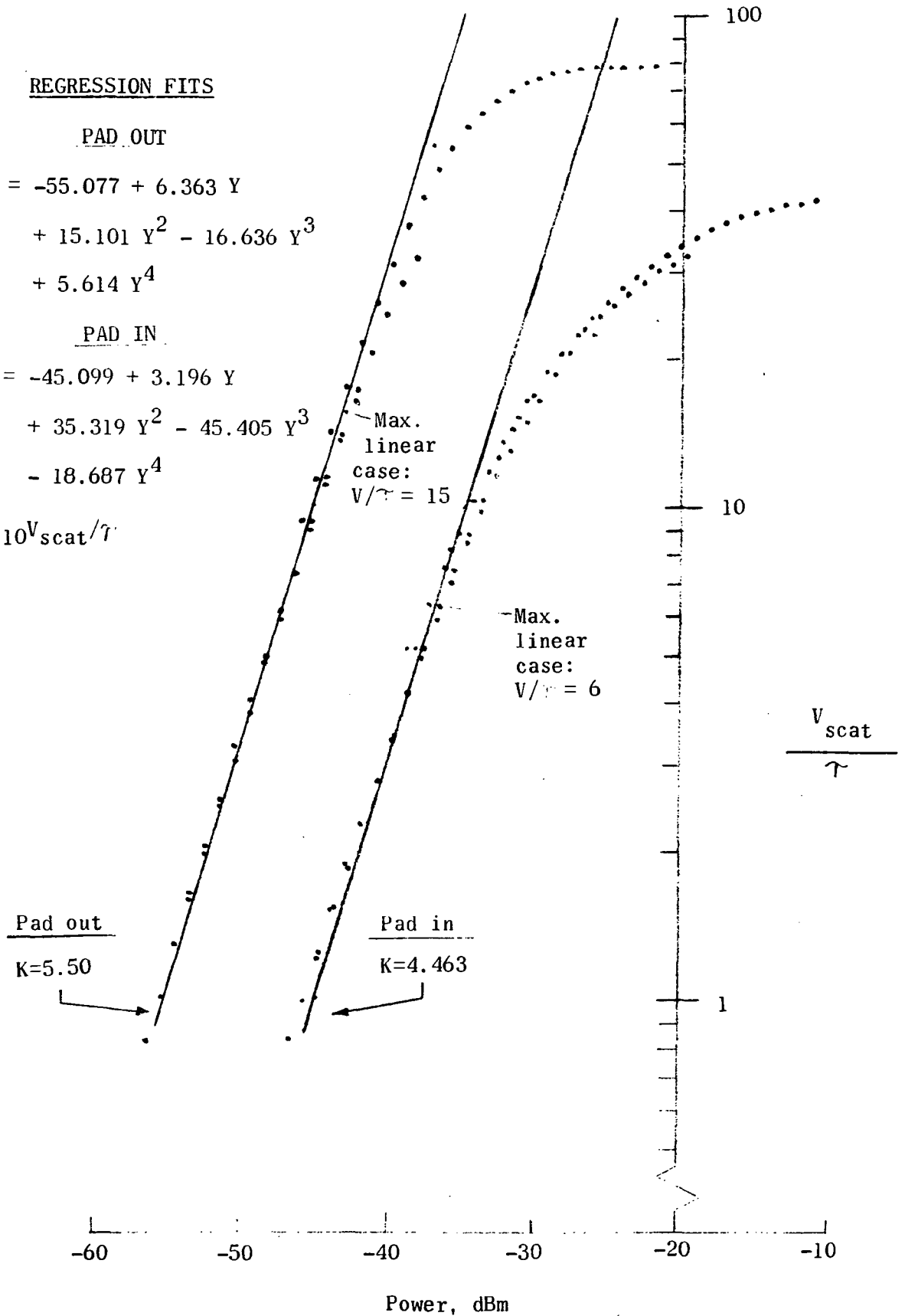
PAD IN

$$P(\text{dBm}) = -45.099 + 3.196 Y$$

$$+ 35.319 Y^2 - 45.405 Y^3$$

$$- 18.687 Y^4$$

$$Y = \log_{10} V_{\text{scat}} / \tau$$



ORIGINAL PAGE IS  
OF POOR QUALITY

Figure 30. - Normalized scat voltage vs. power. Saturated-to-unsaturated scatterometer condition, with 10 dB pad in and out.

C 2

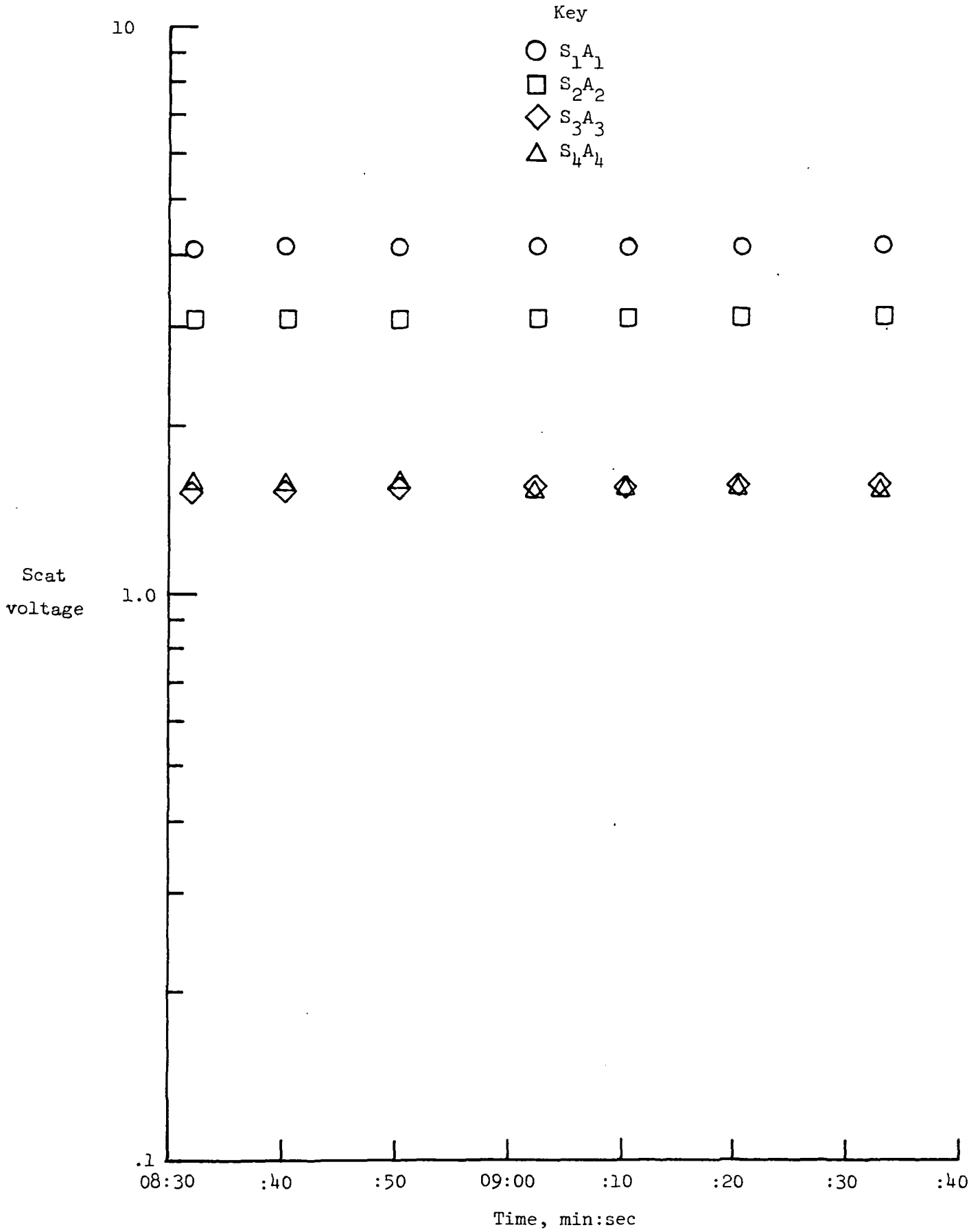


Figure 31.- Calibration stability.

a. Short term - Test 55, April 1973, 13.9 GHz.

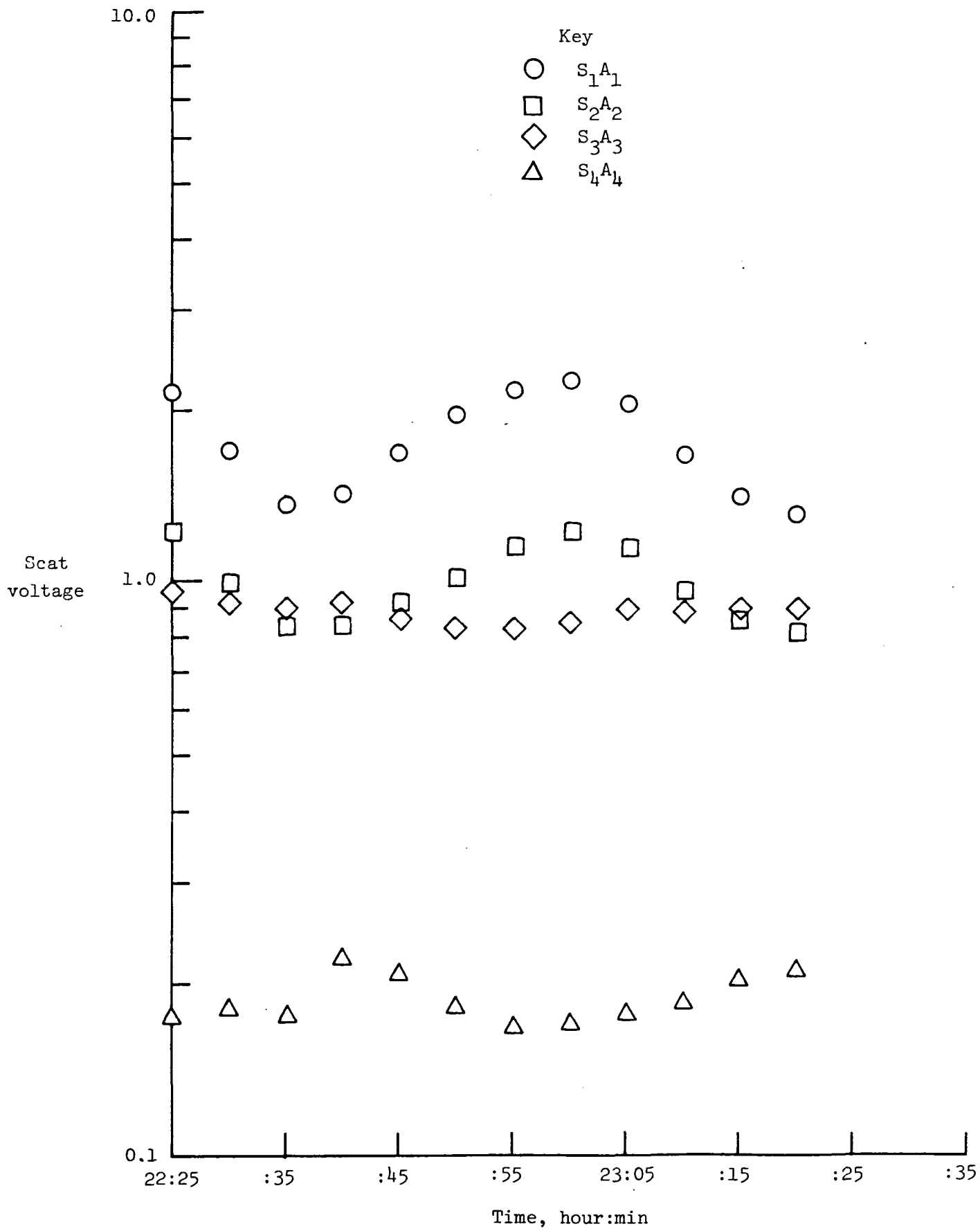


Figure 31.- Continued.

b. Long term - October 73 test 16.

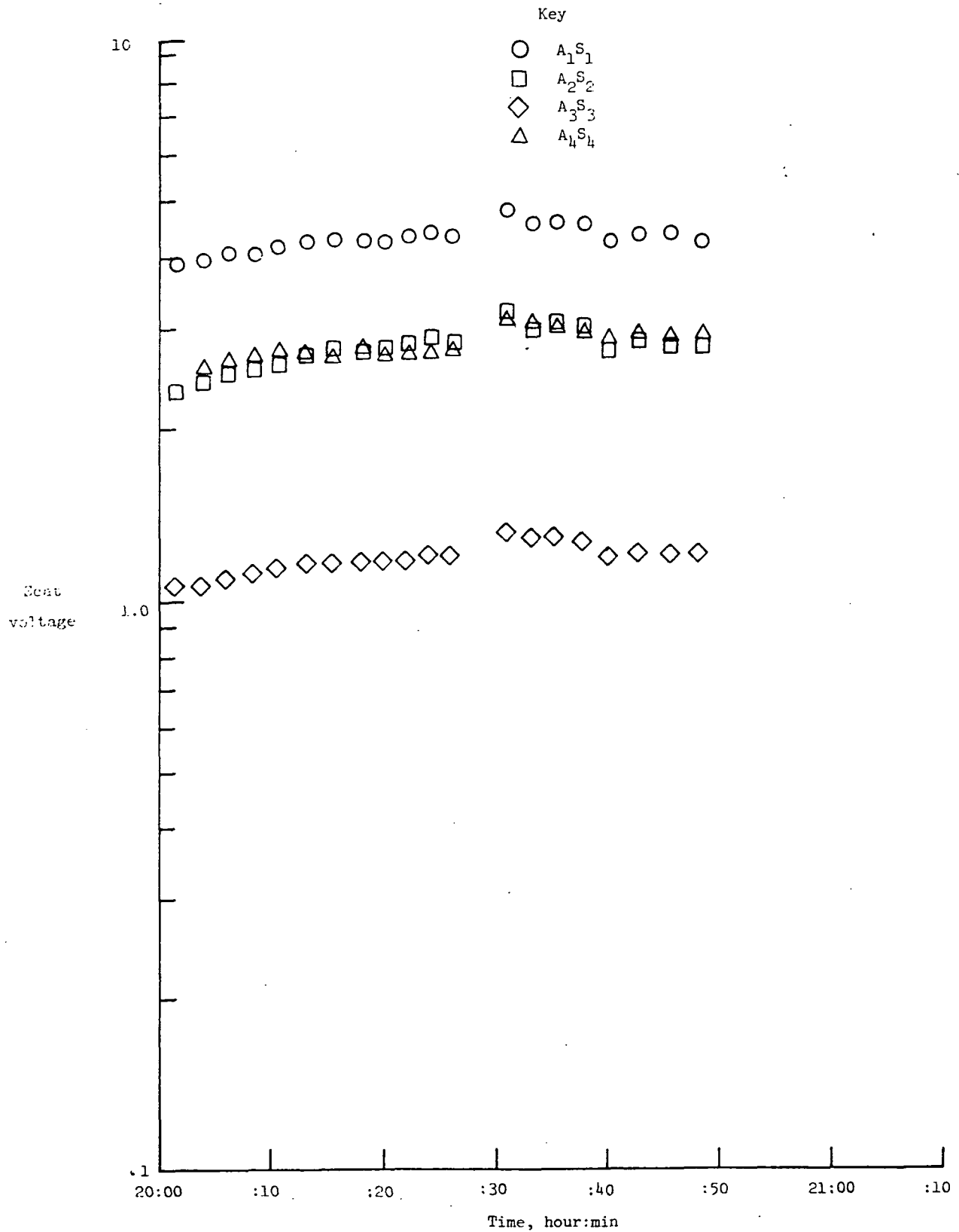


Figure 31.- Concluded.

c. Long term - after installation of second 10 MHz local oscillator - Mesa FCF, April 1975.

ORIGINAL PAGE IS  
OF POOR QUALITY

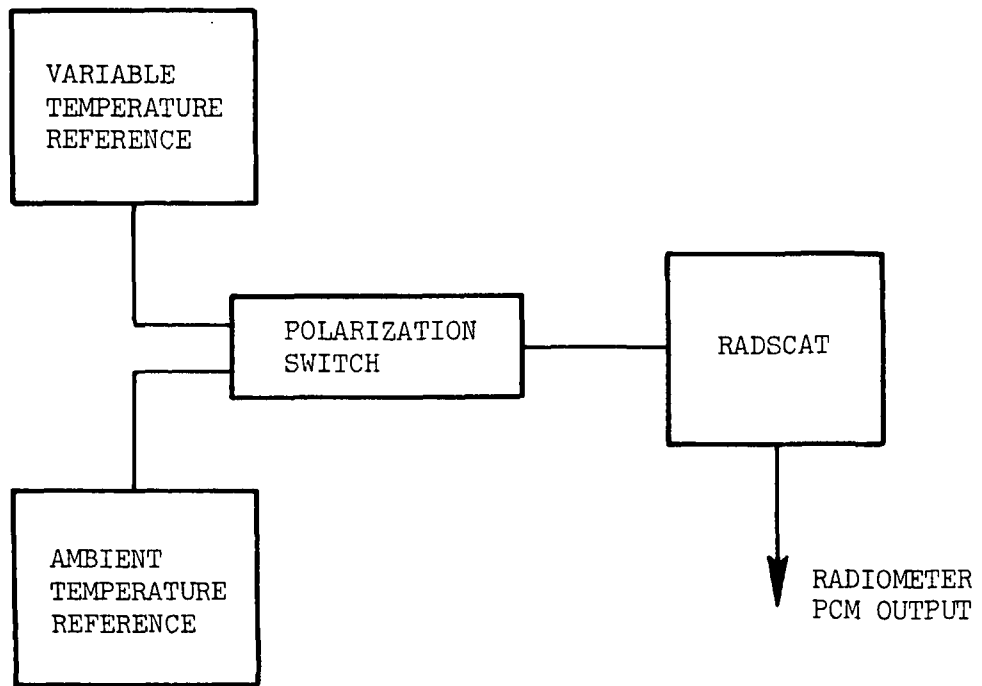


FIGURE 32.- RADSCAT RADIOMETER CALIBRATION EQUIPMENT SET-UP.

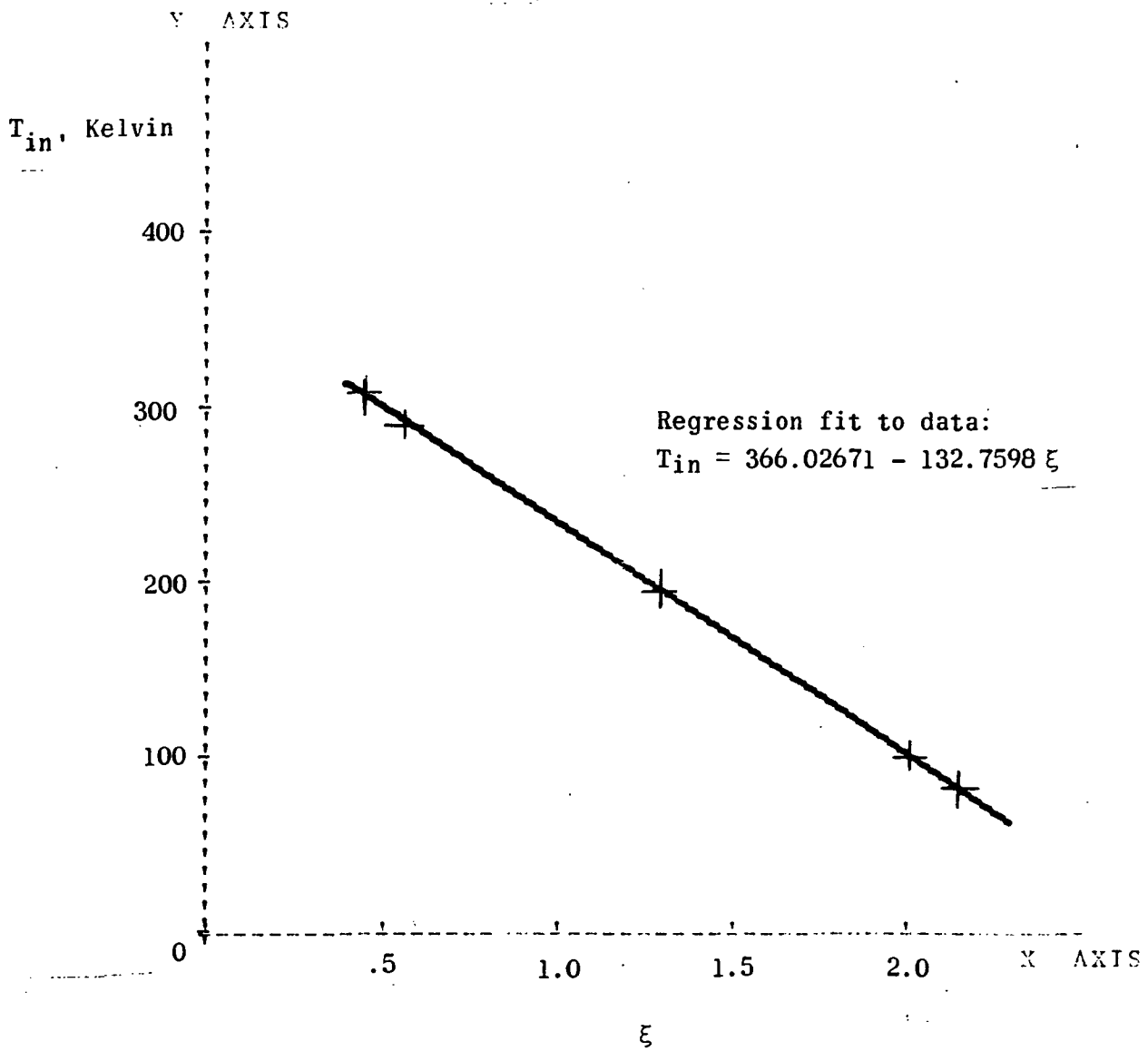


Figure 33.- Typical RADSCAT Radiometer calibration test results (10/18/72).

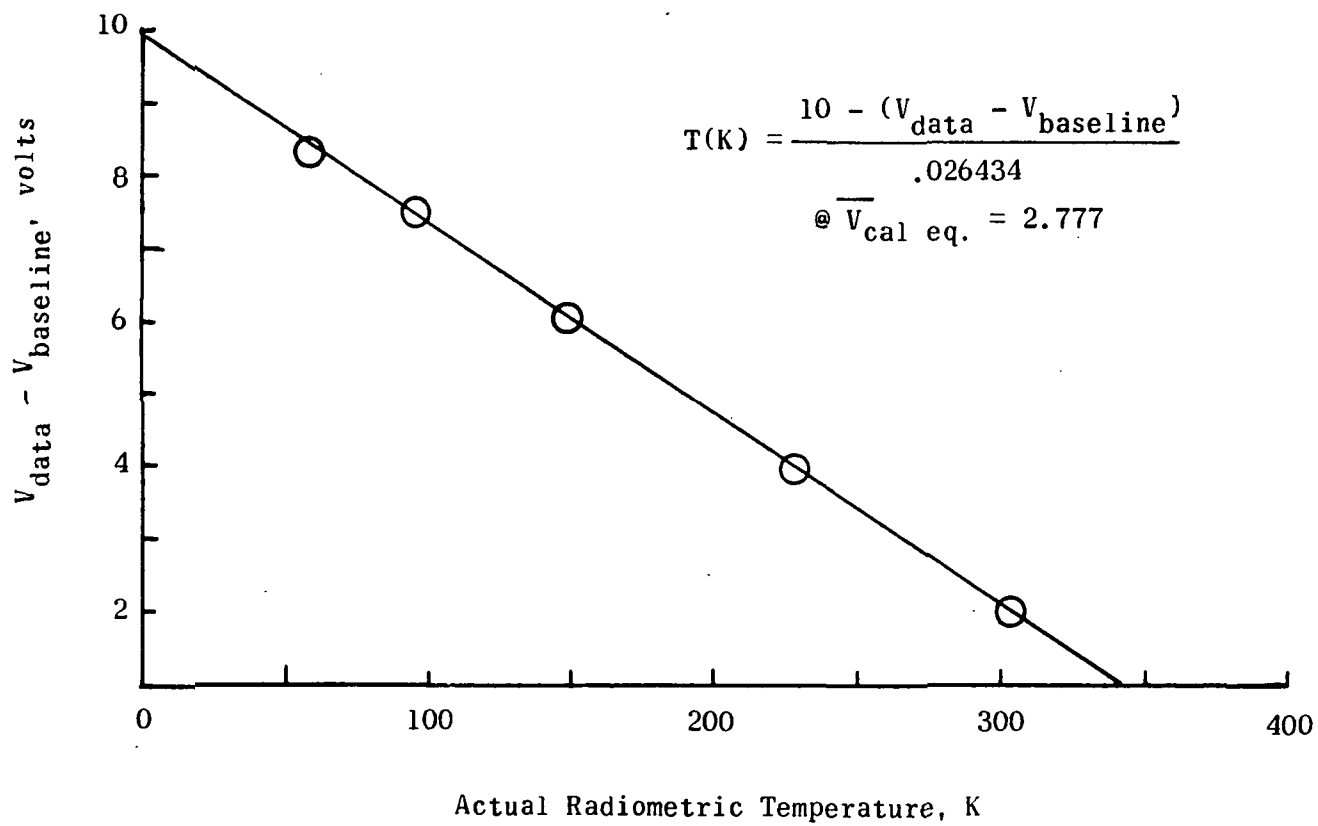


Figure 34.- RAD linearity - LaRC Test 3.



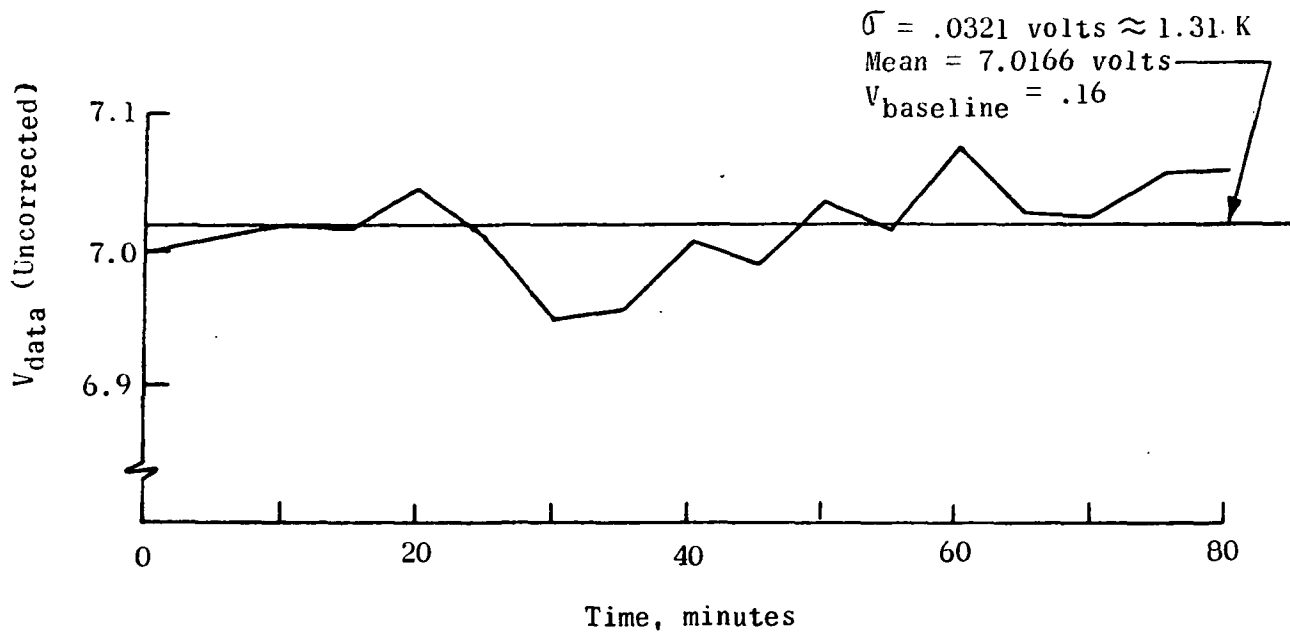


Figure 35.- RAD long term stability (100 K).

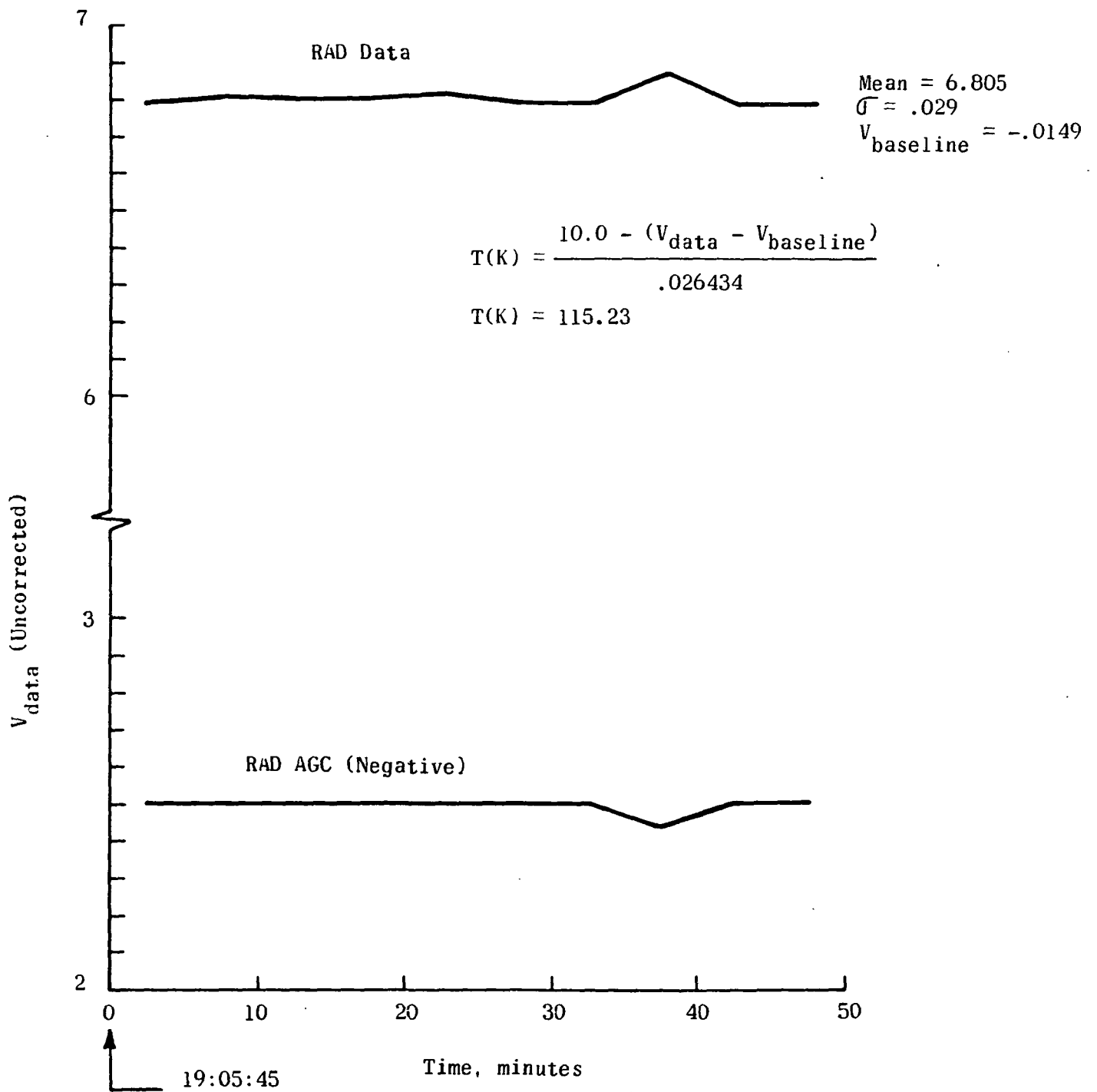


Figure 36.- RAD stability - Houston Ground Tests.

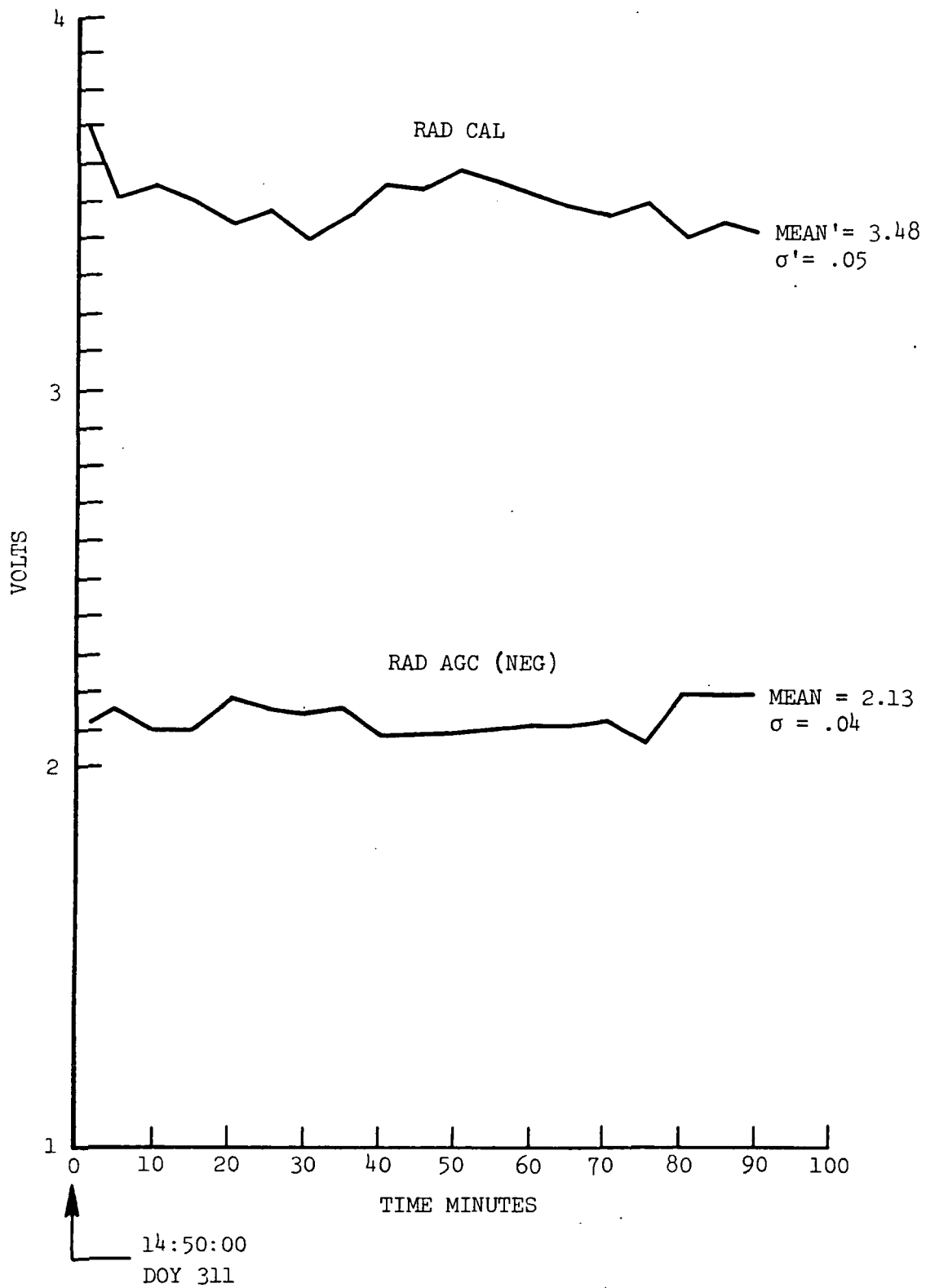


Figure 37.- Radiometer Stability Test No. 46.

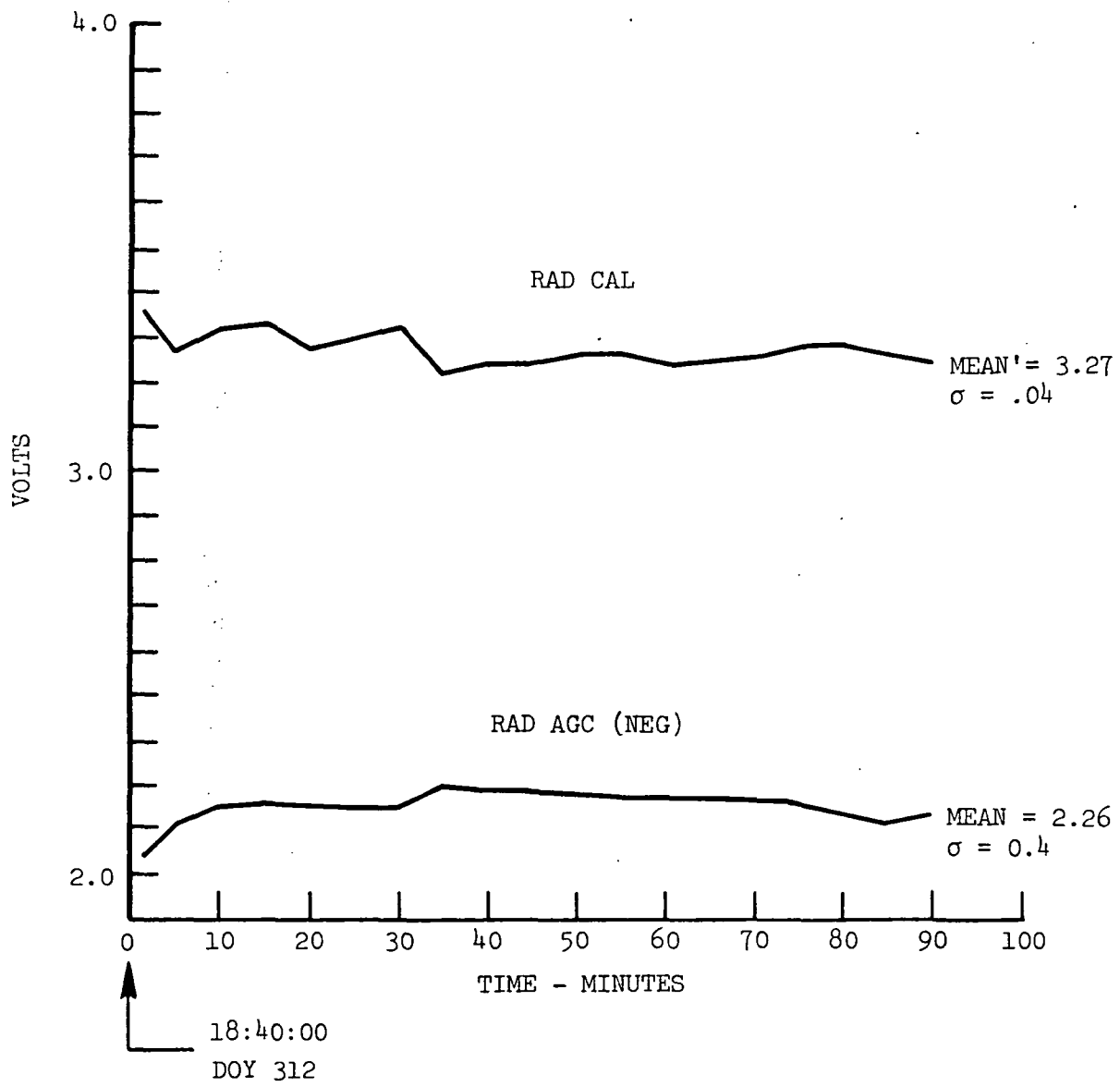
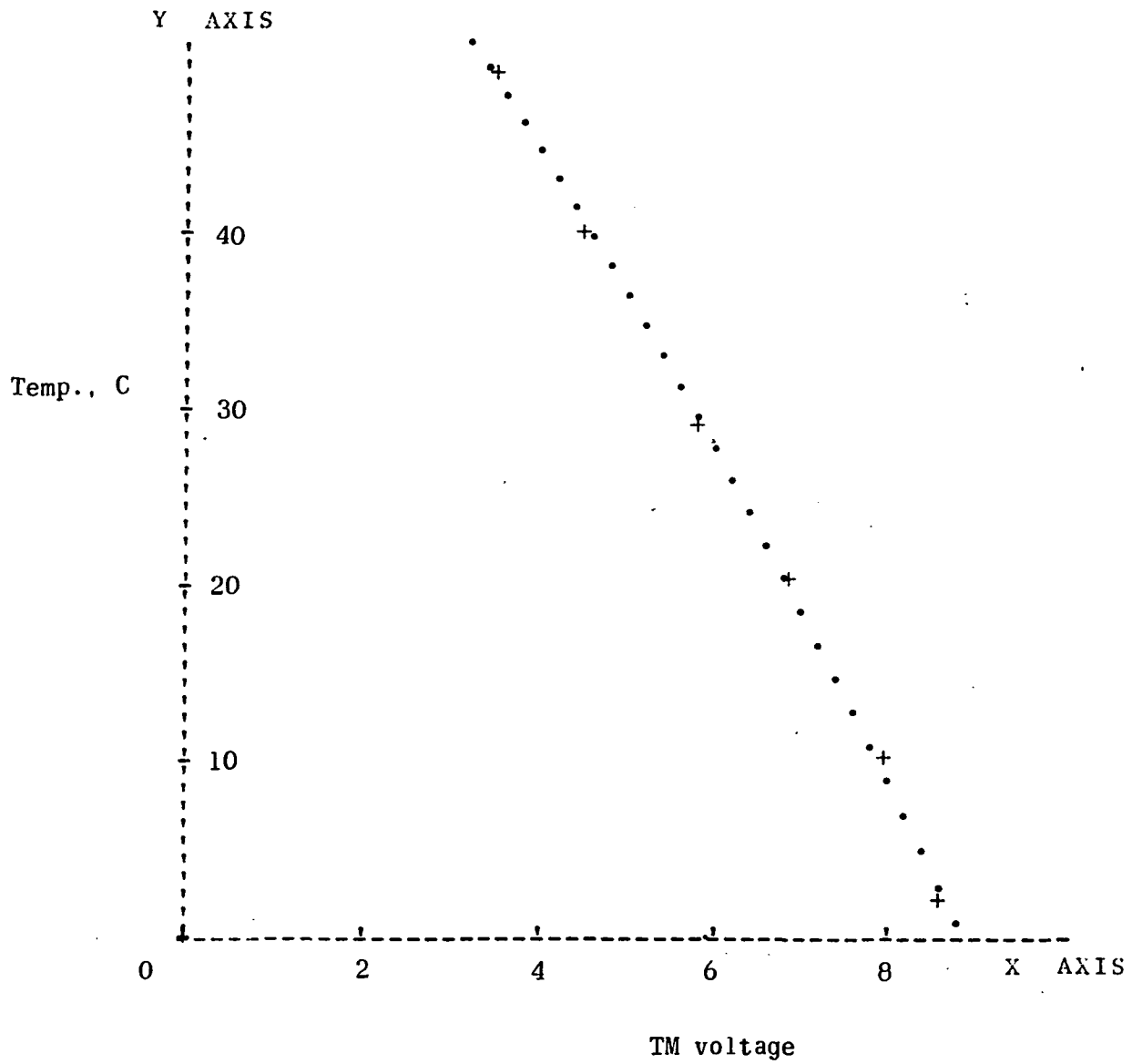


Figure 38.- Radiometer Stability Test No. 50.



Regression Constants

b(0) = 72.43083  
 b(1) = -6.03483  
 b(2) = - .24134

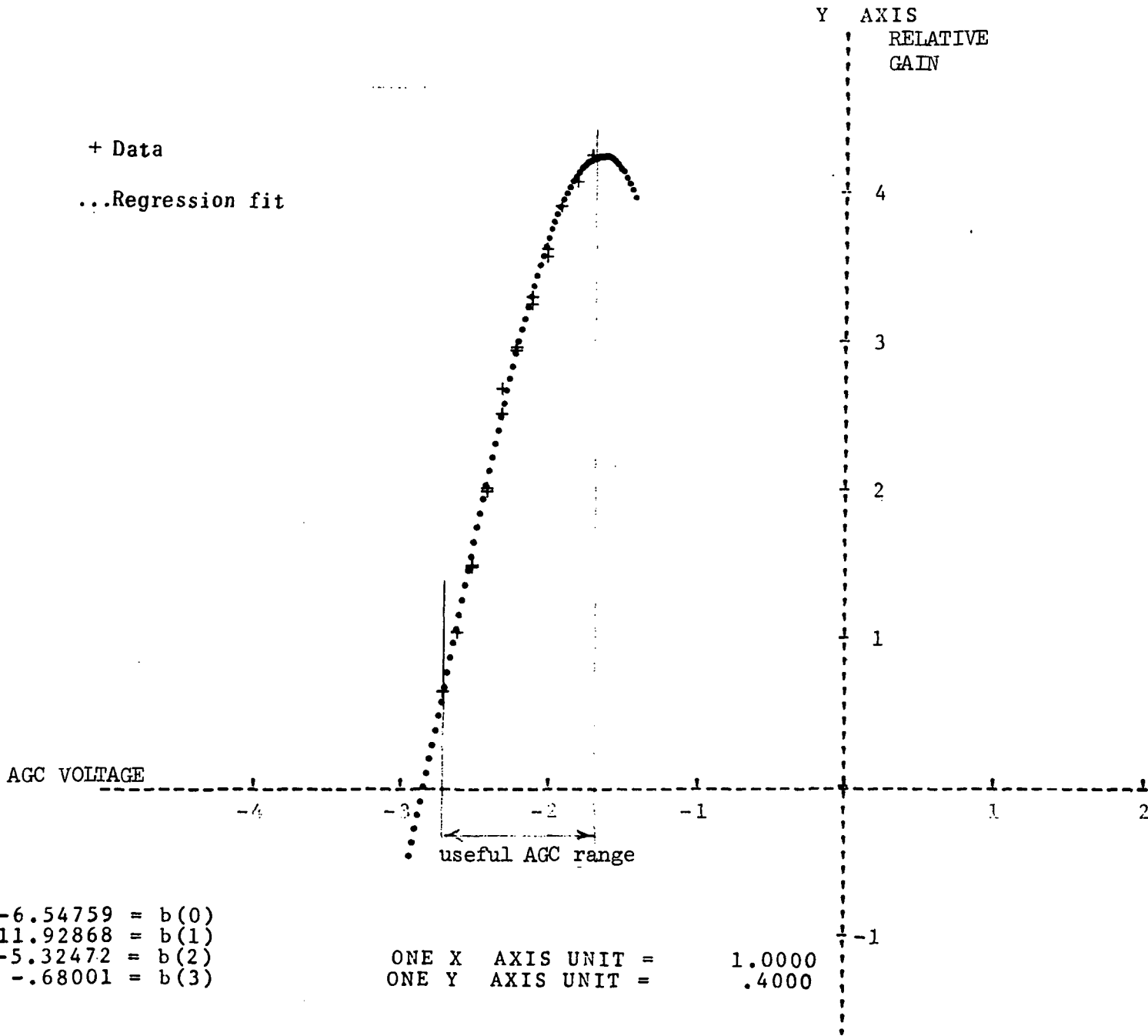
+ Data

...Regression fit

Figure 39.- Typical plot of temperature- TM voltage conversion curve for thermistor 1, and regression fit to data (2nd Order).

th  
n ORDER REGRESSION ANALYSIS

$$y = b(0) + b(1)x + \dots + b(n)x^n$$



(a) 9.3 GHz - Test 10-1, 3/27/73.

Figure 40.- RADSCAT radiometer AGC curve.

th  
n ORDER REGRESSION ANALYSIS

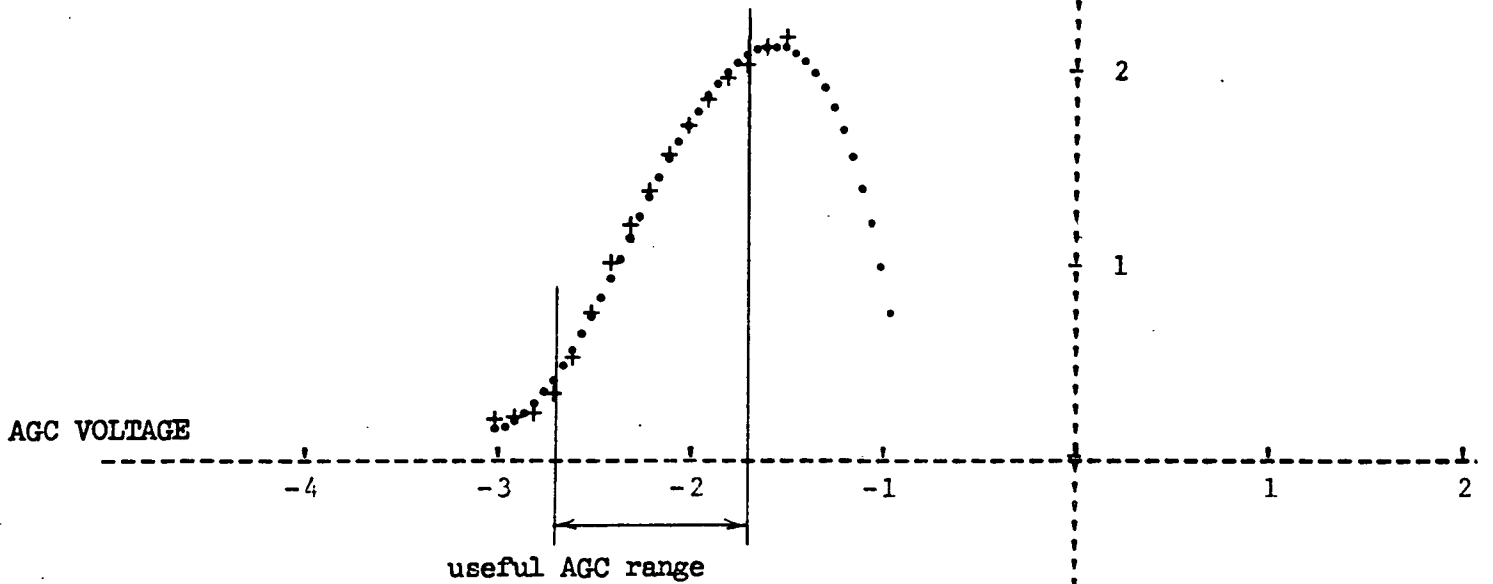
$$y = b(0) + b(1)x + \dots + b(n)x^n$$

Y AXIS

RELATIVE  
GAIN

+ Data

...Regression fit

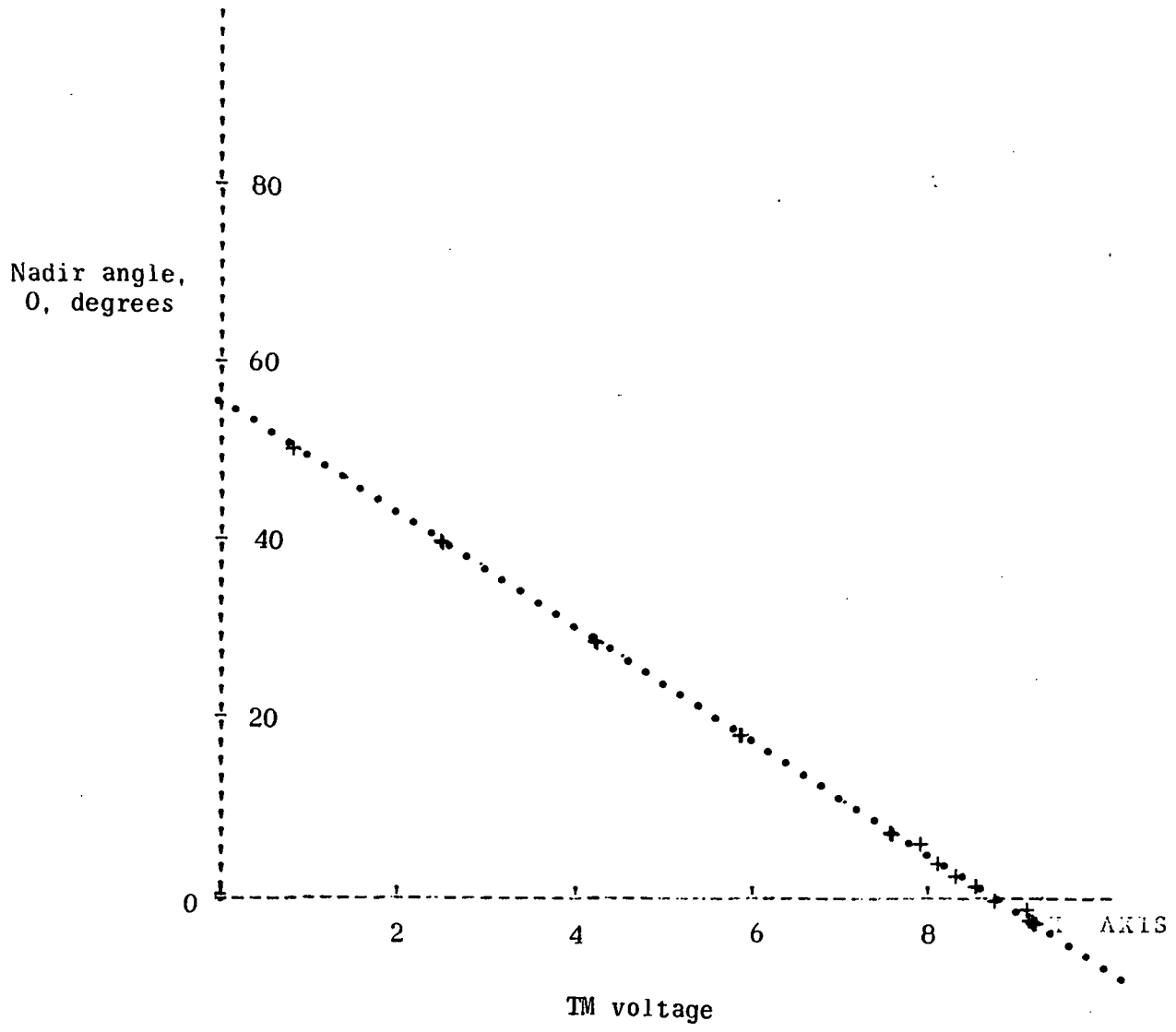


-3.72394 = b(0)  
-18.23593 = b(1)  
-8.81586 = b(2)  
-1.27742 = b(3)

ONE X AXIS UNIT = 1.0000  
ONE Y AXIS UNIT = 1.0000

(b) 13.9 GHz - Test 10-2, 3/27/73.

Figure 40.- (Concluded).



Regression Constants

b(0) = 55.57864                   + Data  
 b(1) = -6.39927                   ...Regression fit

Figure 41.- Antenna angle - TM voltage conversion curve,  
 and regression fit to data (1st order).



Appendix 1: Scatterometer Transfer Function

The derivation of the scatterometer transfer function was developed in reference 1 and is presented in this section. The transfer function converts the instrument output voltages to normalized radar cross section. The RADSCAT scatterometer model is shown in figure Al-1. For convenience the transmitting signal paths  $G_{VT}$ ,  $G_{HVT}$ ,  $G_{HT}$ , and  $G_{VHT}$  and the receiving signal paths  $G_{VR}$ ,  $G_{HVR}$ ,  $G_{HR}$ , and  $G_{VHR}$  have been separated into individual gain (loss) elements. Each element accounts for the total insertion loss (mismatch and dissipative loss).

During the RADSCAT calibration period, the transmitter power is sequentially routed (during four 100 msec periods) through the SCAT CAL attenuators  $A_1$ ,  $A_2$ ,  $A_3$  and  $A_4$ , and the respective channel output is noted. The resulting output voltage for the  $i$ th channel is

$$V_i^{(c)} = d^2 P_x G_c G_R A_i \alpha_i I_i \tau_c \quad (A1-1)$$

where  $d$  = the effective duty factor  $2 \mu s / 80 \mu s$

$P_x$  = peak transmitted power

$\tau_c$  = calibration integration period

(c) = superscript meaning calibration mode

The factor  $d^2$  occurs in the above expression because only the carrier component of the received spectrum is accepted by the receiver. Solving for the transmitter power yields

$$P_x^1 = \frac{V_i^{(c)}}{d^2 G_c G_R A_i \alpha_i I_i \tau_c} \quad (A1-2)$$

During measurements at VV polarization and incident angle  $\theta$ , the received power at the antenna termination is

$$P_r = \frac{\lambda^2}{256\pi^2} \frac{G^2 \theta_{eq}^2}{R^2 \cos \theta_o} \sigma_{VV}^o P_t = K \sigma_{VV}^o P_t \quad (A1-3)$$

At the input to the receiver the power is

$$P_{VV} = K [(\sigma_{VV}^o P_x G_{VT})^{1/2} e^{j\theta_{VV}} + (\sigma_{VH}^o P_x G_{HVT})^{1/2} e^{j\theta_{VH}}]$$

$$[\sqrt{G_{VR}} e^{j\phi_{VV}} + \sqrt{G_{HVR}} e^{j\phi_{HV}}] + [(\sigma_{HH}^o P_x G_{HVT})^{1/2} e^{j\theta_{HH}} + (\sigma_{HV}^o P_x G_{VT})^{1/2} e^{j\theta_{HV}}]$$

$$[\sqrt{G_{HR}} e^{j\phi_{HH}} + \sqrt{G_{VHR}} e^{j\phi_{VH}}]^2 \quad (A1-4)$$

where  $\sigma_{mn}^o$  = normalized cross section for transmission at polarization n and reception at polarization m.

$\theta_{mn}$  = phase of the mn component of the scattered field.

$\phi_{mn}$  = phase shift of mn receiving signal path.

The signal out of both the antenna the vertical and horizontal ports is the vector sum of the backscattered voltage at the direct and cross polarization.

Similarly for observations at HH polarization the power at the receiver input is

$$\begin{aligned}
 P_{HH} = K & \left[ (\sigma_{HH}^o P_x G_{HT})^{1/2} e^{j\theta_{HH}} + (\sigma_{HV}^o P_x G_{VHT})^{1/2} e^{j\theta_{HV}} \right] \left[ \sqrt{G_{HR}} e^{j\phi_{HH}} \right. \\
 & \left. + \sqrt{G_{VHR}} e^{j\phi_{VH}} \right] + \left[ (\sigma_{VV}^o P_x G_{VHT})^{1/2} e^{j\theta_{VV}} + (\sigma_{VH}^o P_x G_{HT})^{1/2} e^{j\theta_{VH}} \right] \\
 & \left[ \sqrt{G_{VR}} e^{j\phi_{VV}} + \sqrt{G_{HVR}} e^{j\phi_{HV}} \right] \quad (A1-5)
 \end{aligned}$$

The expressions Al-4 and Al-5 may be simplified since cross coupling terms  $\sigma_{mn}^o G_{nMT}$  and  $G_{mnR}$  are small and may be neglected. Also when the waveguide polarization switch is used, the term which contains  $G_{NR}$  ( $G_{VR}$  for HH polarization and  $G_{HR}$  for VV) is small and may be neglected. The simplified expressions are

$$P_{VV} \approx K \sigma_{VV}^o P_x G_{VT} G_{VR} \quad (A1-6)$$

$$P_{HH} \approx K \sigma_{HH}^o P_x G_{HT} G_{HR} \quad (A1-7)$$

The corresponding on-scale output voltage for these measurements occur on say, channels  $j$  and  $k$ , respectively. The outputs are given by

$$V_{jm}^{(o)} = P_{VV} d^2 G_R^{A_1} \alpha_j G_j I_j \tau_m \quad (A1-8)$$

and

$$V_{km}^{(o)} = P_{MW} d^2 G_R^{A_1} \alpha_k G_k I_k \tau_m \quad (A1-9)$$

where  $\tau_m$  = measurement integration time

$$m = 1, 2, \dots, 7$$

(o) = superscript meaning operation mode

A subscript is employed on  $\tau$  to identify the different integration periods associated with six angle indicators (1 through 6) for the ALTERNATING and FIXED ANGLE MODES and the integration period  $\tau_1$  for the SHORT SCAT mode.

Now equations (A1-8) and (A1-9) may be employed to express the receiver input power. Thus we may write

$$\frac{V_{jm}^{(o)}}{d^2 G_R^{A_1} \alpha_j G_j I_j \tau_m} = K \sigma_{VV}^o P_x G_{VT} G_{VR} \quad (A1-10)$$

$$\frac{V_{km}^{(o)}}{d^2 G_R^{A_1} \alpha_k G_k I_k \tau_m} = K \sigma_{HH}^o P_x G_{HT} G_{HR} \quad (A1-11)$$

Now  $P_x$  may be replaced by expression (A1-2) for the corresponding output channel to yield the desired results

$$\sigma_{VV}^o(\theta_o) = \frac{V_{jm}^{(o)}}{V_j^{(c)}} \frac{\tau_c}{\tau_m} \frac{G_c A_j}{G_{VR} G_{VT} A_1} \frac{256\pi^2 R^2 \cos\theta_o}{\lambda^2 G^2 \theta_{eq}^2} \quad (A1-12)$$

and

$$\sigma_{HH}^o(\theta_o) = \frac{V_{km}^{(o)}}{V_k^{(c)}} \frac{\tau_c}{\tau_m} \frac{G_c A_k}{G_{HR} G_{HT} A_1} \frac{256\pi^2 R^2 \cos\theta_o}{\lambda^2 G^2 \theta_{eq}^2} \quad (A1-13)$$

It is noted that the receiver gain terms have dropped out.

Missing from these algebraic expressions is the doppler filter gain factor which is a function of the doppler frequency shift. The gain is normalized with respect to the gain at zero doppler since the calibrations are made there. Presently the gain function is sampled at 250 Hz intervals. To compensate the measurement the relative doppler gain must divide the selected channel output,  $V_{jm}^{(o)}$ .

ORIGINAL PAGE IS  
OF POOR QUALITY

ORIGINAL PAGE IS  
OF POOR QUALITY

IDEAL  
ANTENNAS

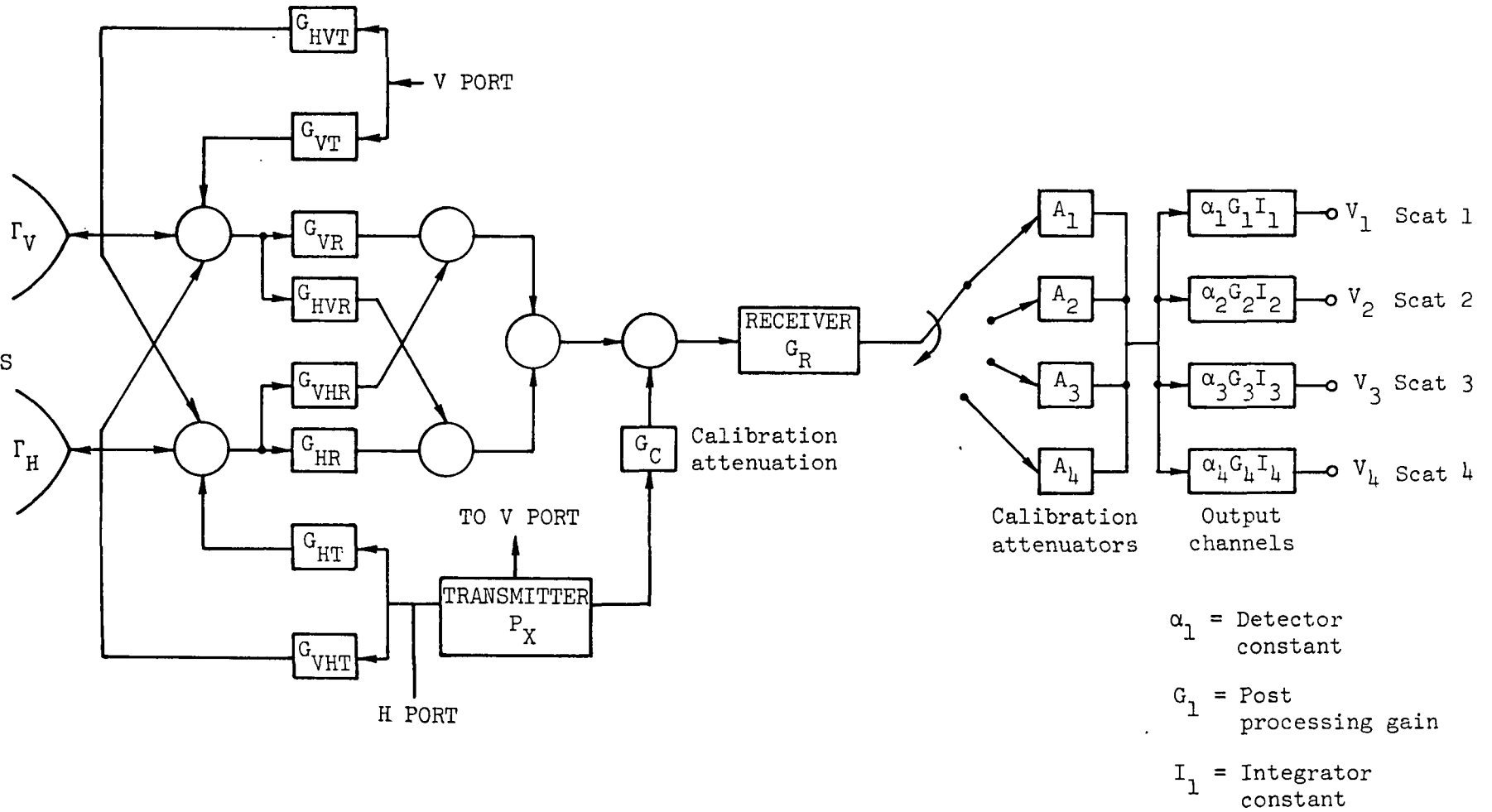


Figure A1-1.- RADSCAT scatterometer model.

## Appendix 2: Radiometer Transfer Function

## Summary

The transfer functions for the AAFE RADSCAT radiometer have been previously developed by others. These approaches derived the radiometer equations using standard transmission line theory. The most general model\* considered the complex voltage reflection coefficients, where as another (ref. 5) used only the absolute magnitude. However, the final equations of both models were simplified to consider only the first order effects of reflections without phase. The model derived in this section differs from these in two respects. First, second order reflections are included where they are significant; second, the equations are developed using different component groupings by subsystems to take advantage of laboratory measurements of RADSCAT transfer functions. Like the others, this model neglects the phase of the reflection coefficient, even though it does consider multiple and second order reflections. This approach is justified because the radiometer signals are broad-band noise which should combine in an incoherent manner.

The block diagram for the radiometer model consists of the microwave portion of RADSCAT from the receiver port of the waveguide polarization switch to the output of the Dicke switch assembly. It is given in figure A2-1. The four radiometer equations are written for the output power which correspond

---

\*Claassen, John: The RADSCAT Radiometry Transfer Function and its Applications to the Reduction of RADSCAT Data. Univ. of Kansas, CRES TM 186-3, Dec. 1971.

to the possible positions of the circulator switches ( $C_1$  and  $C_2$ ) in the Dicke switch assembly. The equations are written in terms of temperature which is conventionally assumed to be related to power by

$$P = KTB$$

where  $P$  = noise power

$K$  = Boltzman's constant

$T$  = radiometric temperature

$B$  = bandwidth

In the equations the following symbols are used.

#### Symbols

$t$  = transmission coefficient

$L$  = dissipative loss in dB

$\Gamma$  = magnitude of voltage reflection coefficient

$t_{fC_i}$  = transmission coefficient in the forward (low loss) direction for circulator  $C_i$

$t_{rC_i}$  = transmission coefficient in the reverse (high loss) direction for circulator  $C_i$

$T_n$  = thermometric temperature of nth component or subsystem

$T_{IN}$  = input radiometric temperature

$T_{REC}$  = output radiometric temperature (input to receiver)

#### Rad Model Development

Equation I ( $C_2$  in antenna,  $C_3$  alternating)

The time average output power (input to the receiver) for the circulator switch  $C_2$  in the antenna position (ie: coupling from ports 1 to 3 equals the forward direction) and switch  $C_3$  alternating between the two



temperature references (hot and warm loads) is:

$$I = T_A t_a + T_B t_{fC_2} + T_C + T_D t_b \quad (A2.1)$$

where

$$\begin{aligned} T_A &= \text{effective temperature at output of circulator } C_7 \\ &= \{[(1 - \Gamma_1^2)t_2[T_{IN}t_1 + T_9(1 - t_1)] + T_3(1 - t_2)](1 - \Gamma_2^2)t_{fC_7} \\ &\quad + T_3(1 - t_{fC_7}) \\ &\quad + [T_3(1 - t_3) + T_{13}(1 - \Gamma_3^2)t_3](1 - \Gamma_{13}^2)(t_{rC_7} + t_{fC_7}(\Gamma_2^2 + t_2^2\Gamma_1^2)t_{fC_7})\} \end{aligned} \quad (A2.2)$$

$$\begin{aligned} t_a &= \text{transmission coefficient from output (port 2) of circulator } C_7 \\ &\quad \text{to the receiver input - with switch } C_2 \text{ connected to the antenna} \\ &= (1 - \Gamma_{10}^2)t_4(1 - \Gamma_4^2)(1 - \Gamma_5^2)t_5(1 - \Gamma_6^2)t_{fC_2} \end{aligned} \quad (A2.3)$$

$$\begin{aligned} T_B &= \text{temperature biases from losses between circulators } C_7 \text{ and } C_2 \\ &= [T_3(1 - t_4)(1 - \Gamma_4^2)(1 - \Gamma_5^2)t_5 + T_2(1 - t_5)][1 - \Gamma_6^2] \end{aligned} \quad (A2.4)$$

$$\begin{aligned} T_C &= \text{temperature bias from losses in } C_2 \\ &= T_4(1 - t_{fC_2}) \end{aligned} \quad (A2.5)$$

$$\begin{aligned} T_D &= \text{equivalent (time average) Dicke reference temperature} \\ &= 1/2\{[T_{HT}t_7 + T_4(1 - t_7)][(1 - \Gamma_9^2)(1 - \Gamma_{16}^2)t_{fC_3}] \\ &\quad + T_{11}(1 - \Gamma_{17}^2)t_{fC_3} + 2T_4(1 - t_{fC_3})\} \end{aligned} \quad (A2.6)$$

$$\begin{aligned} t_b &= \text{transmission coefficient from ports 2 to 3 of circulator } C_2 \\ &\quad \text{(with switch in the antenna position).} \\ &= [(1 - \Gamma_8^2)(1 - \Gamma_{11}^2)][t_{rC_2} + t_{fC_2}(\Gamma_6^2 + t_5^2(\Gamma_5^2 + \Gamma_4^2))t_{fC_2}] \end{aligned} \quad (A2.7)$$

Equation II ( $C_2$  in calibrate,  $C_3$  alternating)

Next the equation is written for the average output power when the circulator switch  $C_2$  is in the calibrate position (ie: coupling from ports 2 to 3 equals the forward direction) and switch  $C_3$  is alternating

between the two temperature references. This equation can be expressed as the average of two equations III and IV.

$$II = 1/2\{III + IV\} \quad (A2.8)$$

where equation III is for switch  $C_3$  in the hot load position and equation IV is for switch  $C_3$  in the warm load position.

Equation III ( $C_2$  in calibrate,  $C_3$  in hot load)

$$III = T_A t_c + T_B t_{rC_2} + T_C + T_E t_d \quad (A2.9)$$

where

$$\begin{aligned} t_c &= \text{transmission coefficient from output (port 2) of circulator } C_7 \\ &\text{to the receiver input - with switch } C_2 \text{ in the calibration position.} \\ &= [(1 - \Gamma_{10}^2)t_4(1 - \Gamma_4^2)(1 - \Gamma_5^2)t_5(1 - \Gamma_6^2)][t_{rC_2} + t_{fC_2}(\Gamma_{11}^2 + \Gamma_8^2)t_{fC_2}] \end{aligned} \quad (A2.10)$$

$T_E$  = effective temperature of hot load with switch  $C_3$  in the hot load position

$$\begin{aligned} &= \{[T_{HT}t_7 + T_4(1 - t_7)][(1 - \Gamma_9^2)(1 - \Gamma_{16}^2)t_{fC_3}] + T_4(1 - t_{fC_3}) \\ &\quad + T_{11}(1 - \Gamma_{17}^2)t_{rC_3}\} \end{aligned} \quad (A2.11)$$

$t_d$  = transmission coefficient from ports 2 to 3 of circulator  $C_2$  (with the switch in the calibration position).

$$= [(1 - \Gamma_8^2)(1 - \Gamma_{11}^2)][t_{fC_2} + t_{rC_2}(\Gamma_6^2 + t_5^2(\Gamma_5^2 + \Gamma_4^2))t_{rC_2}] \quad (A2.12)$$

Equation IV ( $C_2$  in calibrate,  $C_3$  in warm load)

$$IV = T_A t_c + T_B t_{rC_2} + T_C + T_F t_d \quad (A2.13)$$

where

$T_F$  = effective temperature of warm load with switch  $C_3$  in the warm load position

$$= \{ [T_{HT} t_7 + T_4 (1 - t_7)] [(1 - \Gamma_9^2)(1 - \Gamma_{16}^2) t_{rC_3}] + T_4 (1 - t_{rC_3}) + T_{11} (1 - \Gamma_{17}^2) t_{rC_3} \} \quad (A2.14)$$

From the law of thermodynamic equilibrium, if all T's were set equal to the ambient temperature then equations I, III, and IV should also equal the ambient temperature. Any differences are due to errors in the transmission coefficient used. A list of the transmission coefficients used are given in table A2-I. The temperatures were set equal to unity (which is equivalent to normalizing the equations to the ambient temperature) and the following results were calculated:

$$I = 1.0010$$

$$III = 1.0276$$

$$IV = 1.0390$$

These factors are well within the experimental accuracy of the transmission coefficient measurements. The equations were normalized by these factors to exactly satisfy the thermodynamic considerations. After this normalization the equations are;

$$I = .6398 T_{IN} + .0364 T_9 + .2212 T_3 + .0148 T_{13} + .0151 T_2 + .0598 T_4 + .0083 T_{HT} + .0086 T_{11} \quad (A2.15)$$

$$\begin{aligned} \text{III} = & .0021 T_{\text{IN}} + .0001 T_9 + .0007 T_3 + .9034 T_{\text{HT}} \\ & + .0907 T_4 + .0029 T_{11} \end{aligned} \quad (\text{A2.16})$$

$$\begin{aligned} \text{IV} = & .0021 T_{\text{IN}} + .0001 T_9 + .0008 T_3 + .0753 T_4 + .0028 T_{\text{HT}} \\ & + .9191 T_{11} \end{aligned} \quad (\text{A2.17})$$

and calculation equation II yields;

$$\begin{aligned} \text{II} = & .0021 T_{\text{IN}} + .0001 T_9 + .0007 T_3 + .0830 T_4 \\ & + .4610 T_{11} + .4531 T_{\text{HT}} \end{aligned} \quad (\text{A2.18})$$

The relationships between the radiometer output voltage and equations I, II, III, and IV are now derived through the use of a simplified block diagram given in figure A2-2. The output of the radiometer model,  $T_{\text{REC}}$ , is linearly amplified and then square law detected. The detector output is therefore linear with  $T_{\text{REC}}$ .

The voltage output from the integrator is;

$$V_{\text{OUT}} = gK \tau_m T_{\text{REC}} \quad (\text{A2.19})$$

where

$g$  = amplifier gain

$K$  = square law detector coefficient

$\tau_m$  = integration time in each radiometer mode, ms ( $\tau_{\text{OP}} = 128$  ms;

$\tau_{\text{cal}} = 100$  ms)

$T_{\text{REC}}$  = power input to the receiver (defined by equations I, II, III and IV).

Case I.- Operate mode ( $\tau_{OP} = 128$  ms, Equation I appropriate)

$$V_{OP} = gK (\tau_{OP}) I \quad (A2.20)$$

Case II.- Calibrate mode ( $\tau_{cal} = 100$  ms, Equation II appropriate)

$$V_{CAL} = qK (\tau_{cal}) II \quad (A2.21)$$

Case III.- Baseline mode ( $\tau = 128$  ms)

As previously discussed, in the baseline mode the output voltage is ideally zero because  $T_{REC}$  is effectively (II - II).

$$(V_{Bl})_{IDEAL} = gK(II-II)(\tau_{OP}) = 0 \quad (A2.22)$$

For the actual case however, nonsymmetry in circulator switches  $C_2$  and  $C_3$  make II-II non zero, and offset voltages for the operational amplifier integrator are also non zero. The resulting baseline voltage therefore represents a bias which must be subtracted from the operate voltage and from  $(\tau_{OP}/\tau_{cal})$  times the calibration voltage. The adjusted equations for the voltages are therefore

$$(V_{OP} - V_{Bl}) = gK (\tau_{OP}) I \quad (A2.23)$$

$$\left(\frac{\tau_{OP}}{\tau_{cal}} V_{CAL} - V_{Bl}\right) = gK \left(\frac{\tau_{OP}}{\tau_{cal}}\right)(\tau_{cal})II \quad (A2.24)$$

Taking the ratio of the equations yields

$$\xi = \frac{(V_{OP} - V_{Bl})}{\left(\frac{\tau_{OP}}{\tau_{cal}} V_{cal} - V_{Bl}\right)} = \frac{I}{II} \quad (A2.25)$$

Solving this equation for the unknown input temperature,  $T_{IN}$ , yields

$$\begin{aligned} T_{IN} = & \xi[1.4367 T_{11} - 1.4123 T_{HT} - .0241 T_4] - .0569 T_9 - .3458 T_3 \\ & + .0364 T_4 + .6975 T_{HT} + .7094 T_{11} - .0232 T_{13} - .0237 T_2 \end{aligned} \quad (A2.26)$$

TABLE A2-1.- RADIOMETER TRANSMISSION AND REFLECTION COEFFICIENTS

TRANSMISSION COEFFICIENTS			REFLECTION COEFFICIENTS	
<u>Element</u>	<u>Loss, dB</u>	<u>Value</u>	<u>Element</u>	<u>Value</u>
L <sub>1</sub>	0.24	0.9462	Γ <sub>1</sub>	0.127
L <sub>2</sub>	0.40	0.9120	Γ <sub>2</sub>	0.070
L <sub>3</sub>	0.40	0.9120	Γ <sub>3</sub>	0.070
L <sub>4</sub>	0.40	0.9120	Γ <sub>4</sub>	0.070
L <sub>5</sub>	0.07	0.9840	Γ <sub>5</sub>	0.111
L <sub>7</sub>	0.07	0.9840	Γ <sub>6</sub>	0.0056
L <sub>fC<sub>2</sub></sub> *	0.25	0.9441	Γ <sub>7</sub>	0.083
			Γ <sub>8</sub>	0.0056
L <sub>fC<sub>3</sub></sub>	0.10	0.9772	Γ <sub>9</sub>	0.111
L <sub>fC<sub>7</sub></sub>	0.40	0.9120	Γ <sub>10</sub>	0.048
			Γ <sub>11</sub>	0.0056
L <sub>rC<sub>2</sub>,C<sub>3</sub>,C<sub>7</sub></sub> **	25 dB	0.0031	Γ <sub>12</sub>	0.111
			Γ <sub>13</sub>	0.057
			Γ <sub>15</sub>	0.0056
			Γ <sub>16</sub>	0.0056
			Γ <sub>17</sub>	0.0056

\*f denotes low loss "forward" direction

\*\*r denotes high loss "reverse" direction

ORIGINAL PAGE IS  
OF POOR QUALITY

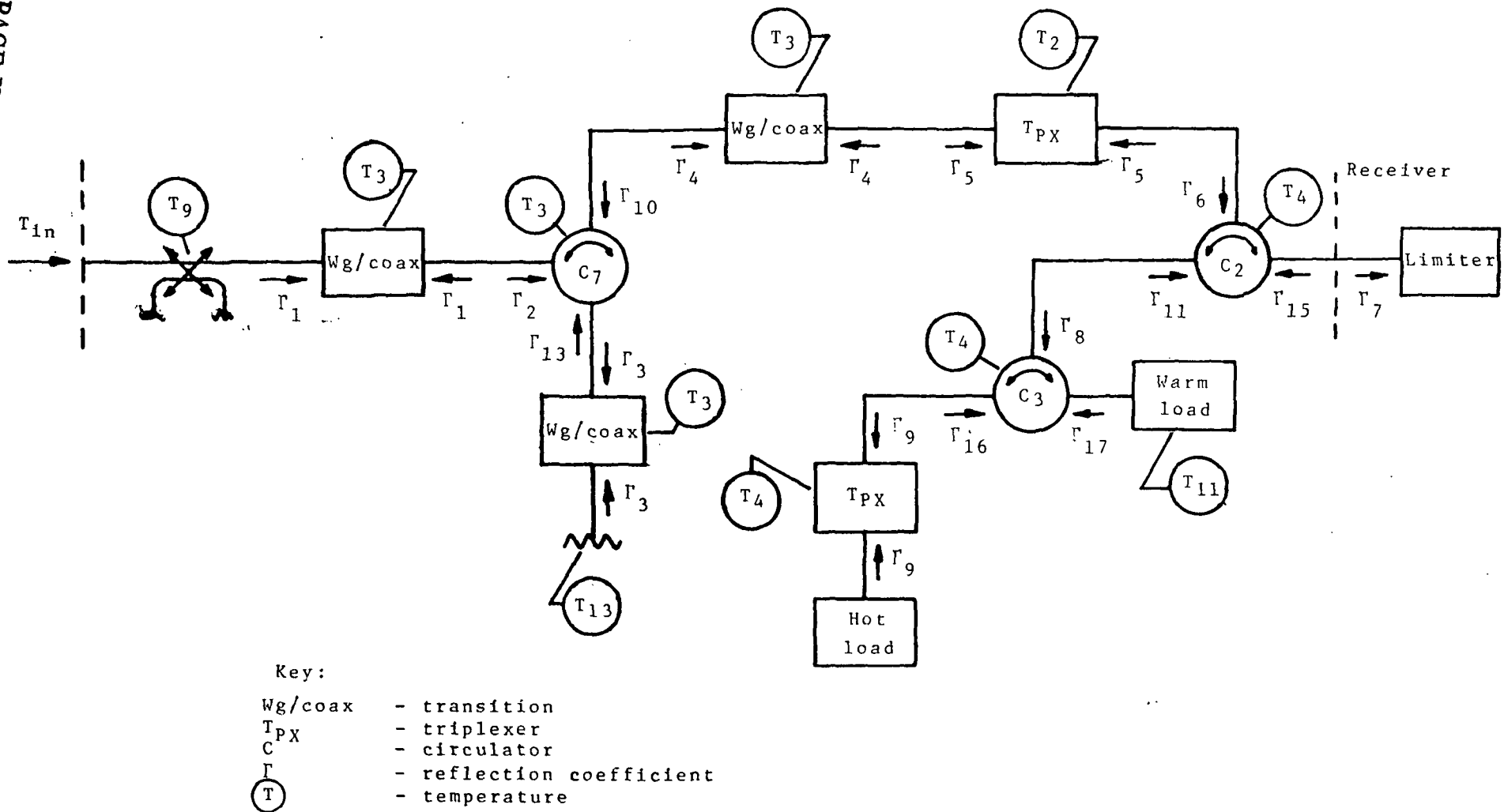


Figure A2-1. - Radiometer block diagram.



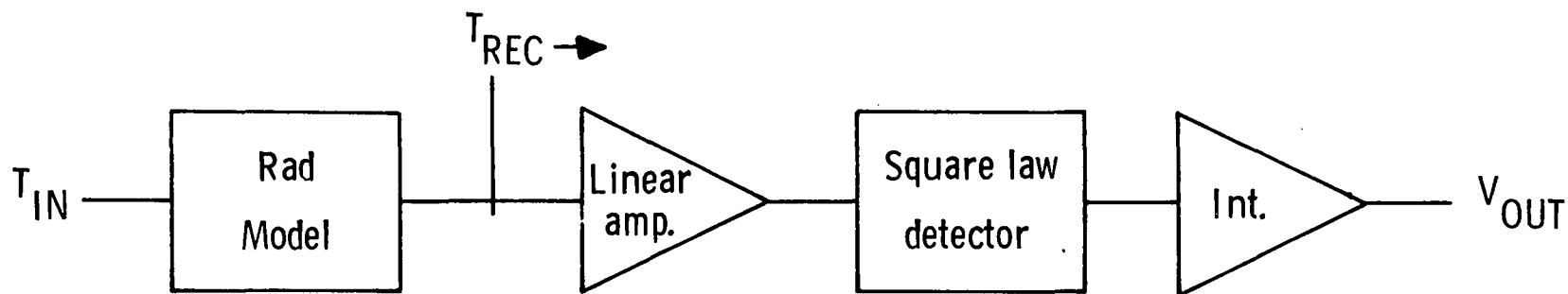


Figure A2-2. - Simplified Radiometer diagram.

## Appendix 3

## Characteristics of the AAFE RADSCAT Antenna\*

## Summary

This appendix gives design and performance information about the antenna supplied for the AAFE RADSCAT. This antenna was basically a parabolic reflector of 113 cm diameter having a feed to diameter ratio of .359. At microwave frequencies, this antenna produced a pencil beamwidth pattern (3 dB beamwidth of  $\sim 1.5^\circ$  at 13.9 GHz). This antenna was used by the RADSCAT instrument until January of 1975, when it was damaged and replaced. Characteristics of the replacement antennas are not discussed here but are available in Reference 2.

## Antenna Design

Reflector and Feed - The antenna design was based on the previously developed rear fed parabolic antenna. The antenna is equipped with interchangeable feeds for dual linear polarization operation at two specific frequencies (9.3 and 13.9 GHz). The effective diameter of the reflector is 44.5 in. and has an F/D of 0.359 (equal to the S-193 reflector). The reflector is a parabolic spinning of 1/8 in. thick aluminum alloy with a 1-1/4 in. dia. beaded rim for stiffening. The feed for 13.9 GHz was previously developed using quartz for the taper dielectric material. Custom Materials Hi K707L with a dielectric constant of 3.9 (equal to Corning 7940 quartz)

\*This information is from "Field Service Procedure Handbook for the AAFE Composite RADiometer-SCATterometer (RADSCAT)", Volume I, by General Electric, Report 735D 4228, April 1973.

was used, however, for the RADSCAT program. Figure A3-1 shows the 13.9 GHz feed assembly mounted in the parabolic reflector. The dimensions for the 9.3 GHz feed were scaled to the 13.9 GHz feed by the frequency ratio. The feed point was located at the focal point of the reflector.

Ortho-Mode Transducer - The ortho-mode transducer (OMT) is used to produce two orthogonal polarization inputs to the circular waveguide of the antenna feed. The Ferrotec models DMT-127 and DMT-135 were chosen based on electrical performance, availability, mechanical interchangeability and interface with the circular guide. The measured isolation between the orthogonal arm of the OMT for the complete antenna assembly radiating into free space is 50 dB for the 9.3 feed and 35 dB for the 13.9 feed.

The insertion loss of the feed/OMT assemblies was measured and found to be:

13.9 GHz	0.16 dB (in line port)
	0.12 dB (coupled arm)
9.3 GHz	0.27 dB (in line port)
	0.26 dB (coupled arm)

#### Antenna Performance

Antenna patterns - Antenna patterns were recorded for the main planes (E and H) of the completed antenna assembly (feed, reflector and OMT) for the dominant and cross polarization. The patterns are shown in Figures A3-2 through A3-5, and the data is tabulated in Tables A3-1, A3-2, and A3-3. Patterns 10, 12, 14, and 16 were integrated by hand calculation at  $0.5^\circ$  intervals to determine main beam efficiency. The efficiency of the main beam is plotted in Figures A3-6 and A3-7, as a function of main beam beamwidth. The main beam efficiency for the RADSCAT antenna is based on three times the 3 dB beamwidth.

VSWR - Final VSWR (voltage standing wave ratio) measurements were performed after pattern tests. The tests were made at the input to the polarization switch. Results are shown in Figures A3-8 and A3-9.

Table A3-1. RADSCAT Antenna Pattern Data

Pattern	9.3 GHz Feed		13.9 GHz Feed	
	Beamwidth (3 dB) degrees	Cross Polarization dB below dominant	Beamwidth (3 dB) degrees	Cross Polarization dB below dominant
E-Plane, In line Arm	2.10	24.0	1.40	47.7
H-Plane, In line Arm	2.38	22.7	1.63	41.0
E-Plane, Side Arm	2.05	22.5	1.42	24.1
H-Plane, Side Arm	2.45	24.0	1.66	21.6

Table A3-2. Measured Antenna Gain

Pattern	9.3 GHz Feed	13.9 GHz Feed
In Line Arm	37.95 dBI	41.5 dBI
Side Arm	37.85	41.6

Table A3-3. Main Beam\* Efficiency (Including Cross Polarization)

Pattern	9.3 GHz Feed	13.9 GHz Feed
E Plane	85.7%	81.88
H Plane	94.3%	95.78
Average ( E & H Plane)	90.0%	88.88
Design Goal	85% min.	85% min.

\*Main Beam = 3 x beamwidth (3 dB)

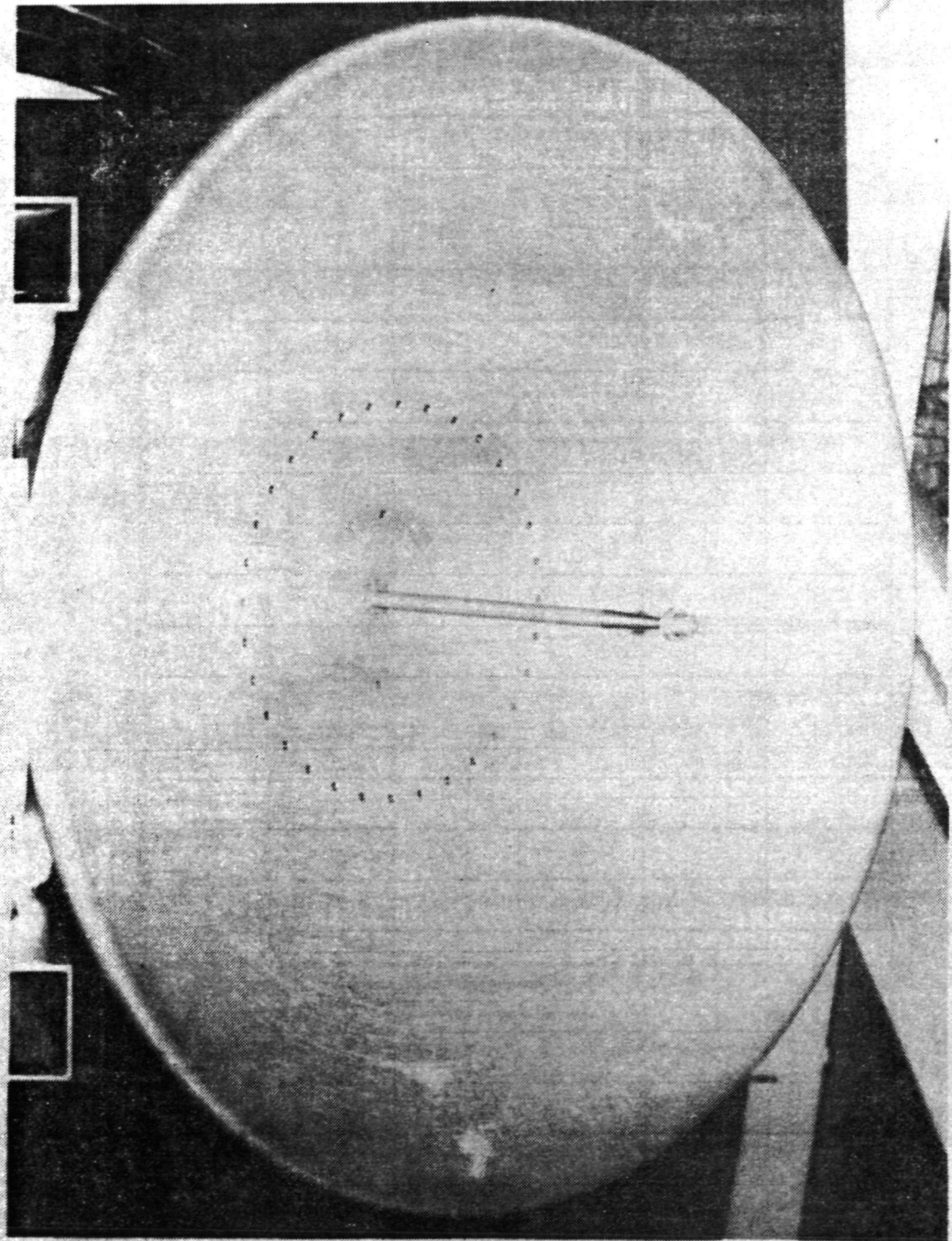
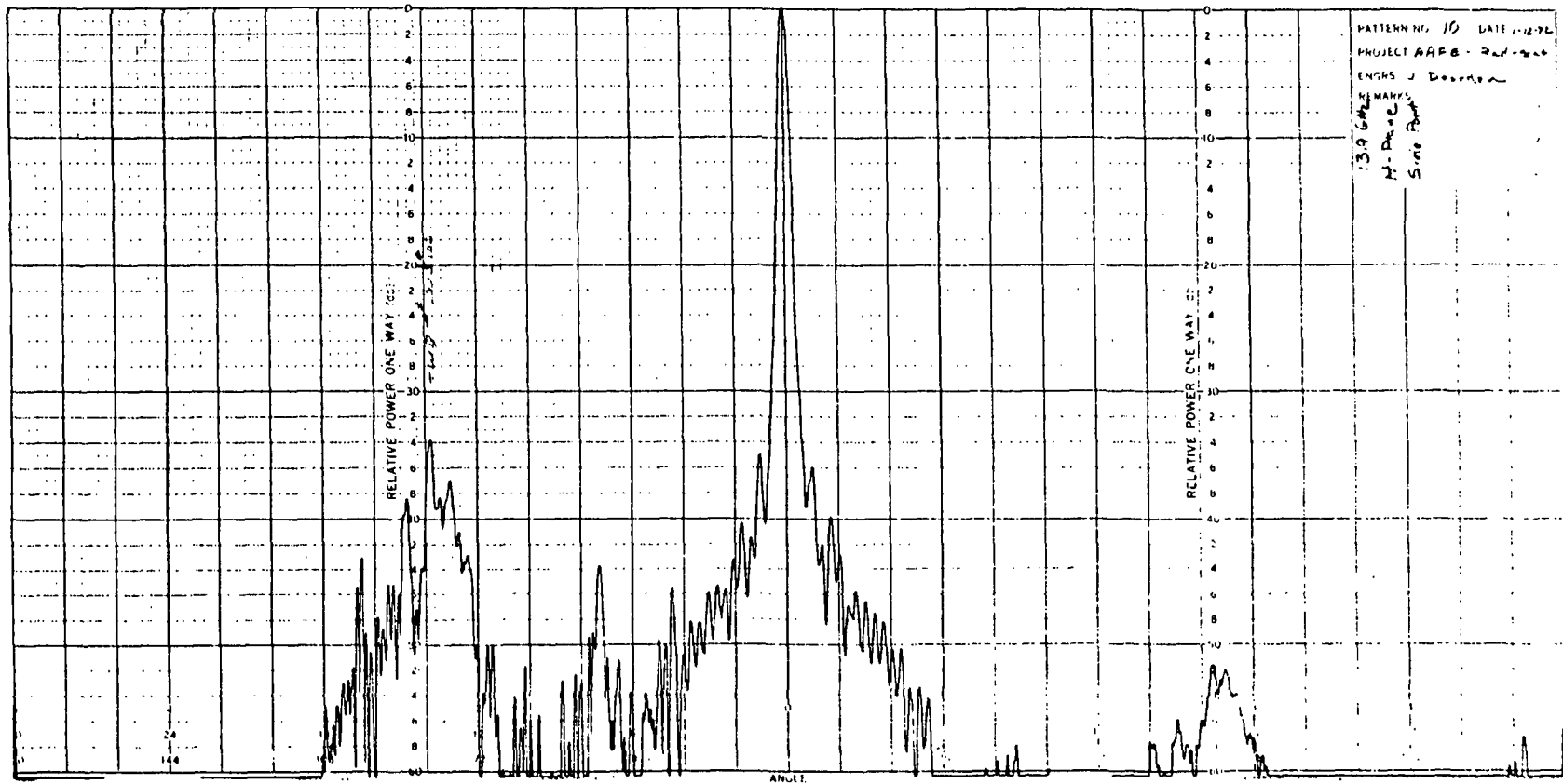
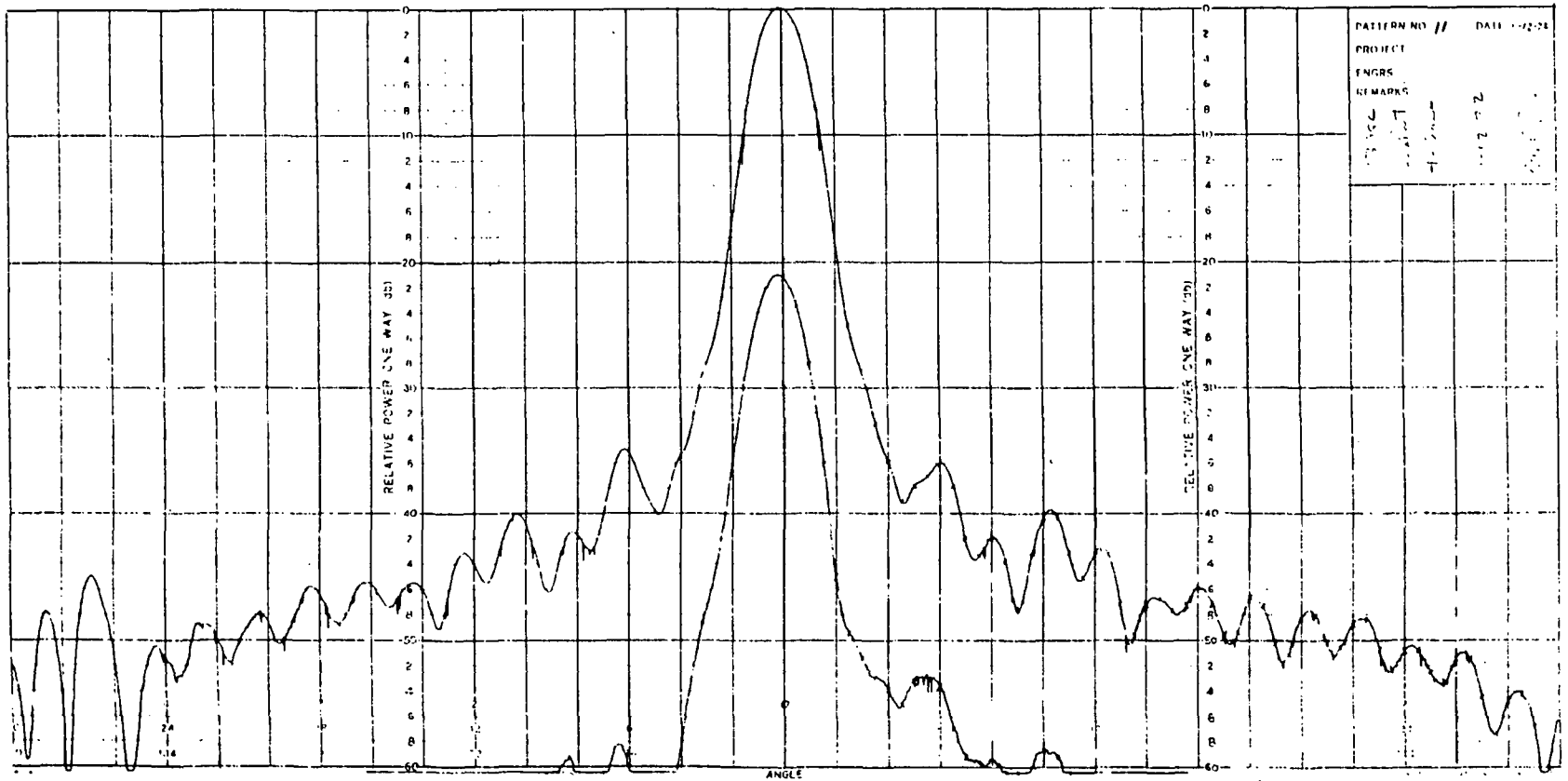


Figure A3-1.- AAFE RADSCAT parabolic reflector with 13.9 GHz feed.

ORIGINAL PAGE IS  
OF POOR QUALITY.



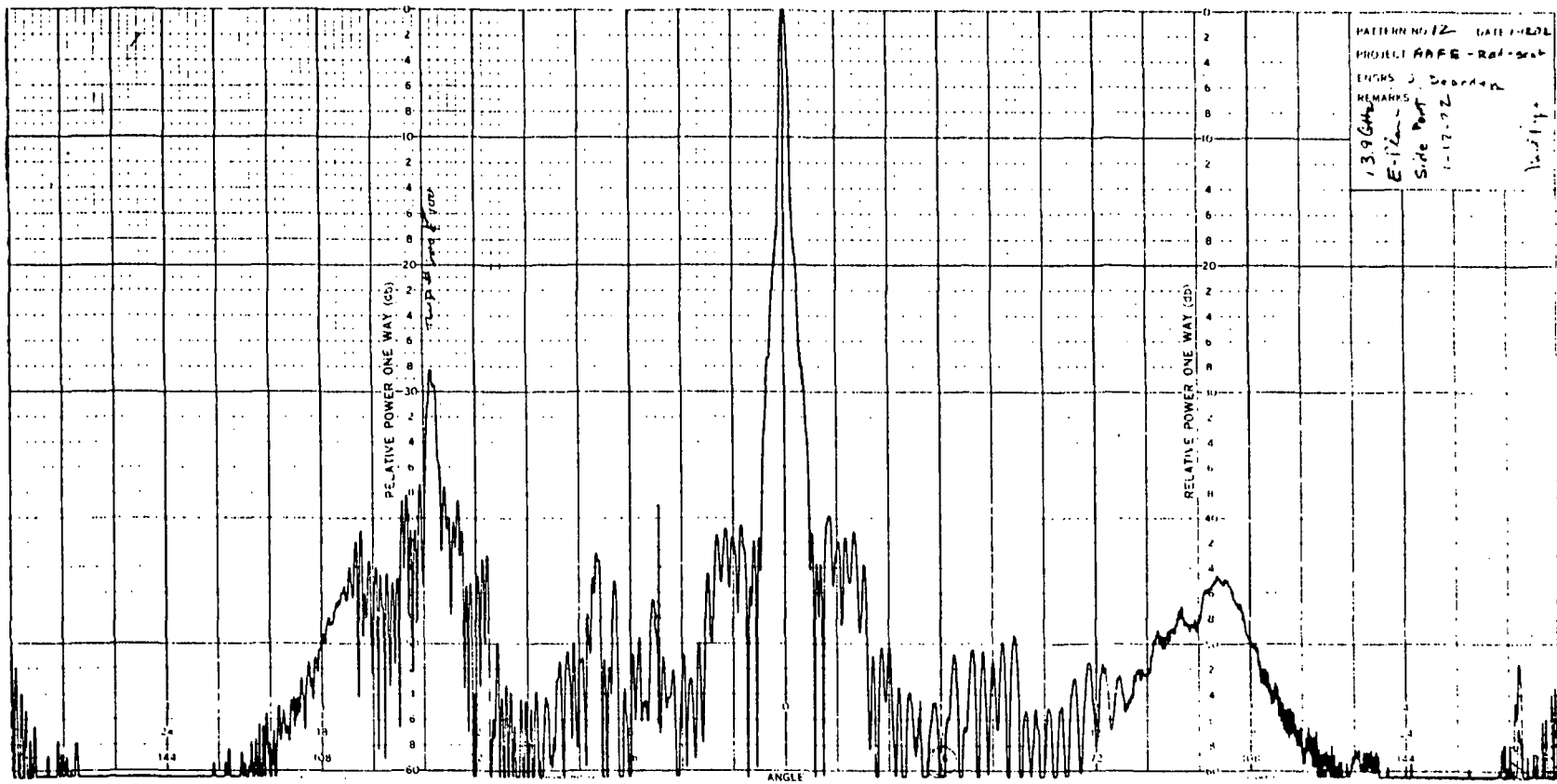
(a) Antenna pattern no. 10 - full pattern  
 Figure A3-2.-H-plane pattern at 13.9 GHz.



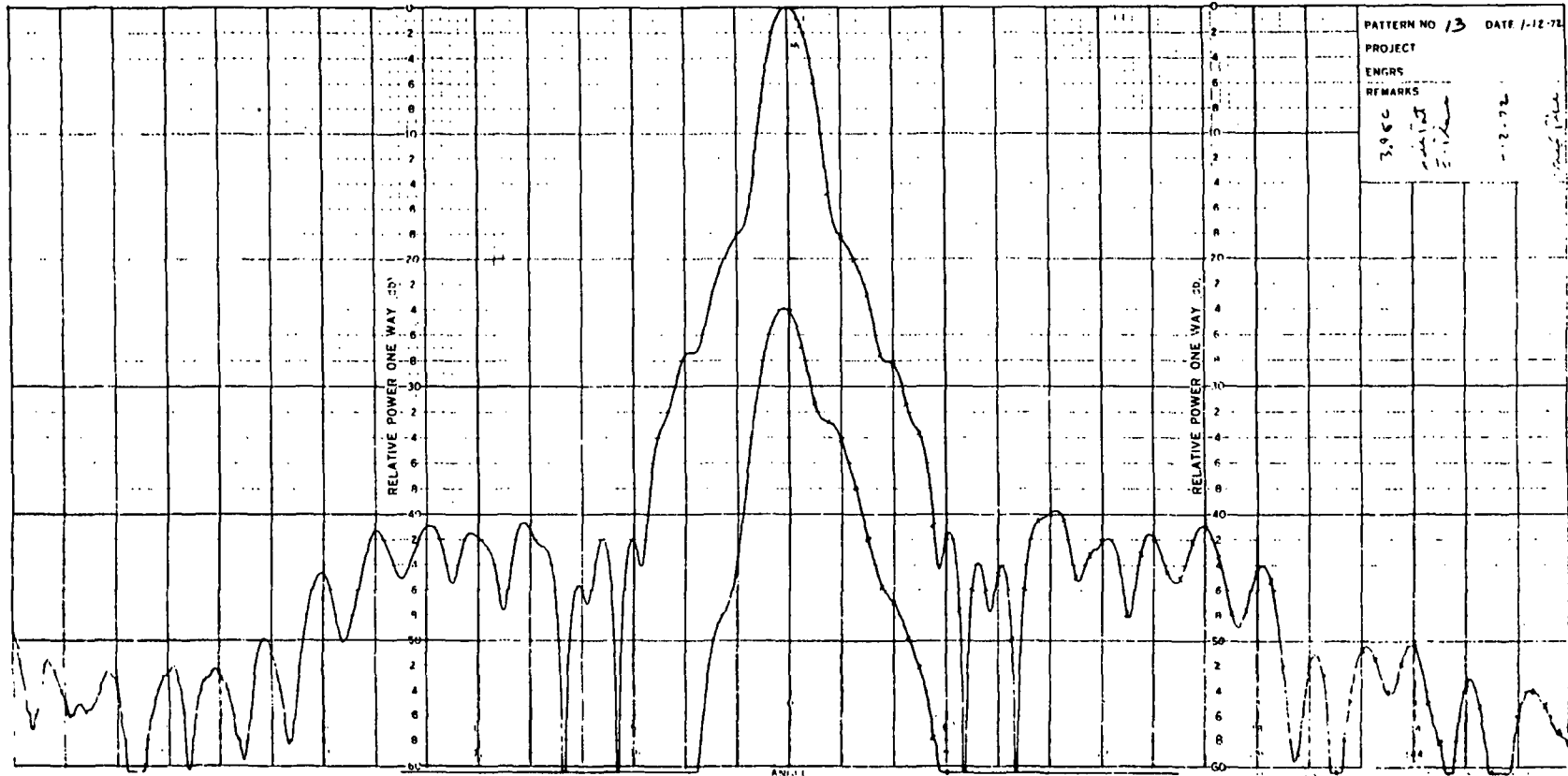
(b) Antenna pattern no. 11 - main beam

Figure A3-2.- (Concluded)

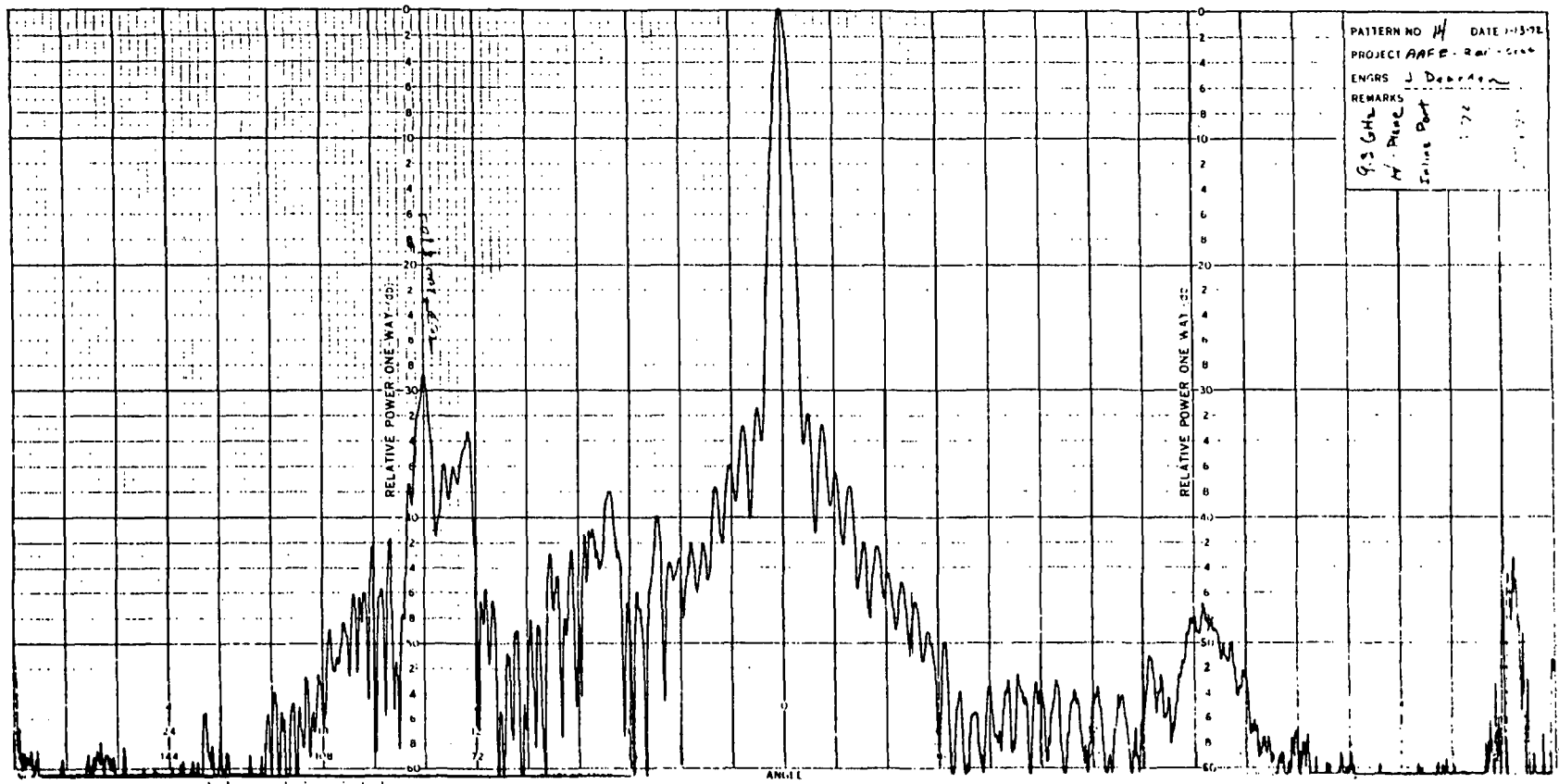




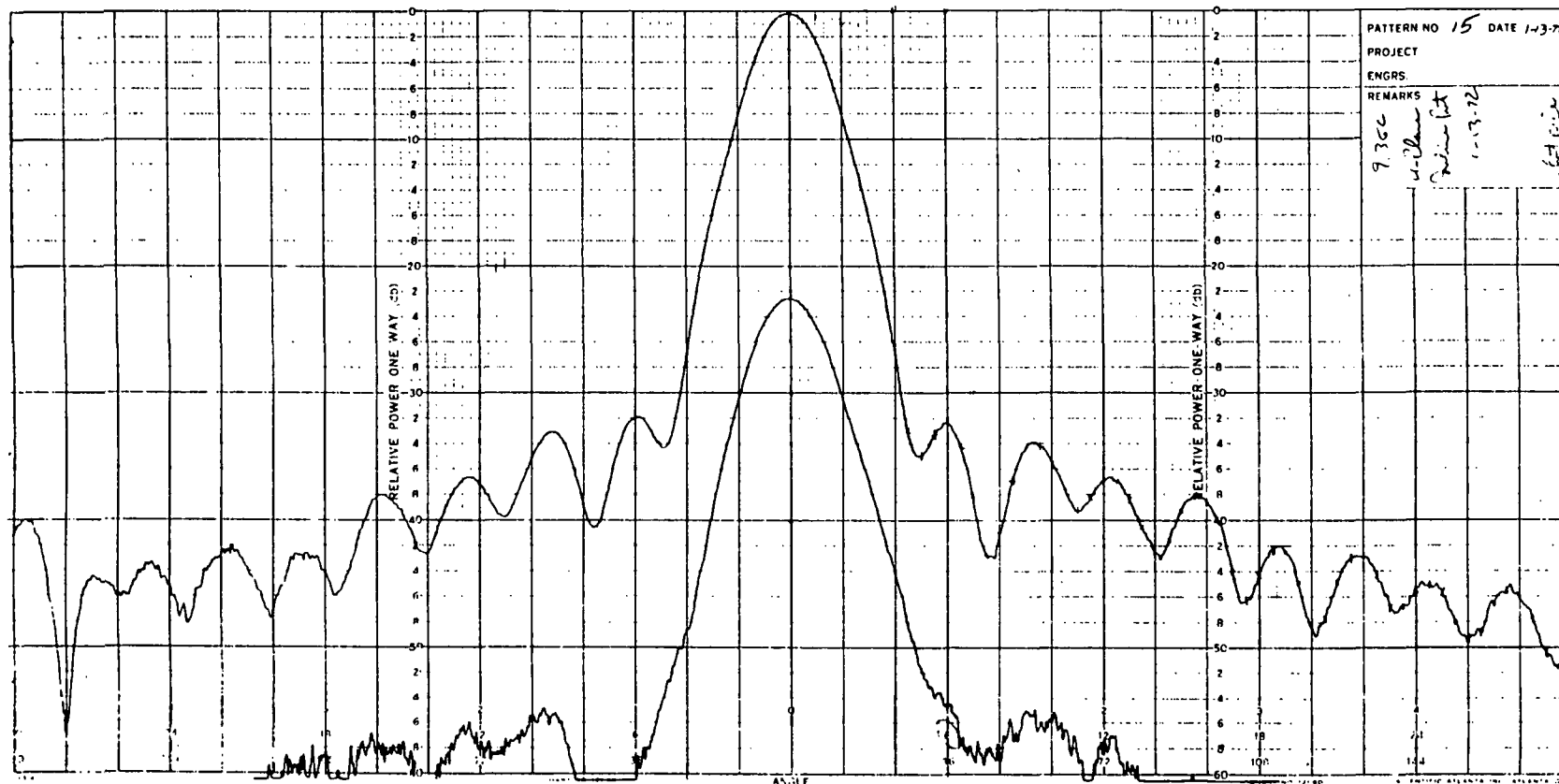
(a) Antenna pattern no. 12 - full pattern  
 Figure A3-3.-E-plane pattern at 13.9 GHz.



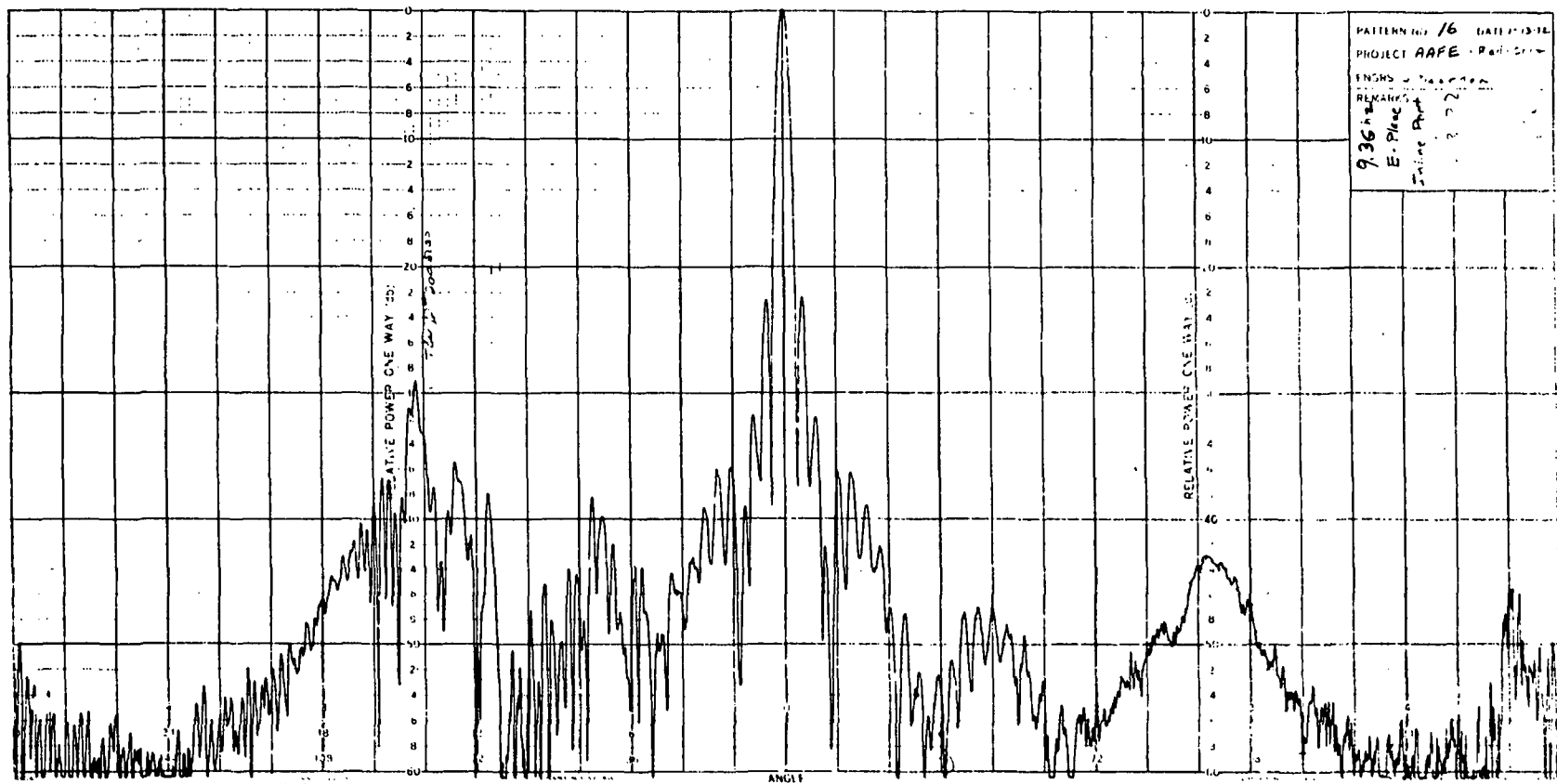
(b) Antenna pattern no. 13 - main beam  
 Figure A3-3.- (Concluded)



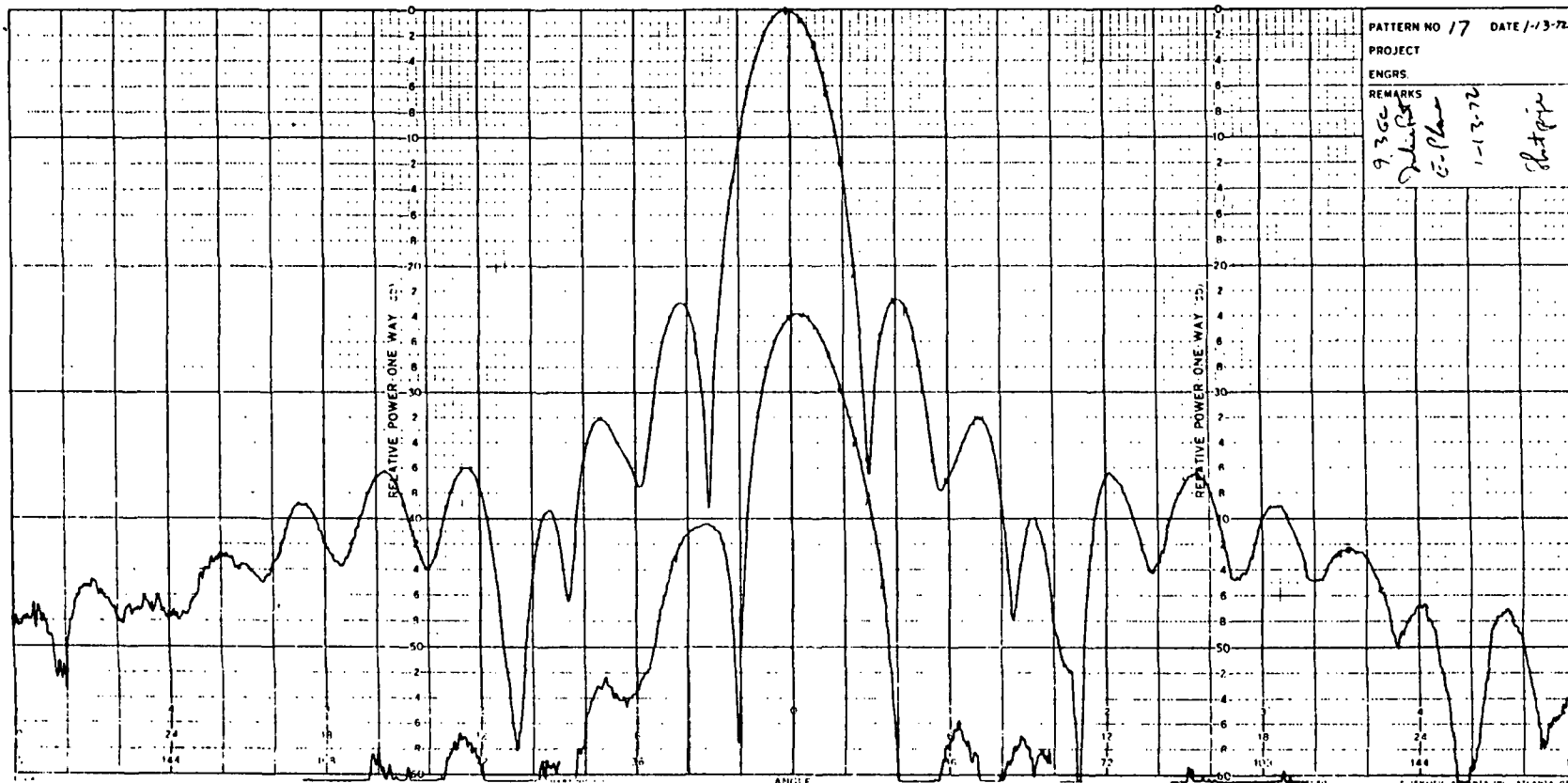
(a) Antenna pattern no. 14 - full pattern  
Figure A3-4.-H-plane pattern at 9.3 GHz.



(b) Antenna pattern no. 15 - main beam  
Figure A3-4.- (Concluded)



(a) Antenna pattern no. 16 - full pattern  
 Figure A3-5.-E-plane pattern at 9.3 GHz.



(b) Antenna pattern no. 17 - main beam  
 Figure A3-5.- (Concluded)

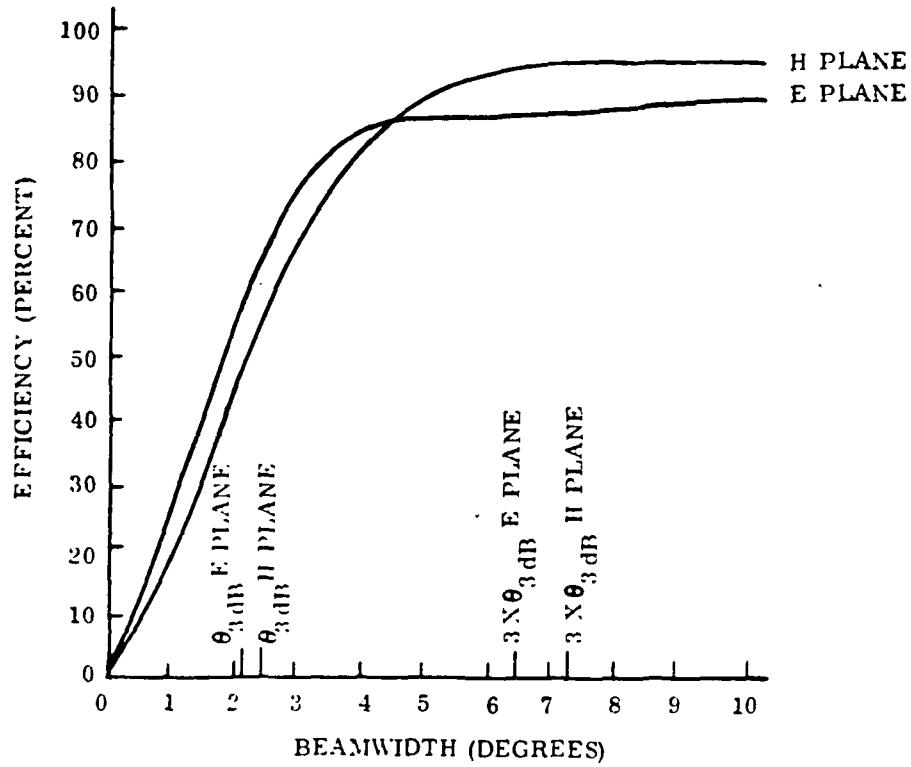


Figure A3-6.- Main Beam Efficiency (Including Cross Polarization) vs Beamwidth (9.3 GHz)

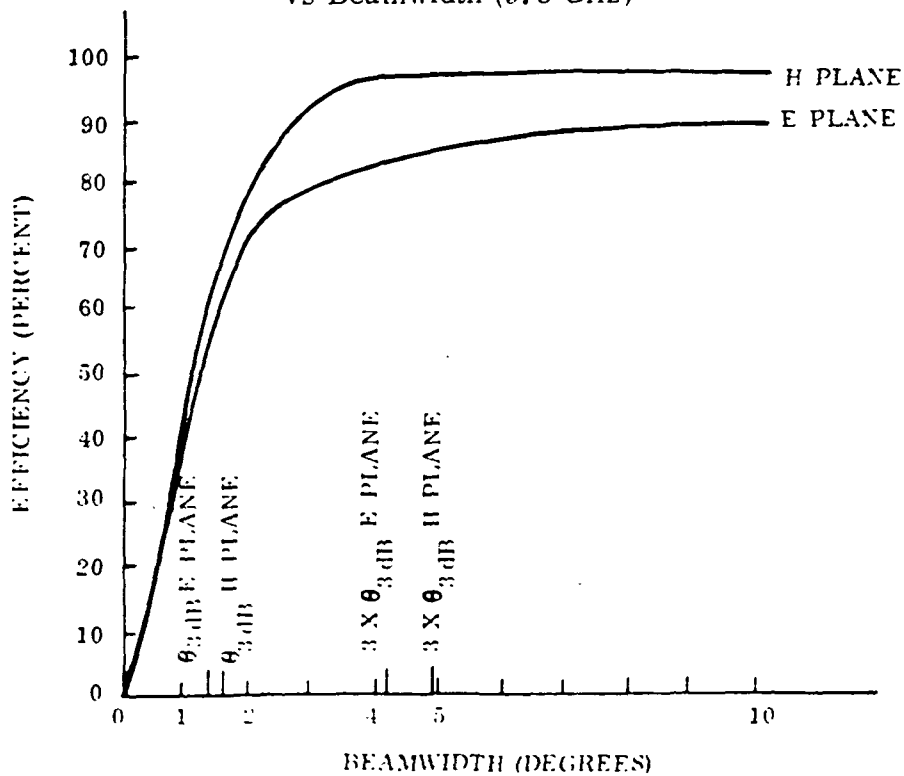


Figure A3-7.- Main Beam Efficiency (Including Cross Polarization) vs Beamwidth (13.9 GHz)

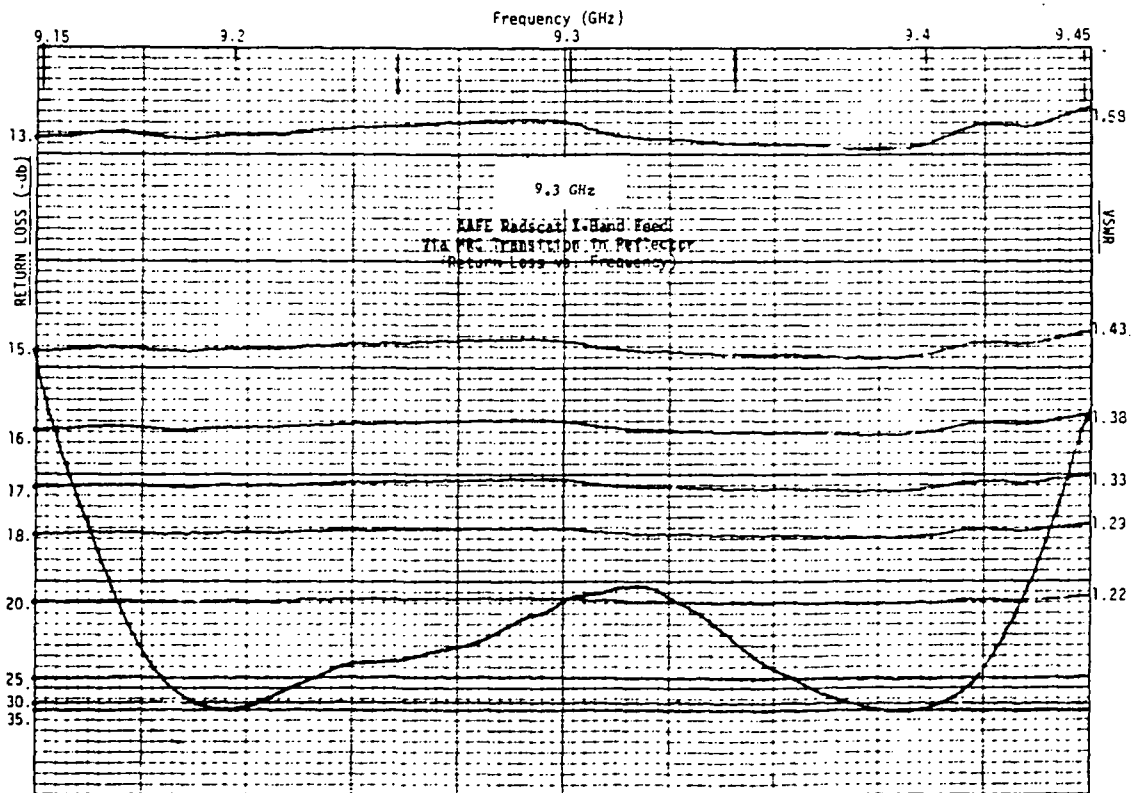
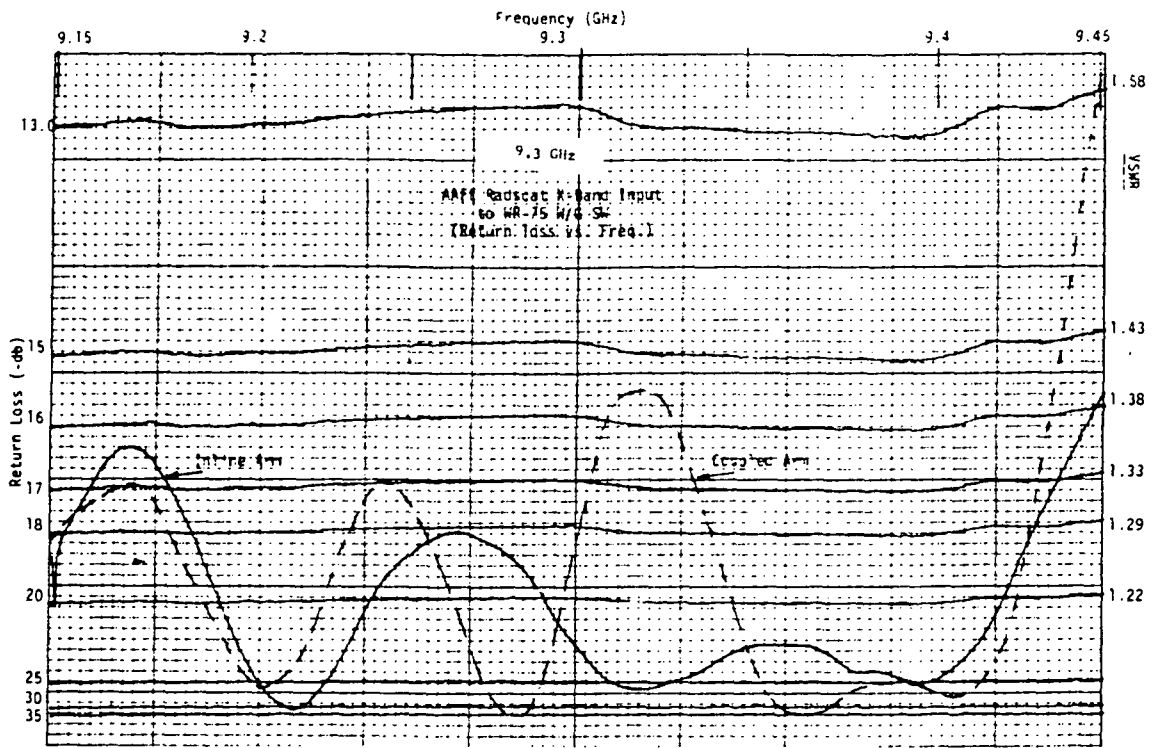


Figure A3-8.- VSWR Test Results (9.3 GHz)



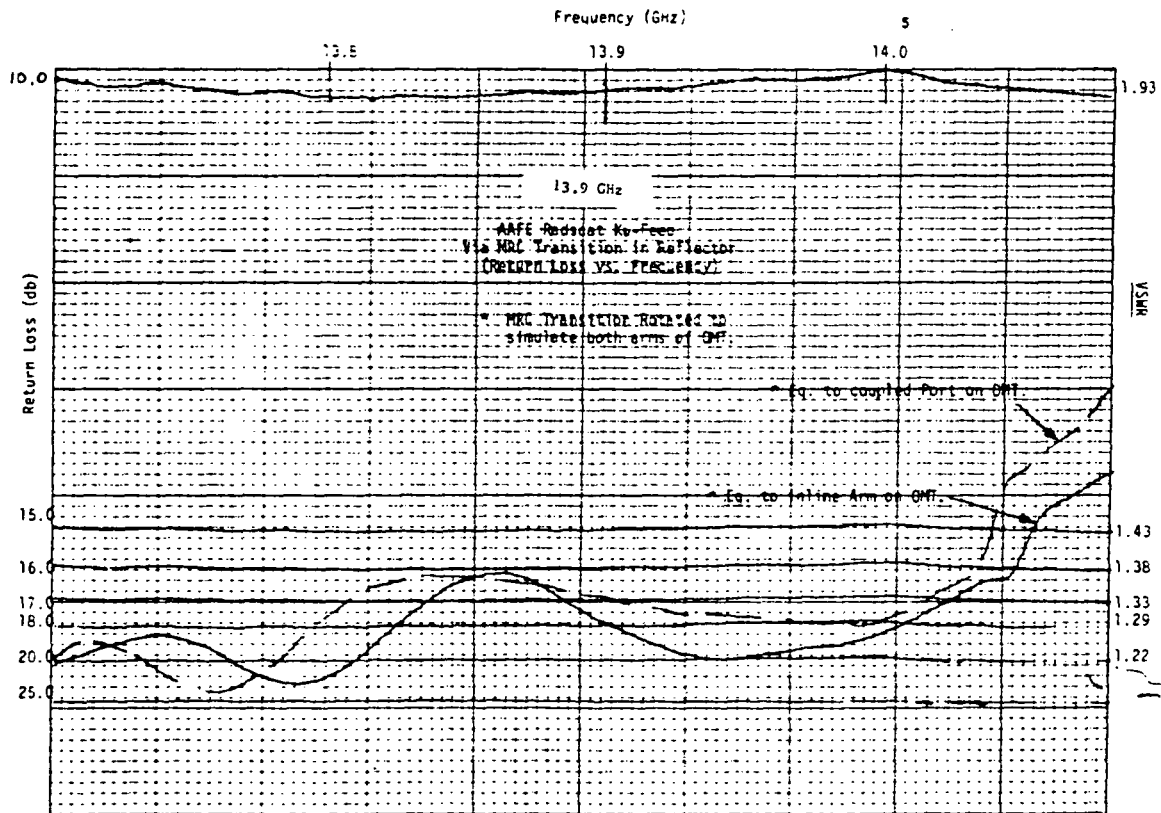
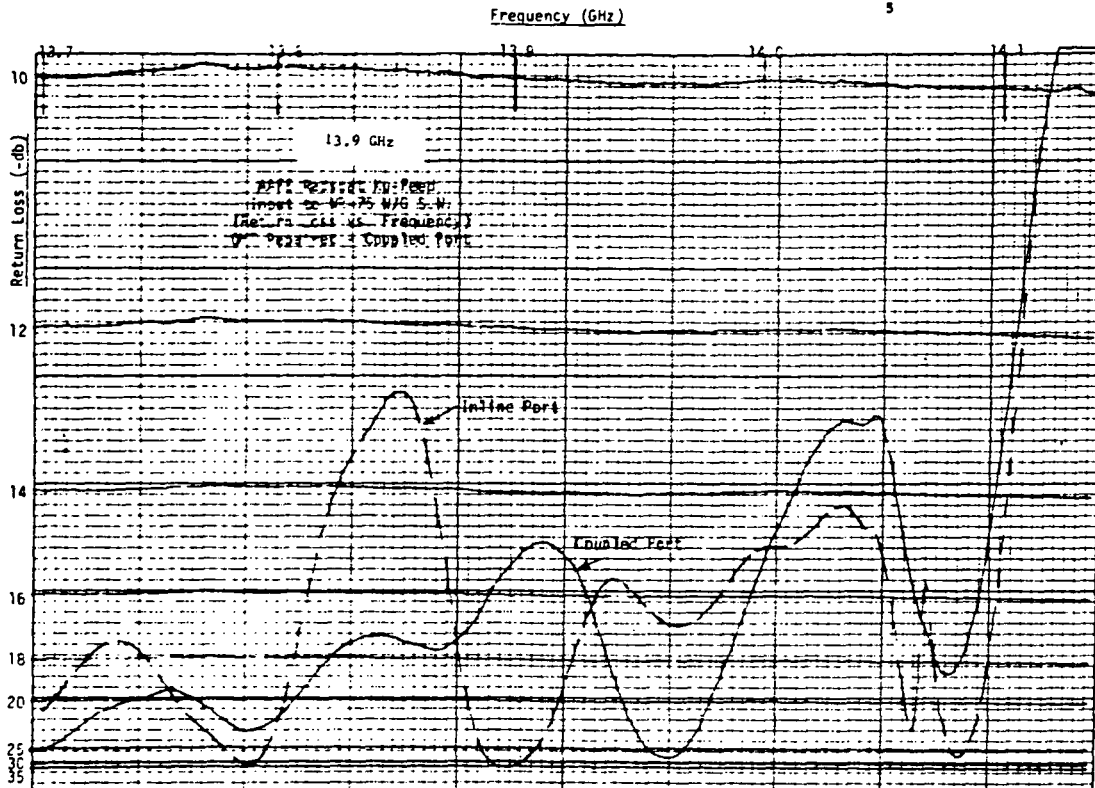


Figure A3-9.- VSWR Test Results (13.9 GHz)

## Appendix 4

## OUTPUT DATA FORMAT

## Bit Definition

The output data is presented for magnetic recording as two PCM data streams, one for Experiment Information, the other for Diagnostic Telemetry. The Experiment Information is provided as two electrically-paralleled channels, while the Diagnostic Telemetry is provided on a single output channel. Both outputs are TTL-derived 0 to +5 volt levels, each with the following characteristics:

Bit rate - 1KBPS

Word length - 10 bits

Coding - Bi-Phase L

## Frame Definition

The Experiment Information format contains 10 words per frame (Figure A4-1) while the Diagnostic Telemetry format contains 10 words per sub-frame (Figure A4-2) the 12 sub-frame per frame (120 words per frame).

WORD NUMBER	1	2	3	4	5	6	7	8	9	10
FUNCTION	FRAME SYNCH		CP	P1	SCAT 1	SCAT 2	SCAT 3	SCAT 4	P2	RAD

NOTE: "CP" denotes CONTROL PANEL parameters

"P1" denotes SCAT PARAMETERS

"P2" denotes RAD PARAMETERS

Figure A4-1. Experiment Information Frame

WORD	1	2	3	4	5	6	7	8	9	10
FUNCTION	FRAME SYNCH		SF X	RAD AGC	RAD AGC	SC	RAD AGC	SC	RAD AGC	RAD AGC
			1			T <sub>1</sub>		T <sub>2</sub>		
			2			T <sub>3</sub>		T <sub>4</sub>		
			3			T <sub>5</sub>		T <sub>6</sub>		
			4			T <sub>7</sub>		T <sub>8</sub>		
			5			T <sub>9</sub>		T <sub>10</sub>		
			6			T <sub>11</sub>		T <sub>12</sub>		
			7			T <sub>13</sub>		T <sub>14</sub>		
			8			T <sub>15</sub>		T <sub>16</sub>		
			9			T <sub>17</sub>		T <sub>18</sub>		
			10			T <sub>19</sub>		T <sub>20</sub>		
			11			T <sub>21</sub>		T <sub>22</sub>		
			12			T <sub>23</sub>		T <sub>24</sub>		

Figure A4-2.- Diagnostic Telemetry Frame.

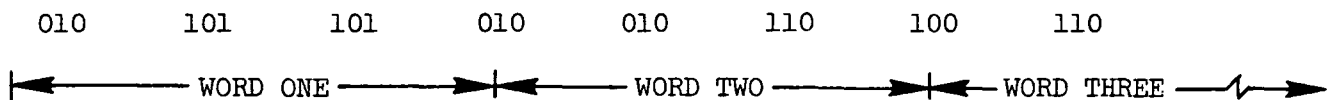
NOTE: "X" denotes "Don't Care"

SF denotes subframe identifier

SC denotes switched channel

Synch Pattern (Experiment and Diagnostic Telemetry Information)

Each frame and sub-frame is identified by a Synch pattern, contained in the leading 24 bits of the first 3 words. The 24-bit pattern is defined as:



## Subframe Identifier (Diagnostic Telemetry Information Only)

The twelve subframes in each Diagnostic Telemetry frame are each identified in the bits following the synch pattern in word three of each subframe (Figure A4-3).

DIAGNOSTIC TELEMETRY SUBFRAME	BIT VALUE - WORD THREE			
	5	6	7	8
1	0	0	0	1
2	0	0	1	0
3	0	0	1	1
4	0	1	0	0
5	0	1	0	1
6	0	1	1	0
7	0	1	1	1
8	1	0	0	0
9	1	0	0	1
10	1	0	1	0
11	1	0	1	1
12	0	0	0	0

Figure A4-3. Sub-Frame Counter Values

## Bit Weighting

## Experiment Information

Bit weighting for RADSCAT information is based on read-out of LEAST SIGNIFICANT BIT (LSB) first. The significance of bits for RAD & SCAT data words is different, and is defined as follows:

Scat Data - The data is defined as 9 bits plus polarity. The bit occupying the first-sent position has values of:

1 = negative polarity

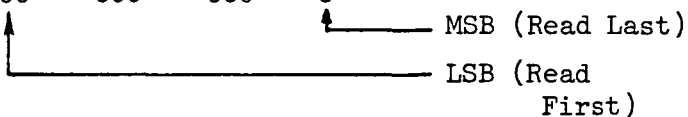
0 = positive polarity

The remaining (9) bits denote the absolute value of the data, with MSB read last. The full-scale range is based on 10 volts, as shown in the examples below:

<u>DATE VOLTAGE</u>	<u>BINARY CODING</u>			
+10	011	111	111	1
+ 5	011	111	111	0
0 <sup>+</sup>	000	000	000	0
0 <sup>-</sup>	111	111	111	1
- 5	111	111	111	0
-10	100	000	000	0

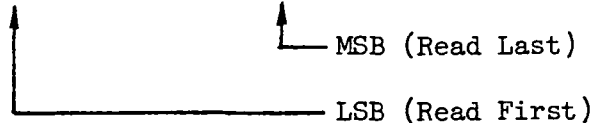
Rad Data - The data is presented as 10 bits, without polarity, covering two cycles from -10 to +10 volts. (The polarity bit is not required due to the hardware-limited voltage range, which eliminates ambiguities). Several examples without regard to the limited voltage range, are given below:

<u>DATA VOLTAGE</u>	<u>BINARY CODING</u>			
+10	111	111	111	1
+ 5	111	111	111	0
0 <sup>+</sup>	000	000	000	0
-10	111	111	111	1
- 5	111	111	111	0
0 <sup>-</sup>	000	000	000	0



The realizable voltage range is approximately from -0.4 volts to +8.0 volts, so that voltages that are decoded as greater than 8.5 volts (absolute value), must be added to -10.0 volts to determine their actual magnitude (with sign). Several examples of actual conversions from Binary coding to Data voltage are given below:

<u>BINARY CODING</u>				<u>ABSOLUTE VOLTAGE</u>	<u>DATA VOLTAGE</u>
010	011	001	1	8.000	8.000
101	100	110	0	2.000	2.000
100	101	000	0	0.400	0.400
001	010	000	0	0.200	0.200
000	000	000	0	0.000	0.000 <sup>+</sup>
111	111	111	1	10.000	0.000 <sup>-</sup>
110	101	111	1	9.800	-0.200
011	010	111	1	9.600	-0.400



## Diagnostic Telemetry

Bit weighting for diagnostic telemetry is based on read-out of MOST SIGNIFICANT BIT (MSB) first. The data is presented as 10 bits, without polarity, covering two cycles from -10 to +10 volts. Due to the hardware-limited voltage range of the measurements made, no ambiguities occur. The limited ranges are described below:

1. Monitor (other than RAD AGC) are all positive voltages, so that the range is limited from 0 to +10 volts, and conversion is direct.

	<u>BINARY CODING</u>			<u>DATA VOLTAGE</u>
1	111	111	111	-0.000
1	100	110	010	8.000
1	001	100	110	6.000
0	110	011	001	4.000
0	011	001	101	2.000
0	000	000	000	0.000

2. RAD AGC ( $T_{21}$ ) is limited to a range of approximately +1.0 to -5.0 volts, so that binary values that are decoded as greater than 5.0 volts absolute must be added to -10.000 volts to determine their actual magnitude (with sign).

	<u>BINARY CODING</u>			<u>ABSOLUTE VOLTAGE</u>	<u>DATA VOLTAGE</u>
0	001	100	110	1.000	1.000
0	000	000	000	0.000	0.000 <sup>+</sup>
1	111	111	111	10.000	0.000 <sup>-</sup>
1	110	011	001	9.000	-1.000
1	100	110	010	8.000	-2.000
1	001	100	110	6.000	-4.000
0	111	111	111	5.000	-5.000

#### Experiment Information Measurements List

Table A4-1 lists the data points contained in the Experiment Information data stream. They are identified by their frame location. (MSB is lowest bit number).

#### Diagnostic Telemetry Information Measurements List

Table A4-2 lists the data points contained in the Diagnostic Telemetry Data stream. They are identified by their subframe/word location. (MSB is lowest Bit number in Table).



## Special Considerations

Certain of the CONTROL PANEL(CP), PARAMETER (P1 & P2) and DIAGNOSTIC TELEMETRY DATA have combinational significance, as follows:

1. SCAT RCV POL (Word 3 - Bit 8) is valid only when the Polarization Circulator is installed, as denoted by T17 greater than 2 volts.
2. PARAMETER WORD 1 (Word 4) is related to SCAT DATA (Words 5-8) in the same frame.
3. PARAMETER WORD 2 (Word 9) is related to RAD DATA (Word 10) in the same frame.
4. SCAT DATA & RAD DATA are valid only when T22/ANTENNA IN MOTION is greater than 2 volts, and when COMPUTER FLAG (Word 3 - Bit 5) is a "one".

Table A4-1.- Experiment Information Data List

Word Number	Bit Number	Function	Remarks	Foot Note
1	1-10	Synch	See text of this Appendix	
2	1-10			
3	1-4			
3	5	Computer Flag	"0" = OFF FLIGHT LINE; "1" = ON FLIGHT LINE	1
	6-7	Altitude	00 = 2 KFT      10 = 10 KFT 01 = 5 KFT      11 = 20 KFT	
	8	Scat Recv. Polarization	0 = Horizontal; 1 = Vertical (Valid only at 13.9 GHz with circulator)	
	9	Zero Calibration	0 = Zero Cal.; 1 = Normal Cal or operation	2
	10	IF Attenuator	0 = 0 dB; 1 = 10 dB	2
4	1	Scat Data Age	1 = New Scat data in words 5-8 of this frame 0 = old(repeated) data	
	2-4	Antenna Angle position	001 = Angle 1   011 = Angle 3   101 = Angle 5 010 = Angle 2   100 = Angle 4   110 = Angle 6 (000 & 111 are invalid antenna position codes)	
	5-6	Operating Mode	00 = Rad Only      10 = Fixed Angle 01 = Short Scat   11 = Alternating Angle	3
	7-8	Frequency	01 = 9.3 GHz; 11 = 13.9 GHz (00 & 10 are invalid codes)	
	9	Scat Transmit Polarization	0 = Horizontal; 1 = Vertical	
	10	Operating State	0 = Calibrate; 1 = Operate	
5	1-10	Scat 1 Output	See text of this Appendix	4
6	1-10	Scat 2 Output		
7	1-10	Scat 3 Output		
8	1-10	Scat 4 Output		
9	1	Rad Data Age	0 = Old (Repeated) Data; 1 = New data in word 10	
	2-4	Antenna Pitch Angle	001 = Angle 1   011 = Angle 3   101 = Angle 5 010 = Angle 2   100 = Angle 4   110 = Angle 6 (000 & 111 are invalid antenna position codes)	
	5-6	Operating Mode	00 = Rad Only      10 = Fixed Angle 01 = Short Scat   11 = Alternating Angle	3
	7-8	Frequency	01 = 9.3 GHz    11 = 13.9 GHz (00 & 10 are invalid codes)	
	9	Rad Receive Polarization	0 = Horizontal; 1 = Vertical	
	10	Operating State	0 = Calibrate; 1 = Operate	
10	1-10	Rad Output	See text of this appendix	4,5

1. Prior to April 1973, this bit identified pol switch.
2. Unused prior to April 1973.
3. 11 designates DFS Mode after May 1974.
4. Prior to April 1973, no polarity bit.
5. Subsequent to September 1973, no polarity bit.

ORIGINAL PAGE IS  
OF POOR QUALITY

Table A4-2.- Diagnostic Telemetry Data List

Sub Frame	Word Number	Designation	Function - 2/74 and before	Function - Relocation 9/28/74	Function - Relocation 1/22/75
All	4	AGC	Antenna Gimbal Angle	RAD AGC Voltage	No Change
All	5				
All	7				
All	9				
All	10				
1	6	T1	Temp-9.3 GHz Section-Circulator	Temp.-13.9 GHz Dicke Switch	No Change
	8	T2	Temp-9.3 GHz Circulator Input W/G	Temp.-TWTA Output	Temp.-Cal Loop Coupler
2	6	T3	Temp-T/R Circulator	No Change	Temp.-WG/Coax. Input to T/R Circulator
	8	T4	Temp-9.3 GHz Hot Load Triplexer	Temp.-13.9 GHz Input Triplexer	Temp.-T/R Circulator
3	6	T5	Temp-9.3 GHz TDA Input	Temp.-OMT	Temp.-WG/Coax. Output of T/R Circulator
	8	T6	Temp-9.3 GHz Circulator Termination	Temp-WG/Coax. Input to T/R Circulator	Temp.-13.9GHz Arm of Triplexer
4	6	T7	Temp-9.3 GHz Limiter	Temp.-WG/Coax. Output of T/R Circulator	Temp.- Output WG of TDA
	8	T8	Temp.-TWTA Output Coupler	Temp.-f <sub>B</sub> Transmitter CFS	Temp.-Mixer/IF Amplifier Panel
5	6	T9	Temp W/G Input to Adapter AD3	Temp.-Cal Loop Coupler	Temp.- f <sub>A</sub> Transmitter CFS
	8	T10	Temp. 11.7 GHz Circulator	Temp.-H-Pol Feed WG	Temp.-Wave Switch/Gate Assy.
6	6	T11	Temp-13.9 GHz Circulator Termination	Temp.-13.9 GHz Warm Load	No change
	8	T12	Temp-13.9 GHz Pol Circ.	Temp.-V-Pol Feed WG	Pol. switch
7	6	T13	Temp-W/G Sw. S2	Temp-Baseplate by S1	Temp.-V-Pol Feed WG
	8	T14	Temp.- 9.3 GHz Image Rej. Filter	Temp.-13.9 GHz Hot Load Triplexer	Temp.-H-pol Feed WG
8	6	T15	Temp-Antenna Rim	No Change	No Change
	8	T16	Temp-Orthomode Transducer	Temp.-Pol. Switch	Temp.-OMT
9	6	T17	Polarization Switch Selection	No Change	No Change
	8	T18	Antenna Angle	No Change	No Change
10	6	T19	Spare	Temp.-Crystal Filter #1	No Change
	8	T20	28 VDC Monitor	No Change	No Change
11	6	T21	Rad AGC Voltage	No Change	No Change
	8	T22	Antenna in Motion	No Change	No Change
12	6	T23	Spare	Temp.-Crystal Filter #2	No Change
	8	T24	Spare	No Change	Temp.-Hot Load

ORIGINAL PAGE IS  
OF POOR QUALITY.